INSTITUT FOR BÆRENDE KONSTRUKTIONER OG MATERIALER

DTU

Strength of Cracked Concrete

Part 2
Micromechanical Modelling of Shear Failure in Cement Paste and in Concrete

JIN-PING ZHANG

DEPARTMENT OF STRUCTURAL ENGINEERING AND MATERIALS
TECHNICAL UNIVERSITY OF DENMARK Series R No 17 1997

STRENGTH OF CRACKED CONCRETE

Part 2 --- Micromechanical Modelling of Shear Failure in Cement Paste and in Concrete

Jin-Ping Zhang

Strength of Cracked Concrete
Part 2.. Micromechanical Modelling of Shear Failure in Cement Paste and in Concrete

Tryk: LTT
Danmarks Tekniske Universitet
Lyngby
ISBN 87-7740-199-9
ISSN 1396-2167
Bogbinder:
H. Meyer, Bygning 101, DTU

PREFACE

This paper has been prepared as the second part of the thesis to obtain the Ph.D. degree at the Technical University of Denmark.

The first part of the thesis is

Part 1 - Shear Strength of Conventional Reinforced Concrete Beams, Deep beams, Corbels, and Prestressed Reinforced Concrete Beams without Shear Reinforcement

which has been published at the Department of Structural Engineering, Report R-311, 1994.

The work has been carried out at the Department of Structural Engineering under the supervision of Professor, Dr.techn. M.P.Nielsen.

I wish to express my sincere appreciation to my supervisor for his inspiring advice and encouragement, and to the entire staff at the department for their help during the time I have been here.

Financial assistance from the Danish Council for Scientific and Technical Research (STVF) is gratefully acknowledged.

Lyngby, 1996

Jin-Ping Zhang

SUMMARY

This report examines the shear failure mechanism in cement paste and in concrete by means of the theory of plasticity.

The micromechanical model of shear failure proposed in this paper is based on the fact that cement paste, as well as concrete, is in a microcracked state during loading or even prior to loading. Hard particles, coming from unhydrated cement grains and aggregate particles, exist in the matrix. In cement paste, the unhydrated cement grains cause yield surfaces to be formed in front of them. In this way the brittle behaviour of cement paste and concrete in uniaxial stress states might be explained. In concrete, the load induced cracks are mainly in the direction of the axial load, and the function of the aggregate particles is to displace the yield line in the cement paste to steeper positions.

The model shows that shear failure in cement paste and the cracking in the direction of the axial loading govern the compressive failure in concrete.

The load carrying capacity is also affected by the microcracking state in the cement paste.

The apparent friction angle of concrete calculated from the test results decreases when increasing the uniaxial compressive strength of concrete. This turns out not to be material properties of the cement paste and the aggregates but a result of the composition.

The failure criterion for concrete appears to consist of two parts: the usual Coulomb failure criterion with a varying friction angle and a transition curve which may be calculated by the model.

The comparison with push-off type experiments indicates that the plastic solutions for shear failure may be applied to macrocracked concrete by multiplying the usual effective compressive strength of concrete with a factor

of 0.5.

The model is compared with experimental results of cement paste, concrete in triaxial compressive stress states, concrete in tensile stress states, and push-off type tests. Good agreement has been found.

RESUMÉ

I denne rapport undersøges glidningsbrudmekanismer i cement pasta og i beton ved hjælp af plasticitetsteorien.

En mikromekanisk model, der er baseret på det faktum, at så vel cement pasta som beton er i en mikrorevnet tilstand både under belastning og før belastning, foreslås. I cement pasta eksisterer der hårde partikler i form af uhydratiserede cementkorn. Disse hårde partikler fører til dannelse af flydelinier foran kornene, og kan forklare, hvorfor cement pasta og beton opfører sig som et skørt materiale for enaksede spændingstilstande. I beton findes revner fremkaldt af belastningen hovedsageligt i retningen af den største trykhoved spænding, og stentilslagets virkning er i det væsentlige at flytte flydelinierne i cementpasta til stejlere retninger.

Modellen viser, at glidningsbrud og revnedannelse i retningen af den største trykhoved spænding i cementpasta kan forklare betons opførsel under tryk.

Modellen indeholder også en beskrivelse af mikrorevnedannelsen i cementpasta-en før belastning.

Betons friktionsvinkel viser sig at aftage med betonstyrken. Det viser at dette ikke er en egenskab ved cementpasta eller tilslag, men er en følge af materiale kompositionen.

Betons brud betingelse viser sig at bestå af to områder: en sædvanlig Coulomb brud betingelse med variabel friktionsvinkel og en overgangs kurve, som kan beregnes ved hjælp af modellen.

En sammenligning af modellen med de såkaldte push-off forsøg viser, at plasticitetsteoriens løsninger kan benyttes for revnet beton, når den sædvanlige effektive betonstyrke multipliceres med 0.5.

Modellen sammenlignes med forsøg med cementpasta, med beton under treaksede spændningstilstande, med beton under træk og med forsøg af push-off typen. Der er fundet god overensstemmelse mellem forsøg og modellen.

TABLE OF CONTENTS

page

Preface i

Summary ii

Resumé iv

Notations 1

I. Introduction 3

II. Review 6

2.1 Composition and structure of hardened cement paste 6
2.2 Strength of hardened cement paste 7
2.3 Bond 7
2.4 Coulomb and modified Coulomb Material 8
2.4.1 Failure criteria in τ-σ space 9
2.4.2 Failure criteria in principal stress space 10
2.4.3 Dissipation in yield lines according to the theory of plasticity 11
2.4.4 Failure patterns according to the theory of plasticity 12

III. Micromechanical modelling of shear failure of cement paste in compression 13

3.1 Observations from experiments 13
3.2 Unhydrated cement particles and microcracking 15
3.3 Micromechanical modelling of shear failure of cement paste in compression 17
3.3.1 Shear Failure condition in τ-σ space according to plastic theory 18

3.3.2 Shear failure condition in principal stress space 27
3.4 Parameter studies 29
3.5 Experimental verification 37
3.6 Other test results 42
3.7 Effect of pore pressure 43
3.8 Conclusions and discussion 44

IV. Micromechanical modelling of shear failure of concrete in compression 47

4.1 Bond strength and strength of concrete 47
4.2 Micromechanical modelling of shear failure in principal stress space 49
4.3 Parameter studies 61
4.4 Experimental verification 61
4.5 Friction angle of concrete 72
4.6 Ratio of lateral strains to axial strains in uniaxial compression 74
4.7 Location of failure lines 78
4.8 Effect of microcracking on the uniaxial compressive strength 80
4.9 Lower bound solutions 82
4.9 Conclusions and discussion 85

V. Micromechanical modelling of failure of cement paste and concrete in tension 87

5.1 Failure modelling of cement paste in pure tension 87
5.2 Failure modelling of cement paste subject to shear tension 91
5.3 Failure of concrete in tension 92
5.3.1 Primary failure in tension 93
5.3.2 Secondary failure in tension 94
5.3.3 Comparison with empirical formulas 98
5.4 Conclusions and discussion 100

VI. Push-off type tests 102

6.1 Solutions according to plastic theory 102
6.2 Strength reduction due to cracking 104
6.3 Shear carrying capacity of cracked concrete 106
6.4 Experimental verification 111
6.5 Conclusions 115

VII. Conclusions 116

References 118

Appendix 1 123

NOTATIONS

c : Apparent cohesion of cement paste in triaxial stress states
c_0 : Initial cohesion of cement paste
f_c : Uniaxial compressive strength of concrete
f_{cc} : Compressive strength of unmicrocracked cement paste or apparent compressive strength in triaxial stress states
f_t : Tensile strength of cement paste or concrete
f_{tp} : Tensile strength of cement paste in pure tension
f_{tpc} : Tensile strength of concrete in primary failure in tension
f_{ts} : Tensile strength of cement paste in shear tension
f_{tsc} : Tensile strength of concrete in secondary failure in tension
f_{tt} : Tensile strength of unmicrocracked cement paste or cement paste in triaxial stress states
k : Material constant, $k=(1+\sin\varphi)/(1-\sin\varphi)$
m' : Volume ratio of hard particles in cement paste
N : Normal force along the failure surface
u : Relative displacement in yield line
V : Shear force along the failure surface
W_i : Internal work per unit length
W_I : Internal work
W_E : External work

α : Angle of yield line in concrete
β : Angle of sliding surface in cement paste in front of the hard particles
γ : Angle of yield line in cement paste
Δ : Displacement of yield line due to aggregates
η : Damage factor in cement paste due to microcracking
κ_a : Volume ratio of aggregates in concrete
λ : Effectiveness factor of aggregates in concrete
μ : Coefficient of friction for cement paste, $\mu=\tan\varphi$
ν_s : Sliding reduction factor due to cracking
σ : Normal stress

$\sigma_1,\sigma_2,\sigma_3$: Principal stresses

τ : Shear stress

φ : Apparent angle of friction for cement paste or concrete

Φ : Mechanical degree of reinforcement, $\Phi=A_s f_Y/bhf_c$

I. INTRODUCTION

In uniaxial and triaxial tests of concrete specimens, sliding failure has been observed. According to the theory of plasticity, under the assumption that concrete obeys the Coulomb frictional criterion with the internal friction angle $\varphi=37^{\circ}$, the ratio of lateral strain increments to axial strain increments is 4 and the yield line in the cylinder or prism specimens, subjected to uniaxial compression, has an inclination of h/b=2 (here, h and b are the length of the vertical projection and the horizontal projection of the yield line, respectively), details see [84,1]. However, in the test series reported in [86,1], the ratio of lateral strain increments to axial strain increments for specimens under uniaxial compression is larger than 7 and the failure lines in the specimens tend to be much steeper than that predicted by the plastic theory for a Coulomb material. Further, the rate of the axial strength of concrete as a function of the lateral confining stress is not a constant as expected but decreases with the increasing strength of the concrete.

The discrepancy between the estimation by plastic theory and the experimental facts can not be covered by errors of the tests, and neither can this be explained coherently by the present plastic theory.

The test results from [92,1][95,1] indicate that hardened cement paste seems to be a frictionless material when the lateral confining pressure is sufficiently high.

Up to now, most of the failure criteria of concrete, no matter how complicated their formulations may be, are hypotheses whose application needs to be verified by experiments. The parameters in the criteria are empirically determined. No direct relation between the parameters and the structure and composition of the material is normally established.

In this paper an effort is made to model the failure of cement paste and concrete based on the structure and composition of cement paste and concrete. The main idea is described as follows.

It is an established fact that a fraction of cement in the hardened cement paste will not be hydrated even after a long period of curing. It has been found that for hardened cement paste with a gel/space ratio of 1.0, those with a higher proportion of unhydrated cement displayed a higher strength [47,1]. Therefore, normally it is assumed that the strength of unhydrated cement grains is higher than the strength of the surrounding paste or cement gel. Obviously, the existence of hard unhydrated cement particles and microcracks influences the strength of the cement paste significantly. Plastic theory is applied in the analysis. We assume that, at failure, it is difficult for the yield line to go through the hard unhydrated cement particles. Sliding surfaces are formed around the unhydrated cement particles, and the yield line will proceed around the unhydrated cement grains.

Concrete may be regarded as a two phase composite: aggregates embedded in the hardened cement paste.

Little is known about the properties of cement paste both in compression and in tension, even though it is one of the main components of concrete.

It is also an established fact that microcracks exist in the cement paste, even prior to the application of load.

The bond between aggregates and cement paste is normally the weakest part in concrete and is even more weakened by microcracking in the interfacial zone. Bond cracks might be formed prior to and as well as during the process of loading.

The failure in concrete, based on these facts, may be described in the following way. Under a certain load, sliding failure occurs in the cement paste. When the yield line runs into an aggregate particle, it will follow the path where bond cracks already exist and pass around the aggregate particle since these particles normally are stronger than cement paste. Sometimes, because of lamination of the aggregates the failure will go through the aggregates. Hence, the addition of

aggregates displaces the yield line to another steeper position than that formed in pure cement paste.

A micromechanical model simulating the sliding failure of cement paste and concrete is proposed based on the microstructure of cement paste and concrete. The advantages of the micromechanical model are obvious. Firstly, the failure mechanism may be closely related to the composition and the structure of the material itself. Secondly, new physical information may be gained by means of the model. The parameters in the model are still empirically estimated, but with strong theoretical background. Qualitative estimation of the failure is possible. Thirdly, the principles of the model can be extended to different cases with small modifications.

It should be emphasized that the failure of concrete both in tension and in compression is often considered to be governed by growth of microcracks in what is termed Mode I in fracture mechanics (tensile mode). As pointed out in [93,1], this is probably due to the fact that sliding failure in cement paste is very difficult to observe in thin section analysis. Further, in concrete failure with low confining pressure where the strains are highly localized, a sliding failure line may be difficult to distinguish from a mode I crack because of the crack opening between the hard unhydrated cement particles resulting from the sliding around these particles.

It should be noted that what the model in this paper can predict is the peak value determined in a test. To describe the softening, further assumptions must be made. Softening is not considered in this paper.

The results obtained by the model are compared with the available test results. The comparison shows that the micromechanical model proposed here can predict the failure mode fairly well, and the estimation of the load carrying capacity of cement paste and concrete specimens is in a relatively good agreement with the experimental results.

II. REVIEW

In this section, some general information about hardened cement paste and concrete, and some basic assumptions and formulas in plastic theory are reviewed briefly.

2.1 Composition and structure of hardened cement paste

Cement paste is made by mixing cement and water. The hydration of cement in water causes the formation of a complex cement gel, and thus we get hardened cement paste.

One hypothesis about the hydration process of cement proposes that the hydration of cement proceeds by a reduction in the size of the cement particles, and the hydrated cement bonds firmly to the unhydrated cement grains. However, how the hydration propagates in detail and in what way the bond works are not certain yet. For normal cement, complete hydration is difficult, if not impossible, to achieve under the normal curing conditions. Therefore, an amount of unhydrated cement grains remains in the hardened cement paste even long time after casting.

The structure of hardened cement paste is highly irregular and largely amorphous. On a microscopic scale, the hardened cement paste consists primarily of the so called C-S-H particles (CaO, SiO_2, H_2O) and calcium hydroxide. This is a gel termed the cement gel. Further there are some other minor components, grains of unhydrated cement and also an extensive network of capillary pores which may be dry or filled or partly filled with water. Within the cement gel, so called gel pores exist.

Details about the composition and structure of hardened cement paste can be found in [47,1][58,1] and other related books and articles.

2.2 Strength of hardened cement paste

From the structure of the hardened cement paste, it can be seen that the strength of cement paste depends mainly on: 1) the strength of the cement gel; 2) the bond between the cement gel and the unhydrated cement grains; 3) the capillary porosity.

The bonds responsible for the strength of the cement gel are normally considered to be a mixture of chemical bonds and van der Waals bonds (attractive forces between electrically neutral atoms or molecules) of which the relatively stronger hydrogen bonding is an essential part.

Most researchers agree that the capillary pores play a vital role in the determination of the strength of cement paste. Empirical formulas are proposed relating the strength with the capillary or total porosity. Powers postulated that the strength of hardened cement paste is a function of the gel/space ratio, i.e. the ratio of the volume of gel to the total available space [58,1]. Even though this kind of empirical formulas comply well with test results, they do not, as pointed out by many investigators, cover other factors which are also influential on the strength of hardened cement paste, such as the morphology of the products of hydration, the shape and the distribution of pores, the unhydrated cement particles and the micro cracking state, etc.

Approaches based on fracture mechanics have been introduced to find the relationship between the strength and the microstructure of cement paste. A review on this is given in [83,1].

2.3 Bond

Besides the bonds responsible for the strength of the cement gel, in cementitious composite materials other categories of bond exist:

(1) bond between the unhydrated cement grains and cement gel.

(2) bond between aggregates and hardened cement paste.

The true nature of bond has not been fully understood yet. It is commonly believed that, for bond(1), there are mainly two contributions, i.e. (a) chemical bond; (b) physical attraction due to van den Waals forces. Bond(2) results primarily from the combination of mechanical interlocking of the hydrated cement paste with the aggregate surface and the van der Waals forces between them. The bond due to chemical reactions between the aggregates and cement paste may probably be disregarded in most cases.

The unhydrated cement grains are those left over when the process of hydration can not proceed any more. One hypothesis about the hydration process suggests that the C-S-H particles grow from the unhydrated cement particles. Thus, it can be imagined that the bond between these unhydrated cement particles and the cement gel will be rather strong, if microcracks around the grains are not present.

The mechanical interlocking forces and van der Waals forces between aggregates and cement gel are normally relatively weak compared with the strength of the cement gel and the strength of the aggregates. Hence, the bond between aggregates and hardened cement paste might be considered the weakest part in normal strength concrete.

2.4 Coulomb and modified Coulomb material

Many hypotheses are proposed to describe the failure conditions for concrete. Among them the most commonly used ones are the Coulomb criterion and the modified Coulomb criterion.

Two failure modes need to be distinguished, one is sliding failure, and another separation failure. In sliding failure, displacements have components parallel to the rupture surface. For materials with non zero angle of friction, the sliding is accompanied by a displacement away from the rupture surface. In separation

failure, the displacement is perpendicular to the rupture surface.

2.4.1 Failure criteria in τ-σ space

The sliding failure condition in τ-σ space according to the Coulomb criterion is

$$|\tau|=c-\mu\sigma \qquad (2.4.1.1)$$

Here, τ is the shear stress on the rupture surface, σ the normal stress, positive as tension, c the cohesion of the material, and μ the coefficient of friction.

A material complying with the failure condition (2.4.1.1) is called a Coulomb material.

The modified Coulomb criterion combines the Coulomb sliding failure criterion with a tension cut off. Separation failure occurs when the tensile stress σ at a section exceeds the tensile strength f_t. The condition for separation failure is:

$$\sigma=f_t \qquad (2.4.1.2)$$

A material complying with the failure conditions (2.4.1.1) and (2.4.1.2) is called a modified Coulomb material.

The failure conditions for a modified Coulomb material are depicted in Fig.-2.4.1. Since the stress states dealt with in this paper are mainly compression states, it is convenient to take σ positive in compression and negative in tension as shown in Fig.2.4.1.

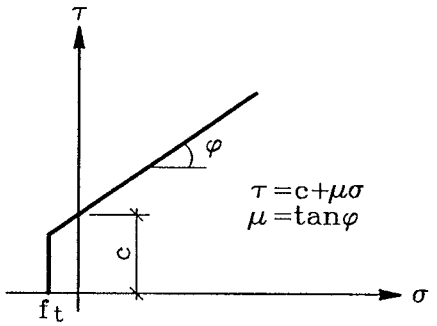

Fig.2.4.1 Failure conditions in τ-σ space for modified Coulomb materials

For normal strength concrete, a frictional angle $\varphi=37^\circ$, and correspondingly a coefficient of friction $\mu=\tan\varphi=0.75$, yields fairly good agreement between the

prediction of load carrying capacity and test results.

2.4.2 Failure criteria in principal stress space

By a simple transformation from τ-σ space to principal stress space, details see [84,1], the failure criteria for modified Coulomb materials in principal stress space are found to be:

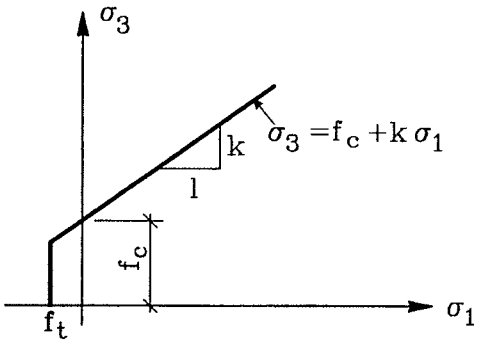

Fig.2.4.2 Failure conditions in σ_1-σ_3 space for modified Coulomb materials

sliding failure:

$$\sigma_3=f_c+k\cdot\sigma_1 \tag{2.4.2.1}$$

separation failure:

$$-\sigma_1=f_t \tag{2.4.2.2}$$

where

$$f_c=\frac{2c\cdot\cos\varphi}{1-\sin\varphi}=2c\cdot\tan(\frac{\pi}{4}+\frac{\varphi}{2}) \tag{2.4.2.3}$$

$$k=\frac{1+\sin\varphi}{1-\sin\varphi}=\tan^2(\frac{\pi}{4}+\frac{\varphi}{2}) \tag{2.4.2.4}$$

σ_1 and σ_3 are the minor and major principal stress, respectively. Note that $\sigma_1<\sigma_3$ and both are positive as compression.

The failure conditions in principal stress space are shown in Fig.2.4.2.

For normal strength concrete with the friction angle $\varphi=37°$, we have k=4 and $c=f_c/4$.

2.4.3 Dissipation in yield lines according to the theory of plasticity

In the theory of plasticity, failure may take place by the formation of a yield surface or, in plane problems, a yield line. A yield line is a line of discontinuity in displacements. The relative displacement u between two rigid parts separated by a yield line forms an angle α with the yield line as shown in Fig.-2.4.3.

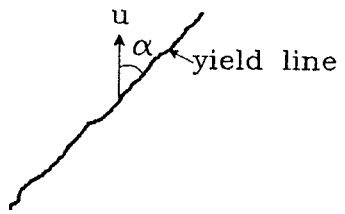

Fig.2.4.3 Yield line showing relative displacement between two rigid parts

For a modified Coulomb material in plane problems, the dissipation per unit length of the yield line, details see [84,1], is:

in plane strain state:

$$W_i=\frac{1}{2}f_c u(1-\sin\varphi) \qquad (\alpha=\varphi) \qquad (2.4.3.1)$$

$$W_i=\frac{1}{2}f_c u(1-\sin\alpha)+\frac{\sin\alpha-\sin\varphi}{1-\sin\varphi}f_t u \qquad (\alpha\geq\varphi) \qquad (2.4.3.2)$$

in plane stress state:

W_i is the same as (2.4.3.2) with no restrictions on α.

In plane strain state with $\alpha=\varphi$, the formula for the dissipation can be rewritten as

$$W_i=cu\cos\varphi \qquad (2.4.3.3)$$

where

$$c=f_c\frac{1-\sin\varphi}{2\cos\varphi}$$

For a material with $\varphi=0$, we have $\alpha=0$ in a plane strain state and

$$W_i=\frac{1}{2}f_c u \qquad (2.4.3.4)$$

2.4.4 Failure patterns according to the theory of plasticity

Upper bound solutions according to the theory of plasticity require geometrically possible yield line patterns. For cylinder or prism specimens under uniaxial and triaxial compression such patterns are shown in Fig.2.4.4.

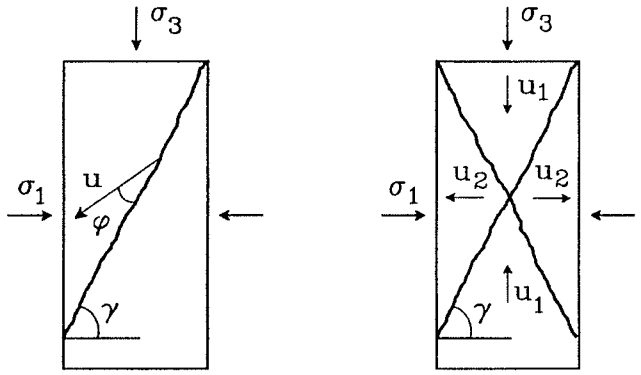

Fig.2.4.4 Yield lines in cylinders or prisms

For a Coulomb material or a modified Coulomb material with a tension cut off in uniaxial compression ($\sigma_1=0$), the upper bound solution yields $\sigma_3=f_c$ and $\gamma=\pi/4+\varphi/2$ for both failure patterns. The result is of course an exact plastic solution.

The same failure patterns may be used for specimens in triaxial compression states. The result is $\gamma=\pi/4+\varphi/2$ and $\sigma_3=f_c+k\sigma_1$, cf. formule (2.4.2.1). Notice the large effect of a side pressure.

With $\varphi=37°$, we get $\gamma=63.5°$ and $\tan\gamma=2$, i.e. the inclination of the yield line will be h/b=2, where h is the vertical projection and b the horizontal projection of the yield line, respectively.

III. Micromechanical modelling of shear failure of cement paste in compression

Since one of the essential ingredients of concrete and mortar is cement paste, the shear behavior of hardened cement paste is treated first.

3.1 Observations from experiments

Not so many tests on hardened cement paste specimens both in compression and in tension have been reported. Cement paste has a very high shrinkage, so the curing and the testing is difficult, and the scatter of the results obtained from the experiments is rather large.

A series of triaxial tests on cement paste cylinder specimens, as well as concrete cylinder specimens, was carried out in the laboratory at the Department of Structural Engineering, Technical University of Denmark [92,1][95,1]. Details about the test set up and the procedures of testing can be found in [92,3].

Fig.3.1.1 shows the results of the triaxial tests for cement paste specimens with different uniaxial compressive strengths. The specimen was a 10cm×20cm cylinder. In the figure, σ_1 is the lateral confining pressure around the cylinder at failure, σ_3 the longitudinal or axial compressive pressure at failure, and f_c the uniaxial compressive strength of the cement paste measured on standard cylinder specimens.

It can be seen that when the lateral confining pressure is close to zero, the axial stress at failure is close to the uniaxial compressive strength, which is quite natural. With an increase of the lateral confining pressure σ_1, the longitudinal compressive stress σ_3 is increased correspondingly but with a decreasing rate. From a certain level of σ_1, the relationship between σ_1 and σ_3 may be described by a straight line with the inclination of 1. If the cement paste is considered as a Coulomb material, this means that, in triaxial stress states with relative large confining pressures, hardened cement paste has the frictional angle $\varphi=0$ and

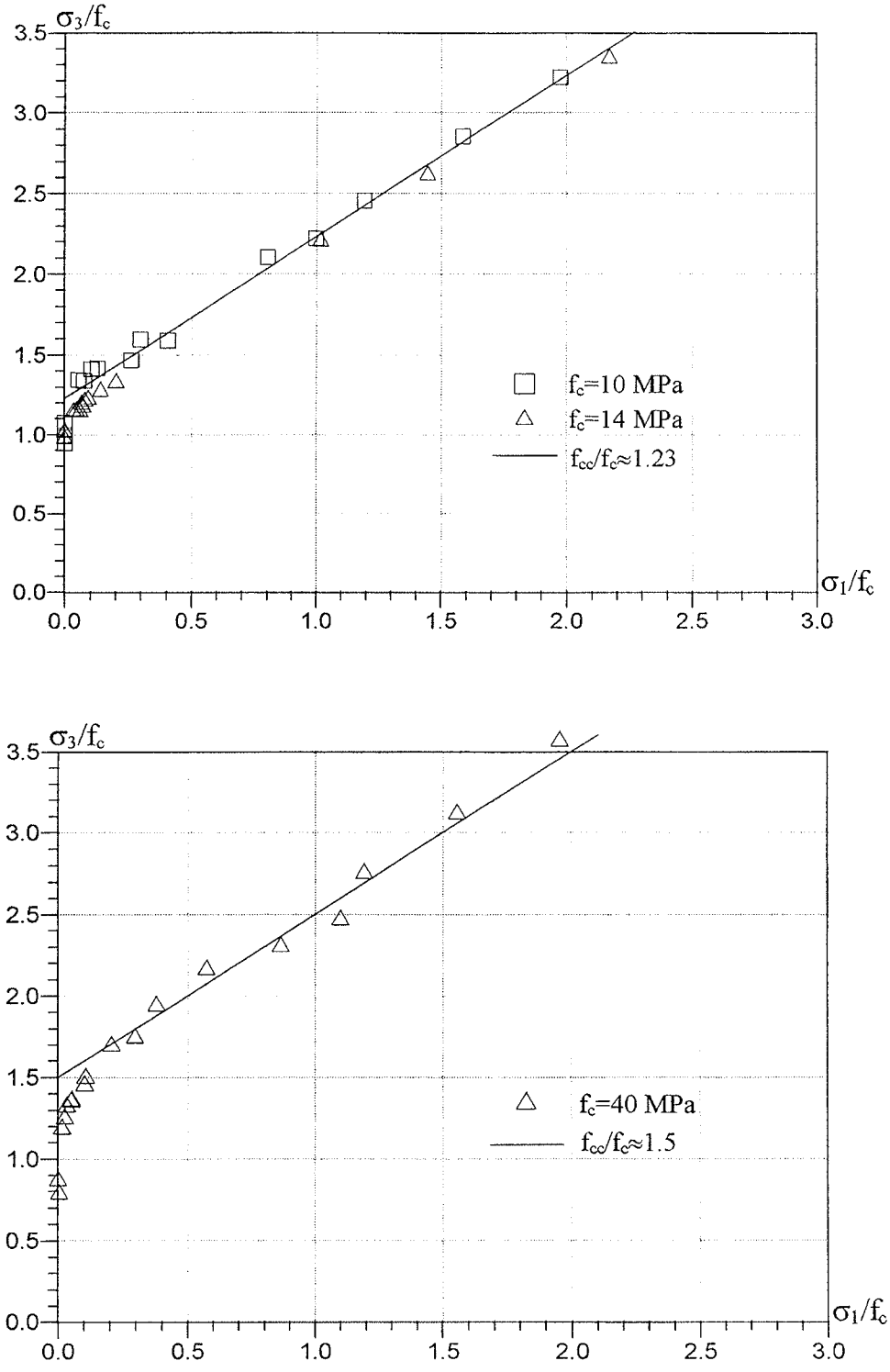

Fig.3.1.1 Triaxial test results for different f_c [92,1][95,1]

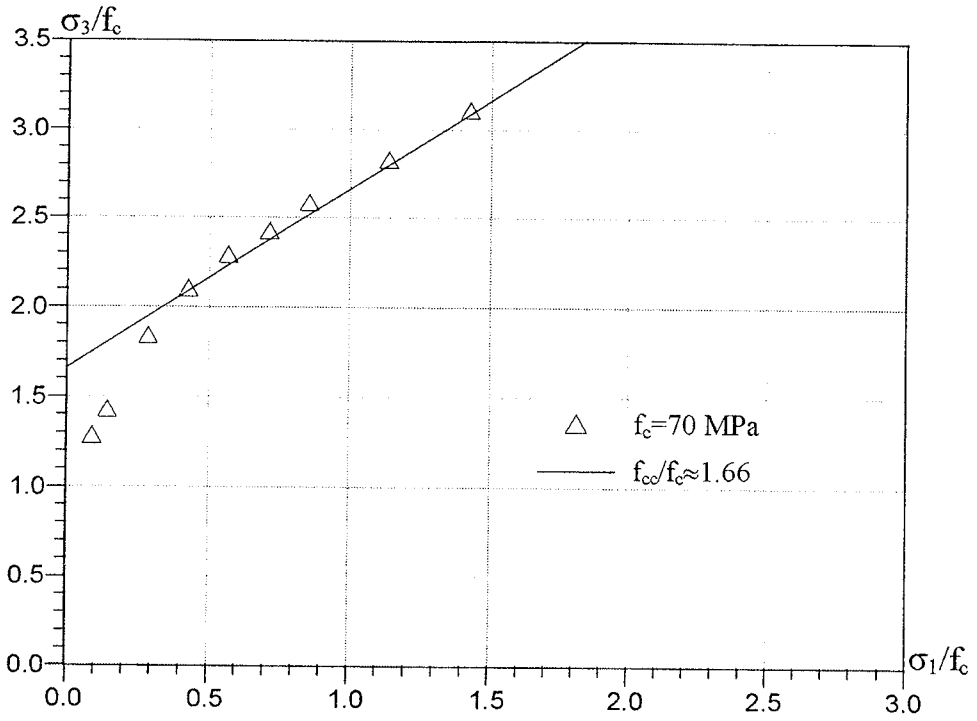

Fig.3.1.1 (continued)

Note: Tests for f_c=70 are from [92,1], the rest are from [95,1]

therefore k=1, cf. formula(2.4.2.1). The point where the extension of the linear part of the curve intersects the σ_3-axis is denoted f_{cc}, which is the apparent uniaxial compressive strength in triaxial stress states. It appears that f_{cc} is higher than the true uniaxial compressive strength f_c. Detailed discussion on f_{cc}, see the following sections.

3.2 Unhydrated cement particles and microcracking

At the microscopic level, hardened cement paste consists, as mentioned before, mainly of cement gel with gel pores, unhydrated cement grains, and capillary pores. The strength of the unhydrated cement grains is estimated to be much higher than that of the hydrated cement gel. If the cement gel and the capillary pores are taken as one phase for convenience, a phase which is referred to as the hydration product in the following, the hardened cement paste can be imagined as a material with hard unhydrated cement grains embedded in a softer matrix

of hydration products.

The physical properties of the unhydrated cement grains and the hydration product are obviously different. During the process of hydration and subsequent loading, discontinuity between these two phases will occur. It has been observed that microcracks do exist, even prior to loading, around the unhydrated cement grains due to volume changes during hydration, shrinkage because of loss of water, etc. This implies that the hardened cement paste is in a state of microcracking even before the application of load.

What here is termed microcracks are not necessarily visible even in thin section analysis. It can be a flaw which is weaker than the surrounding cement paste or a weak bond between the unhydrated cement grain and the hydration product.

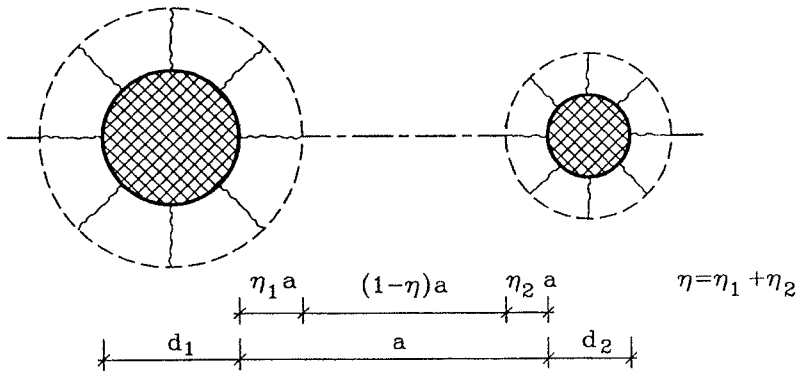

Fig.3.2.1 Microcracks around the unhydrated cement grains in the model

The model developed in this paper is a plane model. The transformation to a plane model will be done by considering a thin slice of the material with a thickness being of the order of magnitude of the size of the unhydrated cement grains.

Since shrinkage will be resisted by the unhydrated cement grains, we will assume that the microcracks, in the above meaning, are located around the unhydrated cement grains as shown in Fig.3.2.1.

In thin section analysis it is observed that the visible microcracks form a pattern with one or more cracks running between the unhydrated cement grains. Therefore, the description in the model of the cracking state in Fig.3.2.1 is highly idealized. If the model is deemed successful, the observed width and length of the visible microcracks in different cement pastes should be correlated to the microcracks of the model. At present the available data, however, makes such a correlation impossible to perform, cf. section 4.8.

The average extension of the microcracks is represented by the average length of the microcracks between the hard particles, and is denoted as ηa, where a is the mean clear distance between two adjacent unhydrated cement grains. The parameter η may be termed the damage factor due to microcracking.

Part of the microcracking before failure may be due to the loading process itself. This part of the microcracking is assumed to be included in the damage factor η.

To simplify the model the real particle system of unhydrated cement grains is transformed to an ideal one having particles with identical form and giving rise to the same volume ratio of unhydrated cement grains as in the real system.

The particle size arrived at in this way is called the average particle size. We will assume the particles to be spherical or cubic whatever is convenient in the calculations.

The average size of unhydrated cement grains and the average distance between them are related to the hydration degree of the components of the cement paste. This will be discussed in detail in Appendix 1.

3.3 Micromechanical modelling of shear failure of cement paste in compression

3.3.1 Shear failure condition in τ-σ space according to plastic theory

As observed in the experiments, sliding takes place in the specimens of cement paste at failure [92,1][95,1]. In terms of plastic theory, this means that a shear failure occurs along a yield line, i.e. a line of displacement discontinuity. Along the failure surface we have a shear force V and a normal force N.

The hardened cement paste, as stated previously, at the microscopic level, may be regarded as a material with unhydrated cement particles embedded in a matrix of the microcracked hydration product. Since the unhydrated cement grains are estimated much harder than the hydration product, it is preferably for the yield lines to go around the hard grains in a zig-zag form instead of passing through the hard particles, and at the same time to choose the least energy demanding route.

An infinite number of yield lines in the microcracked composite are possible. However, to simplify calculations, only straight yield lines are considered. These are assumed either to pass around the unhydrated cement grains the number of which is determined by their volume ratio in the composite or to go through only uncracked cement paste. In the last mentioned case the strength is of course the strength of the uncracked virgin material without any influence from the unhydrated cement grains.

Further, we will only consider an "average yield line" passing the unhydrated cement grains. By this we mean that the average depth of the hard particles along the yield line is half of their radii or quarter of their diameters.

When we are dealing with a yield line passing a number of hard particles, an inclined sliding surface is bound to form in front of every hard particle. From triaxial tests it is observed that cement paste is extremely ductile when subjected to triaxial stress states. The same ductility may be assumed to be present in the local sliding failure in front of the hard particles. Sliding displacements take place along the inclined surfaces, and this will cause a separation displacement

at the top and at the rear of the hard cement grain. Since cement paste is very sensitive to tensile displacements, microcracks will probably be formed at the top and at the rear of the cement particle. The loading will undoubtedly increase the microcracking near the hard particles. As mentioned before, this increase in microcracking is included in the damage factor η. Thus a yield line pattern of shear failure is postulated as shown in Fig.3.3.1.1. The thickness is taken to be an unit of length. To simplify the model, the unhydrated cement grains are as previously mentioned assumed to have the same size, and here to be square shaped. Further they are assumed to be evenly distributed in the matrix of the hydration product.

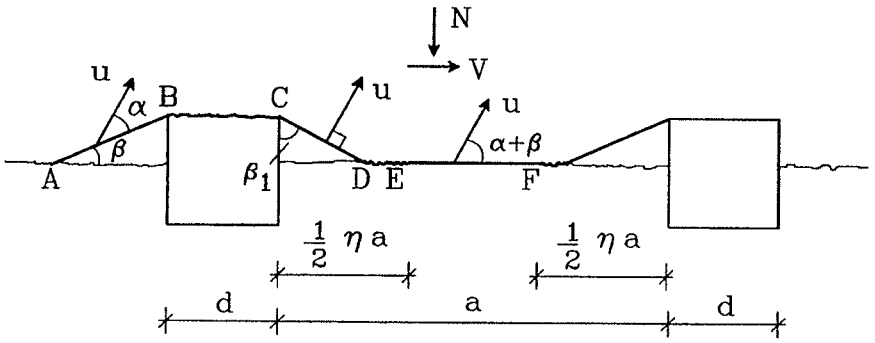

Fig.3.3.1.1 Yield line pattern of shear failure in cement paste

In the figure, a is the average clear distance between two adjacent unhydrated cement particles, d the average size of the hard particles, β the angle of the sliding surfaces with the yield line in front of the hard cement grains, and β_1 the angle determining the inclination of the cracks formed at the rear of the hard grains. The relative displacement u is shown to form an angle α with the sliding surface AB.

The problem we are dealing with here may be considered as a plane strain problem. Since we are dealing with compression states, the angle between the relative displacement and the yield surface is $\alpha=\varphi$. If we hold the observation that the friction angle of hardened cement paste under triaxial stress states is zero, then $\alpha=\varphi=0$, meaning that the sliding displacement is parallel to the sliding surface AB. In this way, the " apparent friction angle " observed in the experiments is actually originating from the inclination of the sliding surfaces

in front of the unhydrated cement grains. When the lateral confining stress is relatively small, the sliding surface is steeper, which results in a larger "apparent friction angle ". When the lateral confining stress gets larger, the sliding surface in front of the hard particles becomes flatter, thus a smaller " apparent friction angle " is observed in the tests. When the confining stress comes to a certain level, the effect of the hard unhydrated cement particles will disappear, and the sliding surface will be formed outside the hard particles in the direction of the shear force, thus a zero friction angle is observed.

The crack along CD is caused by the separation displacement originating from the sliding displacement along the surface AB during loading. For simplicity, we assume that this crack is perpendicular to the direction of the sliding displacement, which results in $\beta+\beta_1=90^\circ$. Thus, the dissipation along CD is zero if the tensile strength along the crack is neglected. We arrive at the same result if we assume that the part CD of the yield line pattern will undergo brittle tensile failure, the dissipation of which will disappear before the whole yield line pattern has been formed. In other words CD is considered as a part of the load induced microcracks. Hence, the yield line pattern becomes as shown in Fig.3.3-.1.2.

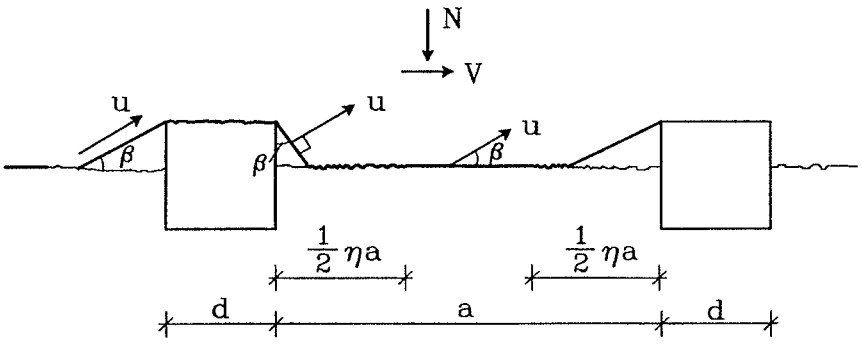

Fig.3.3.1.2 Yield line pattern of shear failure in cement paste with $\alpha=\varphi=0$

Microcracking reduces the strength of cement paste. Little is known about how much this reduction might be. Due to the lack of knowledge and for convenience, it might be assumed that the tensile strength and the cohesion along the microcracks in the cement paste are reduced to such an extent that their contribution to the sliding resistance can be disregarded. Thus, the dissipation

along the microcracks is zero both in the case where the displacement is perpendicular to the yield line and in the case where it has a component along the yield line.

Under the assumptions above, an equivalent failure pattern, i.e. a failure pattern with practically the same dissipation as that in Fig.3.3.1.2, is obtained as shown in Fig.3.3.1.3.

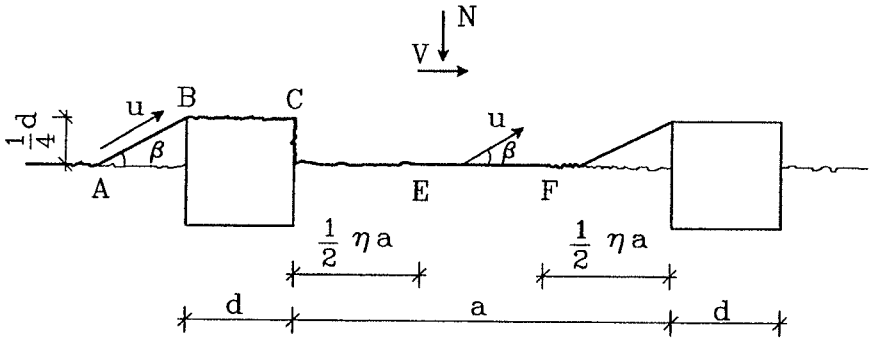

Fig.3.3.1.3 An equivalent yield line pattern of shear failure in cement paste

It is obvious that the compressive strength of the cement paste in an unmicrocracked state will be higher than the standard uniaxial compressive strength which is measured while the cylinder specimens are influenced by microcracking. To distinguish these strengths, we denote the uniaxial compressive and tensile strength of cement paste as f_c and f_t respectively, and the compressive and tensile strength for unmicrocracked cement paste as f_{cc} and f_{tt} respectively. In triaxial compression tests, as mentioned previously, the microcracking does not influence the strength when the confining lateral pressure gets sufficiently large. Hence, it can be envisaged that the material at this stage behaves as unmicrocracked cement paste and has nominal uniaxial compressive and tensile strength equal to f_{cc} and f_{tt} respectively. These strengths are termed the triaxial compressive and tensile strengths respectively. The triaxial compressive strength therefore may be used to evaluate the compressive strength of unmicrocracked cement paste f_{cc}. The value of f_{cc} can be deducted from the triaxial tests of cement paste by determining the intersection point of the extension of the straight line we found in the range of large lateral confining pressures with the σ_3-axis as shown in Fig.3.1.1.

The micro cracks formed by shrinkage etc. are assumed radiating from the unhydrated cement particles into the hydration product. Since the sliding surface AB forms an angle with the direction of the micro cracks, the strength properties along AB are estimated to be little influenced by the microcracking.

According to the theory of plasticity under the assumption of a modified Coulomb material, the internal dissipation along the yield line shown in Fig.3.3.1.3 is found to be:

$$W_I = u \cdot \frac{1}{2} f_{cc} \cdot L_{AB} + u \cdot [\frac{1}{2} f_{cc}(1 - \sin\beta) + f_{tt} \cdot \sin\beta] \cdot L_{EF} \qquad (3.3.1.1)$$

where

$$L_{AB} = \frac{1}{4} \frac{d}{\sin\beta}$$

$$L_{EF} = (1 - \eta)a$$

η - the damage factor due to microcracking

The external work

$$W_E = V \cdot u\cos\beta - N \cdot u\sin\beta$$

V being the shear force and N the normal force along a length of a+d.

Since

$$\sigma = \frac{N}{a+d}$$

$$\tau = \frac{V}{a+d}$$

we have

$$W_E = u \cdot (\tau\cos\beta - \sigma\sin\beta)(a+d) \qquad (3.3.1.2)$$

The work equation $W_I=W_E$ yields

$$\tau=\frac{1}{8}f_{cc}\frac{d}{a+d}\frac{1}{\sin\beta\cos\beta}+[\frac{1}{2}f_{cc}(1-\sin\beta)+f_{tt}\sin\beta](1-\eta)\frac{a}{a+d}\frac{1}{\cos\beta}+\sigma\tan\beta \tag{3.3.1.3}$$

To calculate the ratio d/a+d, consider Fig.3.3.1.4 which shows a plane section through the cement paste. In the figure it has been assumed that the unhydrated cement grains are spherical with diameter d.

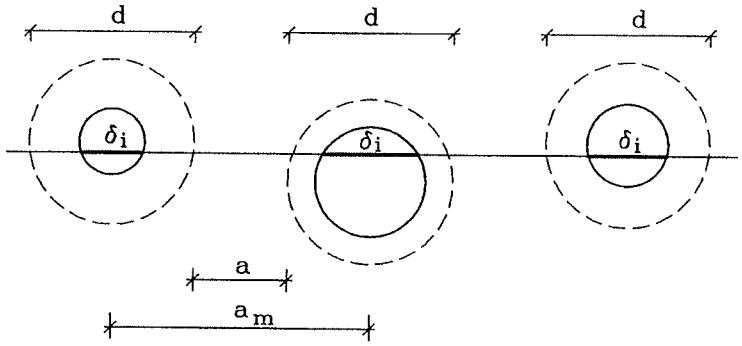

Fig.3.3.1.4 A plane section through the cement paste

The plane section cuts the spheres along circles shown with full line, while the spheres are shown with dotted line. By drawing a line, a number of particles will be cut. The intercept length of each individual particle is denoted by δ_i. According to a well-known theorem in stereology [70,2] which states that the volume ratio, area ratio and linear ratio are equal for a randomly distributed particle system, the sum of δ_i will be

$$\frac{\sum\delta_i}{L}=m' \tag{3.3.1.4}$$

where m' is the volume ratio of hard particles and L the length of a straight line in the plane section considered.

The mean intercept length δ_i of particles according to [70,2] can be expressed by

$$\bar{\delta}_i=\frac{4\bar{V}}{\bar{S}} \tag{3.3.1.5}$$

Here $\bar{V}$ is the mean volume of particles and $\bar{S}$ the mean surface area of particles. For a spherical particle, the mean intercept length becomes

$$\bar{\delta}_i = \frac{2}{3}d \tag{3.3.1.6}$$

Therefore

$$\frac{\sum \delta_i}{L} = \frac{N \cdot \frac{2}{3}d}{L} = m' \quad \Rightarrow \quad N = \frac{3}{2}\frac{L}{d}m' \tag{3.3.1.7}$$

N being the number of particles cut by the line.

The mean distance between the centers of the spheres a_m is

$$a_m = \frac{L}{N} = \frac{2}{3}\frac{d}{m'} \tag{3.3.1.8}$$

leading to

$$\frac{d}{a+d} = \frac{d}{a_m} = \frac{3}{2}m' \tag{3.3.1.9}$$

If the particles are assumed to be cubic, the same values of mean intercept length $\bar{\delta}_i$ and ratio of d/(a+d) will be obtained.

The volume ratio of hard unhydrated cement particles m′ is closely connected with the hydration degree of cement, fly ash and micro silica, see Appendix 1.

Putting eq.(3.3.1.9) into eq.(3.3.1.3) yields:

$$\tau = \frac{3}{16}f_{cc}m' \frac{1}{\sin\beta\cos\beta} + [\frac{1}{2}f_{cc}(1-\sin\beta) + f_{tt}\sin\beta](1-\eta)(1-\frac{3}{2}m')\frac{1}{\cos\beta} + \sigma\tan\beta \tag{3.3.1.10}$$

This is an upper bound solution in which β is a variable. The minimum is obtained by differentiation of eq.(3.3.1.10) with respect to β:

$$\frac{d\tau}{d\beta} = 0$$

$$\Rightarrow \frac{\frac{3}{16}f_{cc}m'\frac{2\sin^2\beta-1}{\sin^2\beta}+[\frac{1}{2}f_{cc}(\sin\beta-1)+f_{tt}](1-\eta)(1-\frac{3}{2}m')+\sigma}{\cos^2\beta}=0 \qquad (3.3.1.11)$$

It is possible to find an analytical solution of eq.(3.3.1.11), but the form of the solution is complicated. Hence, a numerical method is applied instead to obtain the solutions for the specific cases.

As stated above, when the lateral confining pressure is large, the shear capacity of the hardened cement paste is not affected by the hard particles and by the microcracking and the apparent friction angle is $\varphi=0$. At this stage, the hardened cement paste may be regarded as a homogeneous modified Coulomb material with the friction angle $\varphi=0$ and the compressive strength f_{cc}. According to the theory of plasticity, for such a Coulomb material, the shear capacity is $\tau_{max.}=0.5f_{cc}$.

Therefore, the shear capacity obtained from the model must satisfy the condition $\tau\leq\tau_{max.}$.

Now the following parameters need to be determined:

1). f_{cc} - triaxial compressive strength of hardened cement paste or compressive strength of unmicrocracked cement paste. Due to the lack of knowledge about the real structure and failure mechanism of cement paste, the value of f_{cc}, at present, can only be empirically determined. Here it will be determined from triaxial tests as explained in section 3.1.

2). f_{tt} - triaxial tensile strength of hardened cement paste or tensile strength of unmicrocracked cement paste. Little is known about the tensile strength of pure cement paste. It seems from [79,1][85,1] that the order of the magnitude of the tensile strength of cement paste is similar to that of concrete or a little higher. Analogous to the expression for tensile strength of concrete according to the Danish code DS 411, $f_{tt}=\sqrt{0.1f_{cc}}$ (f_{cc} in MPa) is used in the calculations.

3). m' - volume ratio of unhydrated cement particles. As stated in the previous

section, complete hydration of cement in the cement paste specimens, fabricated and cured under normal conditions, is difficult, if not impossible. A fraction of cement will remain unhydrated. The degree of hydration for different types of cement is different. What interests us in this paper is the volume ratio of the hard particles which stems from the unhydrated part of cement, fly ash and micro silica, or the hard particles due to other reasons whose strength may be much higher than that of the hydration product. An approximate way to estimate m′ according to the hydration degree of cement, fly ash and micro silica is suggested in Appendix 1.

4). η - damage factor due to microcracking. This is a parameter reflecting the average extent of microcracks in hardened cement paste. At present, the microcracking is only qualitatively known, quantitative measurements of the extent of microcracking being only scarcely reported in literature. In this paper, the value of η, relevant to a certain strength, is determined by the obvious fact that the maximum compressive stress, obtained in the model with zero lateral confining pressure, should be the uniaxial compressive strength f_c.

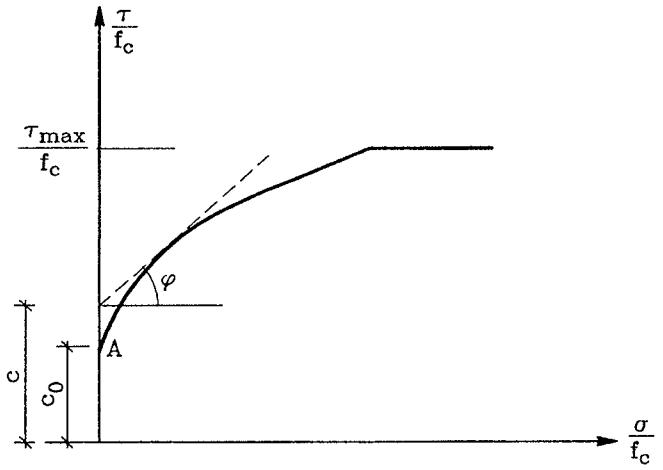

Fig.3.3.1.5 Shear failure condition in τ-σ space

The failure conditions in τ-σ space obtained from the model are shown in Fig.3.3.1.5. A transition part is seen to be present in the failure criterion. The inclination of the tangent line at an arbitrary point is termed the apparent friction

angle at that point, designated by φ, and the point where this line intersects with the τ-axis defines the apparent cohesion c. The point A in the figure indicates the initial cohesion c_0 with the normal stress σ=0.

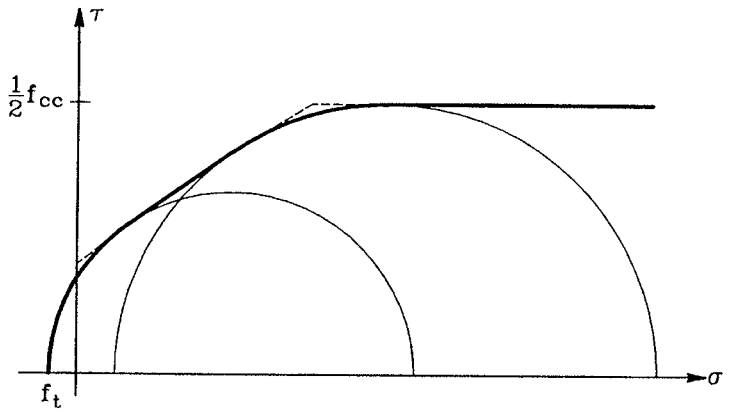

Fig.3.3.1.6 Valid shear failure condition in τ-σ space

For a specific stress state, failure occurs if the Mohr circle determined by theses stresses touches the curve of the failure criterion. In the triaxial compressive stress case, by drawing a Mohr circle which touches both the transition curve and the horizontal line corresponding to $\tau_{max}=f_{cc}/2$, the valid curve for the failure criterion is obtained as shown in Fig.3.3.1.6. The stress states above the valid curve can not be reached. Similarly, by drawing a Mohr circle going through the point $\sigma=-f_t$ on the σ-axis and touching the transition curve might limit the stress states which can be reached.

It is seen that the failure criterion in τ-σ space is composed of three parts determined by two circles and the transition curve obtained from the model, respectively.

These limiting conditions for Coulomb materials with different parameters were studied in [77,1].

3.3.2 Shear failure condition in principal stress space

In the τ-σ space, corresponding to every point on the curve of the failure

criterion, a Mohr circle, which is a tangent to the failure curve, can be drawn as shown in Fig.3.3.2.1. In this way, the corresponding major and minor principal stress at failure are determined by the formulas shown in the figure.

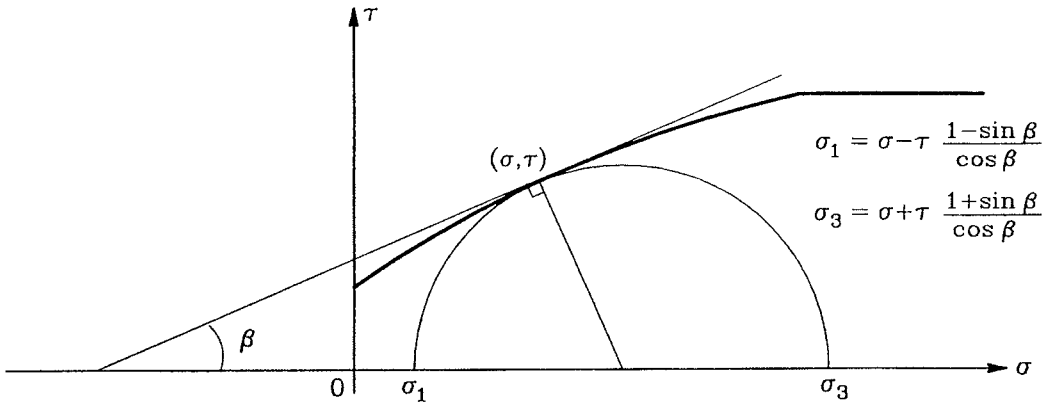

Fig.3.3.2.1 Principal stresses determined from Mohr's circle

As before, σ_1 and σ_3 are positive for compression. The intermediate principal stress σ_2 does not appear in this failure condition.

The type of shear failure condition found in principal stress space is shown in Fig.3.3.2.2.

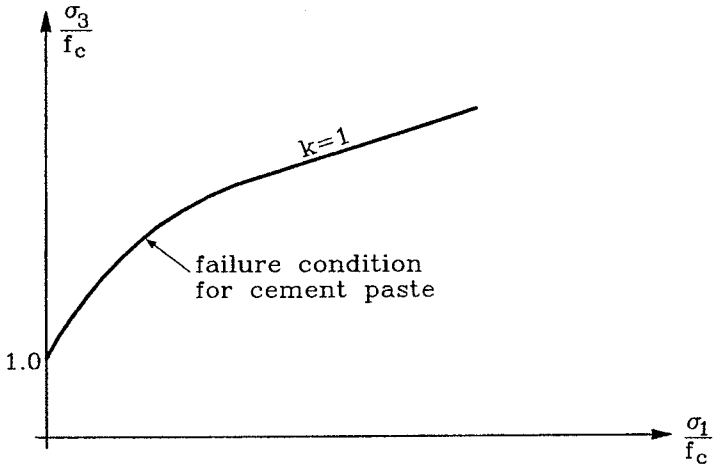

Fig.3.3.2.2 Shear failure condition in principal stress space

3.4 Parameter studies

The influence of the different parameters on the shear resistance of a specific mix of cement paste is evaluated by changing the value of one parameter at one time and by combining several parameters. The values of the parameters applied here are adopted from the test group B010 in [92,1]. The uniaxial compressive strength in these tests were 10MPa.

1). η - the damage factor due to microcracking

This factor reflects the extent of microcracking in hardened cement paste with a specific strength. The cement paste is non microcracked if $\eta=0$, and fully microcracked if $\eta=1$. Normally, $0<\eta<1$. With all the other parameters being the same, the shear failure conditions for cement paste with different damage factors η are shown in τ-σ space and in principal stress space in Fig.3.4.1 and Fig.3.4.2, respectively.

It can be seen that when the confining pressure is relatively small, the damage factor η has a considerable influence on the shear resistance, the cohesion and the apparent friction angle. Obviously, the more the cement paste is microcracked, i.e. the higher value of η, the less strength it will have. But even if the paste is totally microcracked, i.e. $\eta=1$, some initial cohesion still exists. This is due to the sliding resistance around the hard unhydrated cement particles. It should be pointed out once again that a unique value of η may be determined for a specific mix under the condition that $\sigma_3=f_c$ when $\sigma_1=0$.

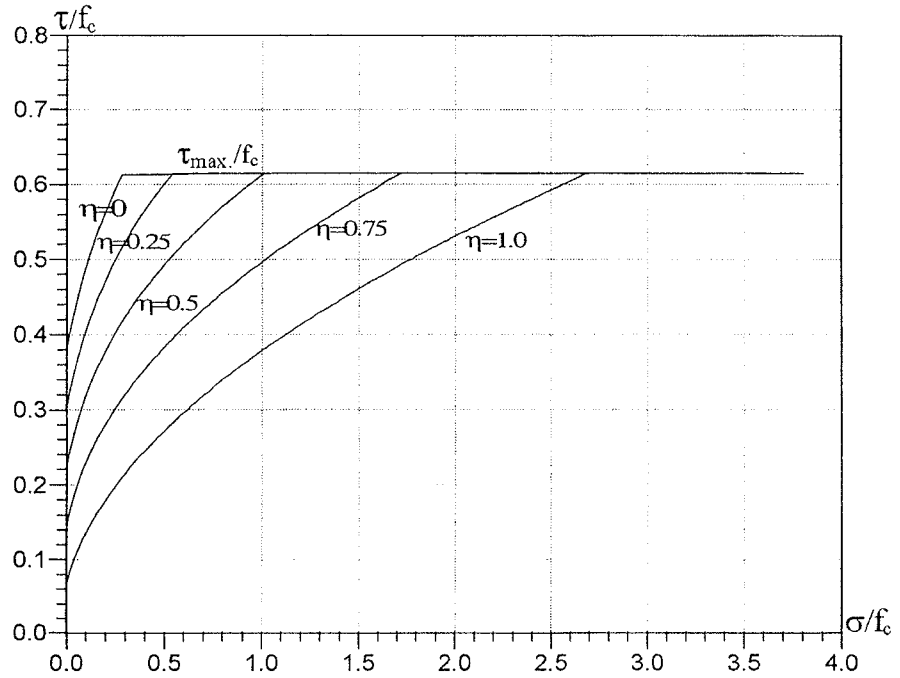

Fig.3.4.1 Shear failure conditions for different η in τ-σ space

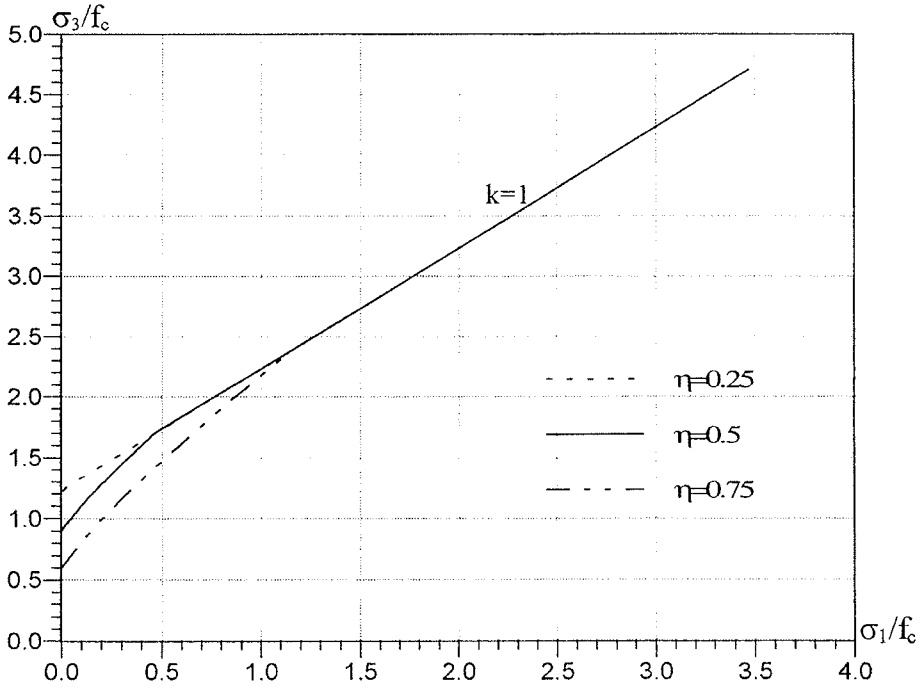

Fig.3.4.2 Shear failure conditions for different η in σ_1-σ_3 space

2). m' - the volume ratio of unhydrated cement particles

This factor reflects the size/distance ratio of the unhydrated cement grains or hard particles in the cement paste. Probably m' and the damage factor η are correlated so that the larger the size of the hard grains, the higher the damage factor. The shear failure conditions in τ-σ space and principal stress space for different m' are depicted in Fig.3.4.3 and Fig.3.4.4.

Increasing the volume ratio of the unhydrated cement grains, the shear resistance becomes greater. The initial cohesion, as well as the uniaxial compressive strength, is influenced by a change of m' to some extent but not as significantly as that caused by the change of η.

3). f_{tt} - triaxial tensile strength of cement paste.

As stated previously, f_{tt} may be regarded as the tensile strength of the unmicrocracked cement paste. The shear failure conditions in τ-σ space and principal stress space for different f_{tt} are depicted in Fig.3.4.5 and Fig.3.4.6.

The figures show that, when f_{tt} is varied from zero to $\sqrt{0.1f_{cc}}$, the initial cohesion is changed considerably, but the general behavior is not altered much, neither is the uniaxial compressive strength. This implies that, in a compressive stress state, the contribution of the tensile strength of the unmicrocracked cement paste to the shear resistance may be ignored, which is of course to be expected.

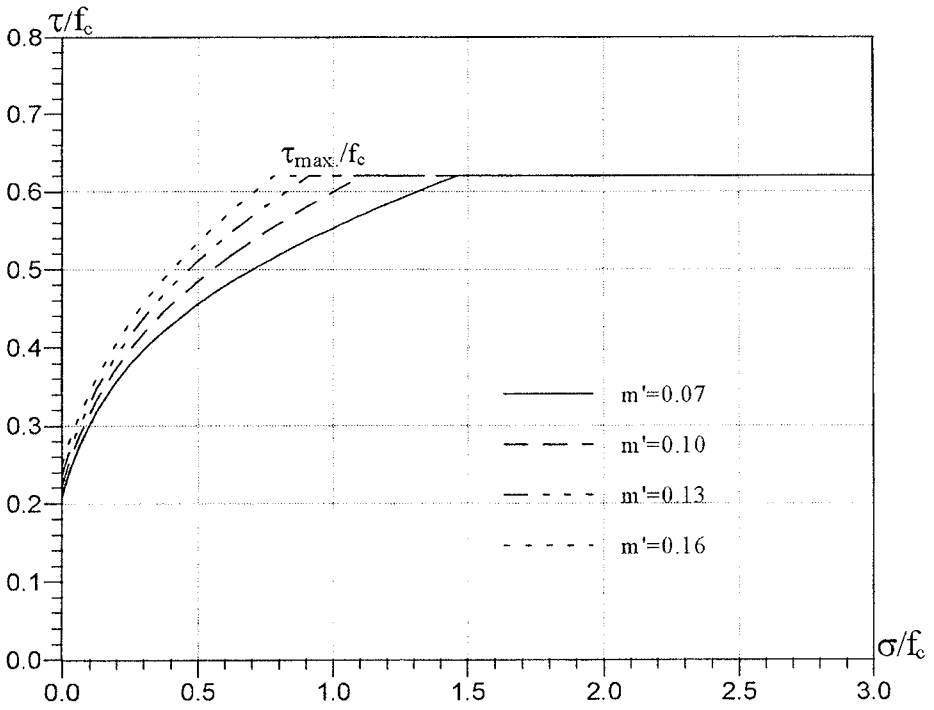

Fig.3.4.3 Shear failure conditions for different m′ in τ-σ space

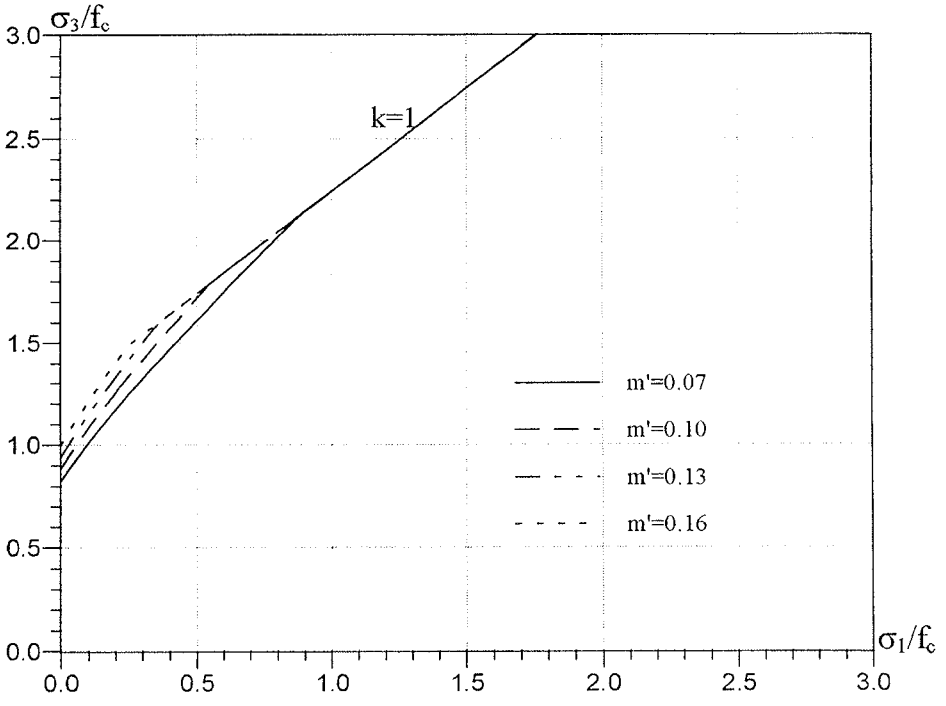

Fig.3.4.4 Shear failure conditions for different m′ in σ_1-σ_3 space

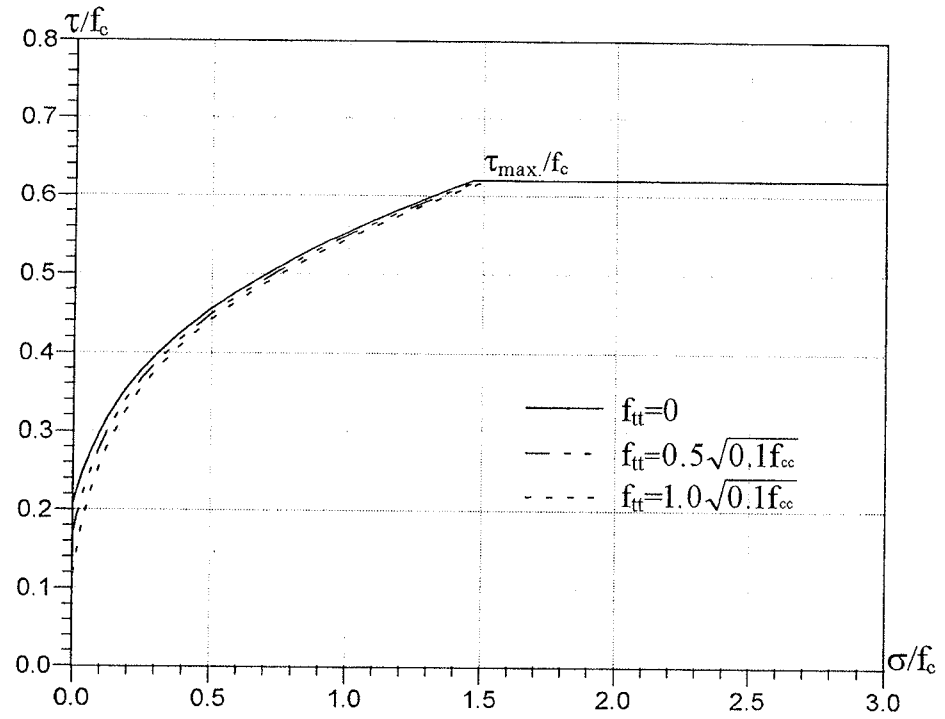

Fig.3.4.5 Shear failure conditions for different f_{tt} in τ-σ space

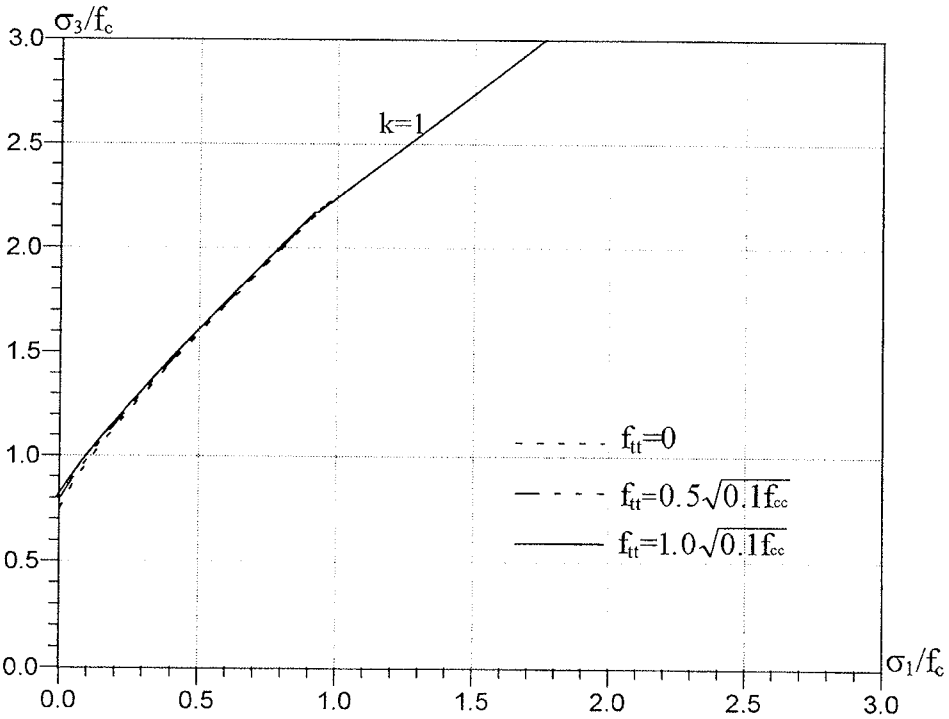

Fig.3.4.6 Shear failure conditions for different f_{tt} in σ_1-σ_3 space

4). Combinations of m′ and η

No quantitative information about the extent of microcracking is available. In the calculation with fixed value of f_{cc}/f_c, η is determined by the condition that $\sigma_3=f_c$ when the lateral confining pressure is $\sigma_1=0$. It is seen that bigger volume ratio of hard particles will give rise to higher microcracking degree in the surrounding cement gel. Based on the condition of constant f_c, η may be determined for different values of m′. The shear failure conditions for different m′ and corresponding η are depicted in Fig.3.4.7 and Fig.3.4.8.

It is seen that in the triaxial compressive stress state, even though the damage factor is increased when the volume ratio of unhydrated cement particles gets higher, the shear resistance is still enhanced. This complies with the observation in [47,1] that cement pastes with a larger portion of unhydrated cement grains will yield higher compressive strengths.

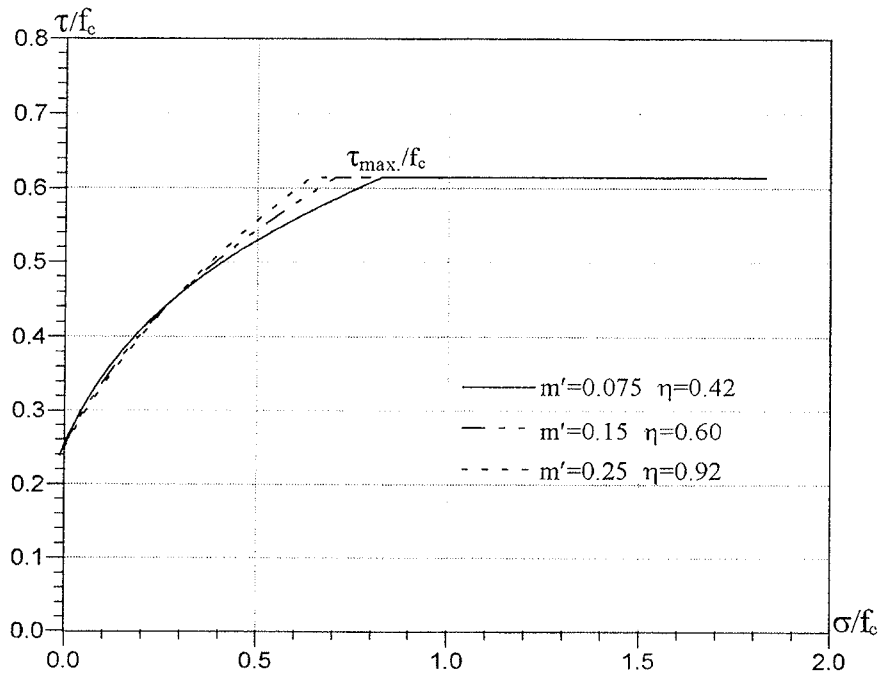

Fig.3.4.7 Shear failure conditions for different m′ and η (constant f_c) in τ-σ space

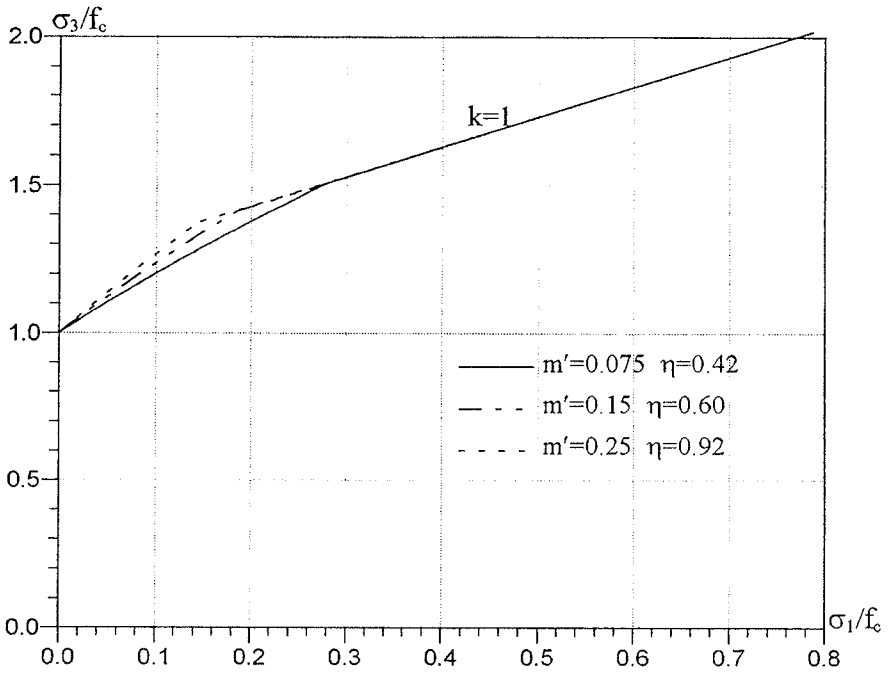

Fig.3.4.8 Shear failure conditions for different m′ and η in σ_1-σ_3 space

5). Combinations of f_{tt} and η

Here f_{tt} is varied while f_c (and f_{cc}) as well as m′ is kept constant, i.e. η is varied at the same time in such a way that f_c is kept constant. Fig.3.4.9 shows the shear failure conditions in τ-σ space.

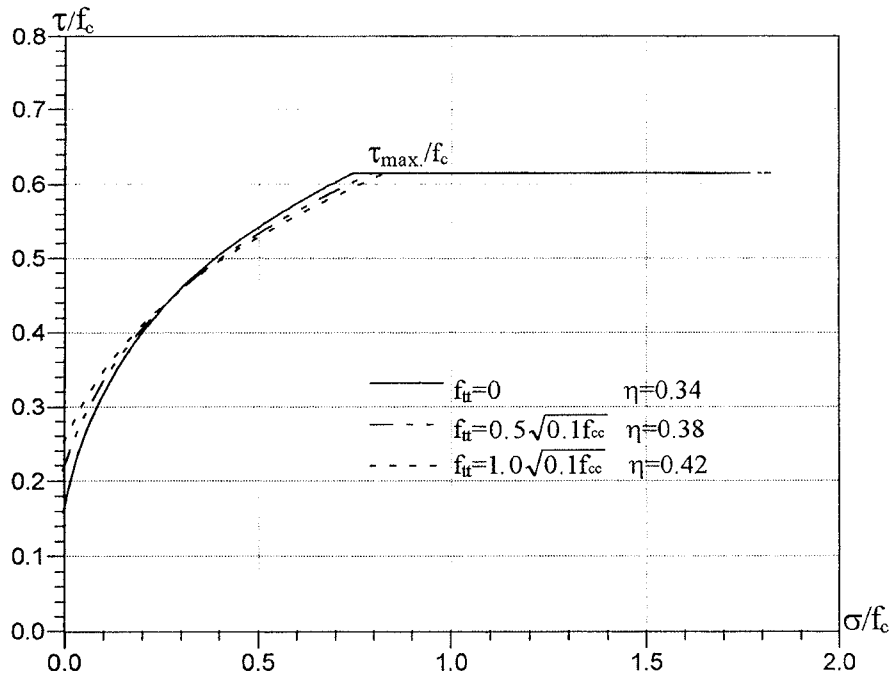

Fig.3.4.9 Shear failure conditions for different f_{tt} and η in τ-σ space

It is seen that for constant f_c the microcracking in the cement paste with a higher tensile strength is more severe than that in a cement paste with a lower tensile strength. According to the calculations, for low confining pressures the shear resistance is smaller in the case of higher tensile strength and at the same time the damage factor is larger. For higher confining pressures the opposite is the case. This indicates that for low confining pressures the effect of increasing damage factor overrides that of increasing tensile strength, and for high confining pressures the opposite is the case.

3.5 Experimental verification

The number of triaxial tests of cement paste specimens is scarce. A systematical test program was carried out at the Department of Structural Engineering, Technical University of Denmark [92,1][95,1]. The test results are studied in detail below.

The volume ratios of hard unhydrated cement particles m′ may be determined by studying the mix design. Details see Appendix 1. For the mixes in the tests, the estimated values of m′ based on the hydration degrees in table A.1 in Appendix 1, are listed in table 3.5.1.

Table 3.5.1 Mix designs and the parameters applied in the calculation

Test group	Cement (kg/m^3)	Fly-ash (kg/m^3)	MS-slurry (kg/m^3)	Water (kg/m^3)	m′	f_c (MPa)	f_{cc}/f_c	η
P20	637	280	-	637	.075	10(14)	1.23	0.29
P40	867	133	120	500	.085	40	1.50	0.42
P070*	1030	-	183	430	.088	70	1.66	0.48

*Note: 1). * results are from [92,1], the rest is from [95,1].*

2). The cement used in both test series is ASTM type III, rapid hardening cement. The degree of hydration at the age of 28 days is estimated, in average, to be m=0.8.

3). The hydration degrees for the hydratable portion of fly ash and micro silica (MS) are estimated to be 0.5 and 0.7, respectively.

4). For test group P20, two values of the uniaxial compressive strength were obtained.

5). The uniaxial compressive strength for test group P070 was deducted from the corresponding triaxial tests. Details see [92,1].

In the table, the ratios of f_{cc}/f_c deducted as shown in Fig.3.1.1, and the damage

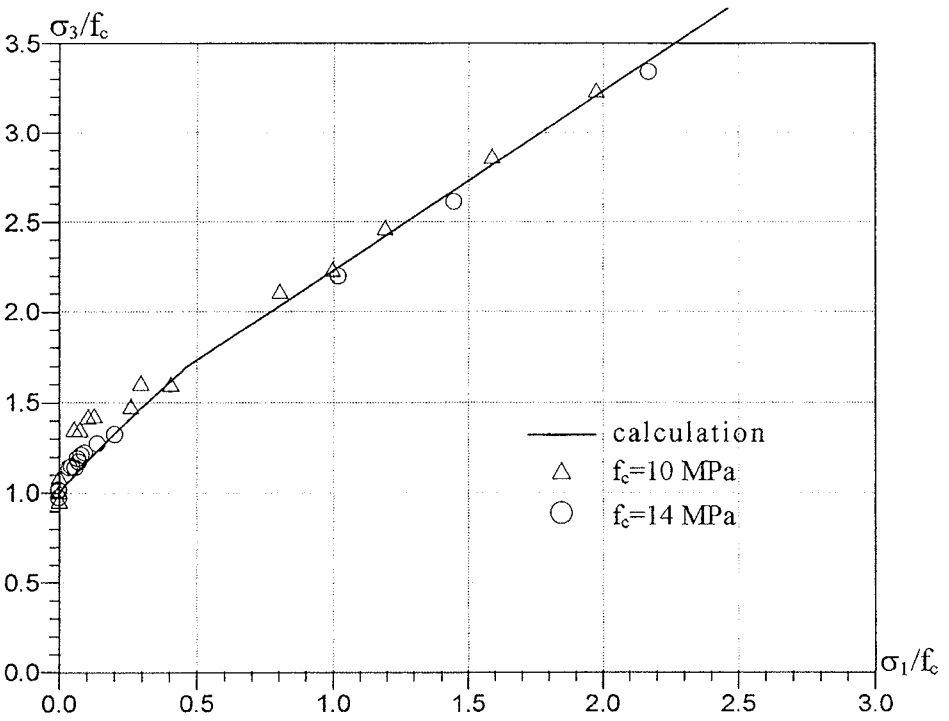

Fig.3.5.1 Comparison with the test results for P20

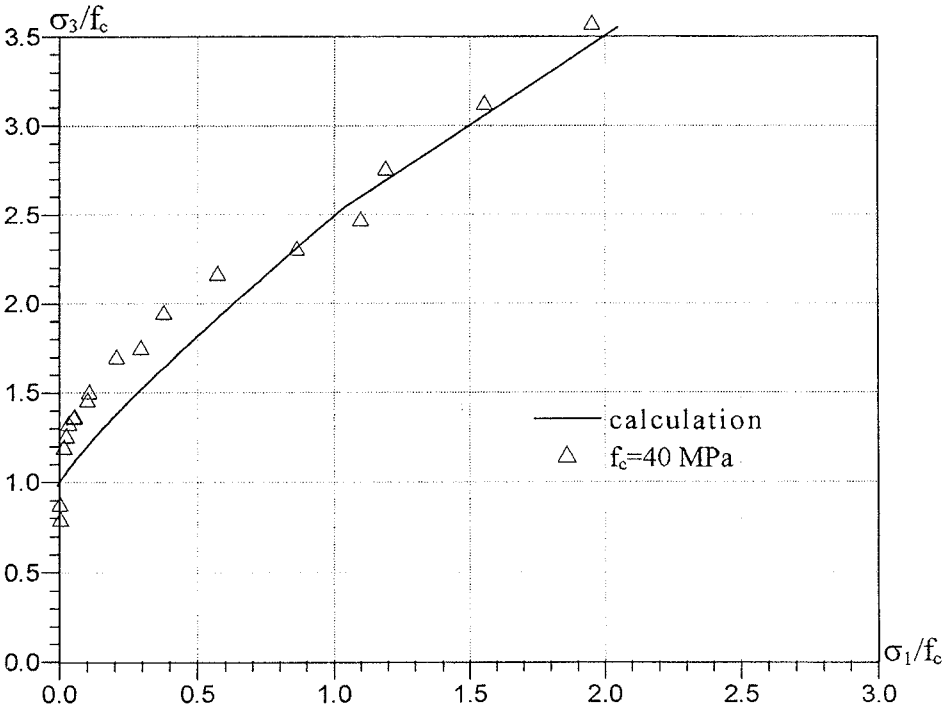

Fig.3.5.2 Comparison with the test results for P40

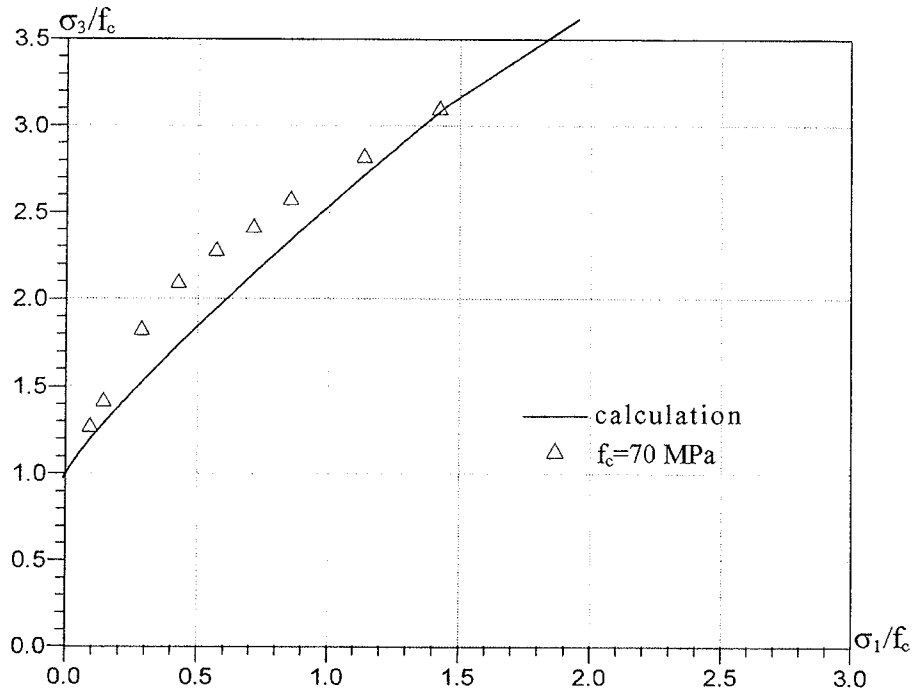

Fig.3.5.3 Comparison with the test results for P70

factors η based on the assumption that $\sigma_3=f_c$ when the lateral pressure $\sigma_1=0$ are also listed.

The tensile strength of the unmicrocracked cement paste is put to $f_{tt}=\sqrt{0.1f_{cc}}$.

The comparison with the test results from [92,1][95,1] are shown in Fig.3.5.1 ~ Fig.3.5.3.

For the test group with $f_c\approx 10$MPa, the agreement between the calculation and the test results is fairly good. For the other two groups with high compressive strengths, the test points in the transition part lie above the calculation. The reason might be due to the estimated volume ratio of hard particles. According to [59,1], the hydration degree of cement is significantly influenced by the water/cement ratio W/C. The hydration degree of cement versus the age for different water/cement ratios is shown in Fig.3.5.4. The lower the value of W/C, the lower the hydration degree. In the calculation above, fixed hydration degrees for cement, micro silica and fly ash were assumed irrespective of W/C ratios.

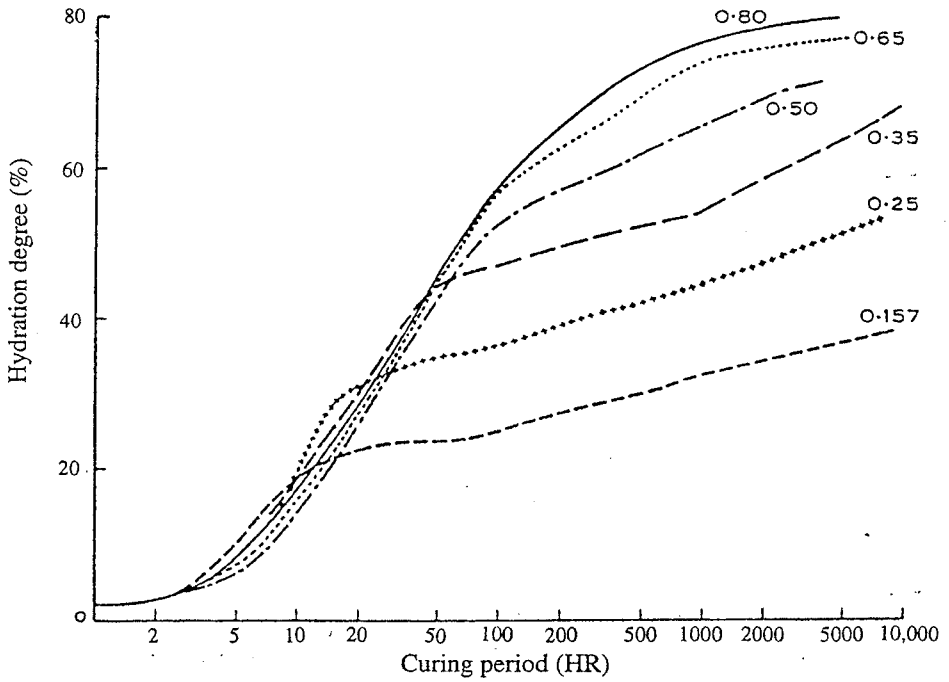

Fig.3.5.4 Hydration degree for different W/C ratios [59,1]

For the test group with $f_c \approx 10$MPa, it may still, according to Fig.3.5.4, be reasonable to assume that 80% of cement is hydrated at the age of 28 days. However, for the other strength groups, this estimation might be too high. Similar tendency might also exist for the hydration process of micro silica and fly ash. This means that the volume ratio of the unhydrated cement particles will be raised. Besides, some particles of the hydration products may not be considered weak compared with the cement gel. Therefore, the volume ratio of hard particles will eventually be higher than what has been estimated only by taking into account the unhydrated cement grains.

When the volume ratio of hard particles in hardened cement paste is estimated by changing the hydration degree of cement according to Fig.3.5.4 and by assuming that all the particles resulting from the hydration of micro silica will be harder than the cement gel, we find the results shown in Fig.3.5.5 and Fig.3.5.6 for P070 and P40. It is seen that the agreement with the test results is improved.

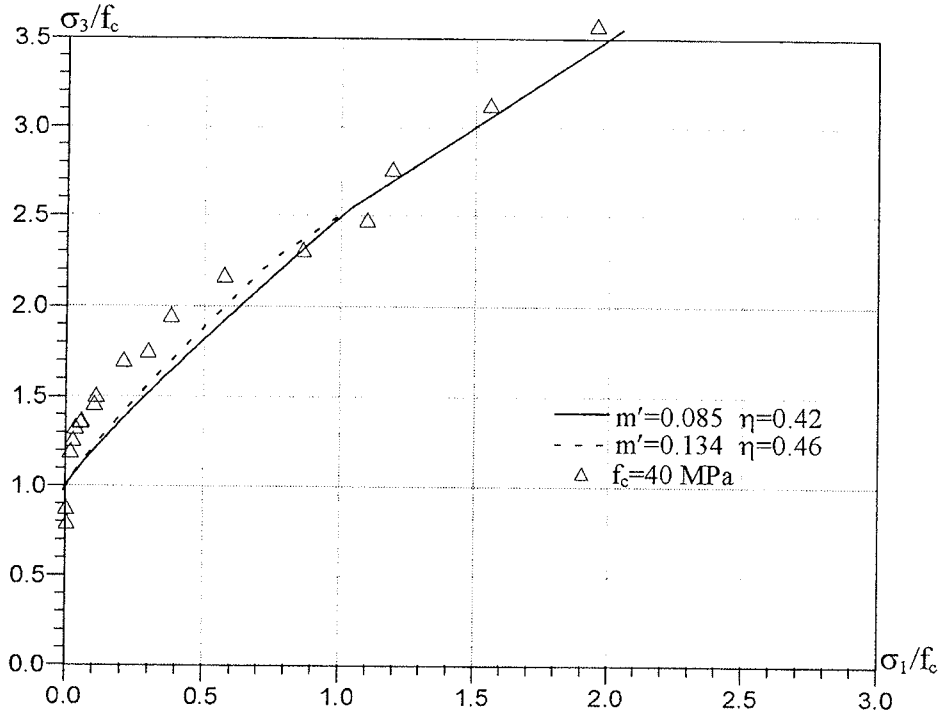

Fig.3.5.5 Comparison with the test results for P40

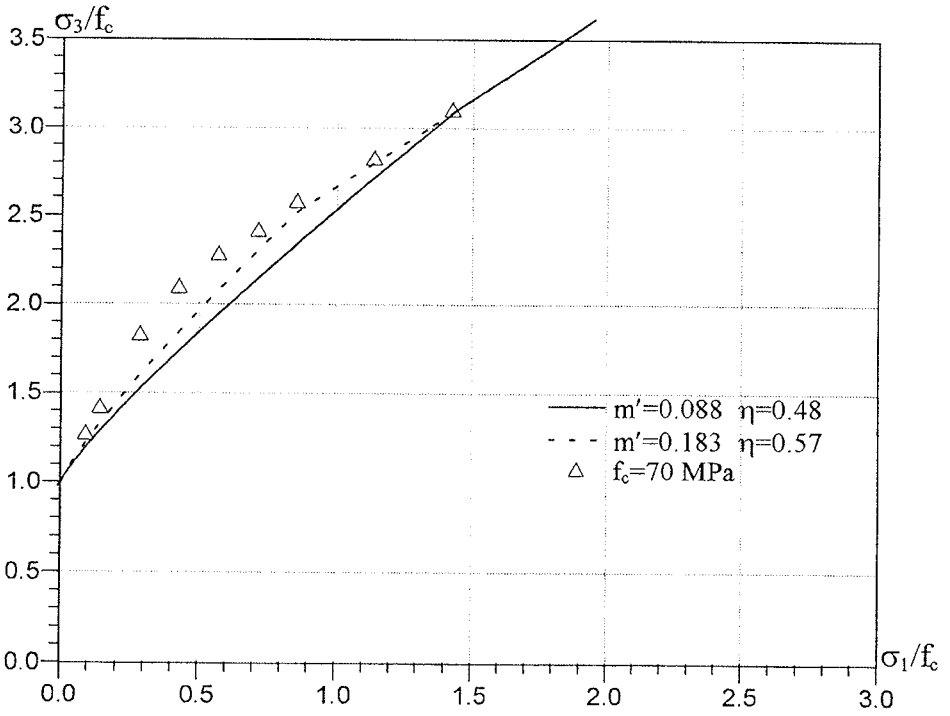

Fig.3.5.6 Comparison with the test results for P70

According to the theory of plasticity for Coulomb materials, the failure surfaces will have an inclination determined by $\gamma=\pi/4+\varphi/2$, see Fig.2.4.4.1. For hardened cement paste, the apparent friction angle $\varphi=\beta$ according to the model of this paper see Fig.3.3.1.3, and the value of β decreases with increasing lateral confining pressure. For sufficiently large confining pressure, the angle β reaches zero and the inclination of the failure surfaces becomes $\gamma=45°$. This implies that the inclination of the failure surfaces is flattening out with increasing confining pressure.

3.6 Other test results

A few other test series on the triaxial behavior of cement paste are described in the literature [54,1][62,2][74,2].

These test results differ from the ones reported in [92,1][95,1]. The uniaxial strength was much lower than the strength obtained even with a low confining pressure contrary to what has been found in the Danish test results, see Fig 3.6.1.

Since the experiments in [54,1][66,2] were done with very small specimens, one might suspect that there have been some difficulties in maintaining constant curing conditions. This view is supported by the very different uniaxial strengths reported in [54,1] for identical paste compositions. If the uniaxial strength is determined by extrapolation of the triaxial test results, the test results reported in [54,1] and [66,2] will be in reasonable agreement with the model developed here.

The test results in [74,2] do not comply with the other test results, neither the Danish ones nor the ones in [54,1] and [66,2]. They show very little increase in strength for high confining pressures indicating that according to these tests there might be a limiting confining pressure beyond which no axial stress may be applied. An explanation for this behavior is lacking.

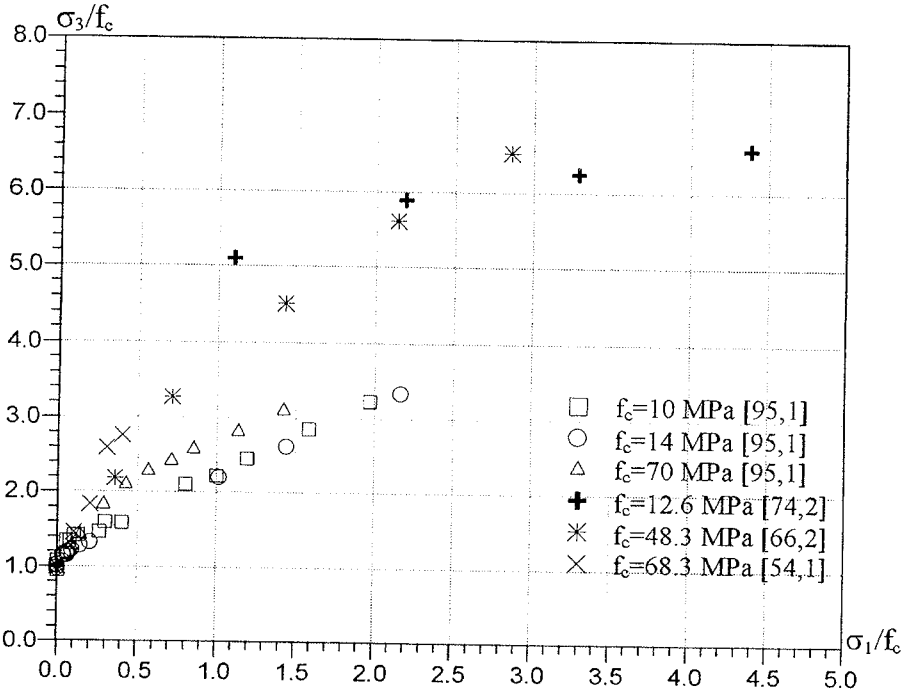

Fig.3.6.1 Test results reported in [54,1][66,2][75,2][95,1]

3.7 Effect of pore pressure

In [66,2] the effect of water pore pressure has been tested.

If the pore system or part of it is open, a water pressure applied on any surface not protected from water penetration will be distributed to all pores and all external surfaces rather fast.

If all the surfaces of the test specimen in this way are subjected to full water pressure, to get the total stresses, the applied pore pressure may simply be added to the applied stresses σ_1 and σ_3.

This means that the failure conditions for the total stresses as a function of the pore pressure can be simply derived from a "mother curve", for instance, the failure condition for pore pressure equal to zero.

Further, this means that if a model describes with sufficient accuracy, the

"mother curve ", the effect of pore pressure may also easily be described.

All the tests reported in [66,2] seem to show the pore pressure behavior explained above. Therefore, they will not be treated further here.

3.8 Conclusions and discussion

From the calculations and comparisons above, the following conclusions may be drawn:

1). Hardened cement paste may be regarded as a plastic material with the friction angle $\varphi=0$. The apparent friction angle observed in tests is probably originating from the sliding surfaces formed in the cement gel around the unhydrated cement particles.

2). The shear resistance of cement paste is mainly influenced by the damage factor η due to microcracking and the volume ratio of hard unhydrated cement particles m'. For cement paste of a particular uniaxial compressive strength f_c, those with larger volume ratio of unhydrated cement particles will have higher shear resistance even though the damage factor is increased at the same time.

3). The tensile strength of unmicrocracked cement paste will affect the initial cohesion of the cement paste, but its influence on the behavior of the shear resistance in compressive stress states is negligible.

From the comparison with the available test results with cement paste specimens, it may be concluded that the micromechanical model proposed here may predict the shear resistance of hardened cement paste with a tolerable accuracy.

As stated before, the parameters applied in the calculation are either empirically deducted or estimated by certain extrapolations of previous knowledge about concrete. No direct information is available concerning these parameters. Some

modifications on the values of the parameters may probably yield better prediction of the behavior. The following suggests some of the parameters which may need further investigation:

1). The hydration degrees of cementitious materials. The degree of hydration directly relates to the volume ratio of the hard unhydrated cement grains m′ in the hardened cement paste. It is known that the water/cement ratio is critical to the process of hydration, as are the curing conditions. Therefore, lower hydration degrees may be expected for higher strength cement paste specimens which have lower water/cement ratio [59,1]. Besides, the scale of the specimens may also have some influence on the hydration degree since the hydration degree is normally measured on samples considerably smaller than the specimens used in tests. Thus, it might be reasonable to expect a lower hydration degree in the specimens under investigation, especially those with higher strength, than what is estimated in the calculation. This will give a larger portion of unhydrated cement particles, which will make the shear failure curve in the transition range steeper and result in a better agreement with the test results.

2). The function of fly ash and micro silica. In the calculation, we assumed that half of the fly ash is hydratable material and half is "dust" which can not be considered strong enough to resist sliding. This assumption is rather rough. There may be a possibility that the hydration of micro silica yields some particles which are stronger than the cement hydration products. Consequently, the volume ratio of the hard particles in cement paste may be higher than what was estimated. More exact figures are not available to the author's knowledge.

3). The micro cracking extent in the cement paste. Besides the microcracks caused by the shrinkage of the cement paste, the addition of micro silica will also influence the microcracking state, as will the casting position of the specimens. An exact measure of the damage due to microcracking is difficult to establish, and this might be one of the reasons for the large scatter in the comparison with the test results.

4). Compressive and tensile strength of unmicrocracked cement paste. Little is known about these. The values used in the calculation are either deducted from the available test results or estimated using common knowledge about tensile strength of concrete. Better agreement with the test results might be obtained with a better understanding of the tensile strength of the unmicrocracked cement paste.

Summing up, more knowledge is necessary to obtain accurate estimation of the model parameters, and more tests related to these may be needed. It should be emphasized here that the model proposed is only a plane model created to illustrate how cement paste specimens fail in shear. No high accuracy of the predictions by the model should be expected. On the other hand it is rather amazing that such a simple model as the one described here may yield results qualitatively in complete agreements with tests.

One main conclusion therefore is that the compression behavior of cement paste is governed by its shear behavior and it is only to a very limited extent governed by crack growth in the way it is studied in fracture mechanics.

The second, equally important, main conclusion is that the apparent brittleness of cement paste in uniaxial cases and triaxial cases with low confinement stress is not due to any lack of basic ductility in the material itself, but due to the presence of the hard, unhydrated cement particles. The brittleness may thus be compared with the apparent brittleness one has in a mild steel bar under tension when the bar is being notched. Despite being the extremely ductile material, the bar will behave in a brittle way judged on a global scale.

IV. Micromechanical Modelling of Shear Failure of Concrete in Compression

4.1 Bond strength and strength of concrete

Concrete is a complex composite material. On a macroscopic level, it is a material with aggregates and hardened cement paste held together by the bond between them. It is obvious that the strength of such a material depends on the following:

1). properties of the cement paste
2). properties of the aggregates
3). size, shape, distribution and orientation of the aggregate particles
4). bond between the cement paste and the aggregate particles.

Agreement has not yet been reached as to the relative importance of these factors and how to model each part rationally.

For simplicity, concrete is normally modelled as a two phase material with strong aggregate particles, both fine and coarse, dispersed in a softer matrix of hydrated cement paste. In this way, it is seen that the strength properties of concrete are controlled primarily by the cement paste, but modified by the addition of the aggregates. Regarding the deformation properties, the aggregates play an important role leading to much higher stiffness of concrete compared to cement paste, and they have also a major role by reducing the overall shrinkage.

The bond between the cement paste and aggregates mainly originates from the mechanical interlocking actions and the van den Waals forces between the particles. Little chemical reaction takes place. Thus, it is apparent that the interfacial region of cement paste and aggregate particles is normally the weakest link in concrete. The bond is strongly dependent on the texture and the cleanness of the aggregate surface and it may be weakened by cracks due to drying shrinkage, carbonation shrinkage, bleeding, volume change during hydration etc. even prior to loading, which have been recorded in [63,1]. When

being loaded, cracks tend to develop and propagate, preferentially along the cement paste-aggregate interface in the direction of the maximum compressive stress.

As to the effect of aggregates on the strength of concrete, the results obtained up to now are controversial. It is observed in [63,1] that, for a given water-cement ratio, the uniaxial compressive strength of mortar may be as much as 30% higher than that of concrete made with it, and the uniaxial compressive strength of cement paste is about 50% higher than that of corresponding concrete. However, it is seen from the graphs presented in [79,1] that the compressive strength is decreased when small amounts of aggregates are added in the cement paste, whereas it is increased once again when the amount of aggregates passes a certain limit. It seems that the uniaxial compressive strength of concrete with normal volume aggregate ratios, i.e. more than 60% of the total volume, is close to that of cement paste, whereas the strength of mortar is lower than that of both concrete and cement paste. According to [79,1], the tensile strength of cement paste, mortar and concrete display a similar tendency. However, it is observed in [92,1][95,1] that the differences of the uniaxial compressive strength of cement paste, mortar and concrete are not noticeable for the same water/cement ratio. This result is close to the common belief that the water/cement ratio is the primary factor in determining the strength of cementitious materials.

The reasons for these scatters and controversies are not yet clearly understood. It is well known that the scatter in the measurements of the strength of cement paste and concrete is rather large. Besides the difficulties in maintaining a constant mix even with fresh cement from the same batch, the casting position and the curing conditions may also have some, in certain cases considerable, influence on the strength. The main reason is probably the effect of voids and microcracking. The introduction of aggregates will certainly increase the microcracking extent in the cement paste, and this will tend to reduce the uniaxial strength, both in compression and in tension, of cement paste. Hence, we would expect from this reason that the uniaxial strength of concrete is lower

than that of mortar, which in turn is lower than that of cement paste for the same effective water/cement ratio. However, if the specimens are cured carefully, and the state of the microcracking is not altered too much due to the presence of the aggregates, the strength of cement paste, mortar and concrete might be expected to be the same.

Therefore, it is assumed in this paper that, when the microcracks caused by the presence of aggregates may be disregarded, cement paste, mortar and concrete has the same uniaxial compressive strength.

4.2 Micromechanical modelling of shear failure in principal stress space

As for the cement paste, the problem dealt with here is transformed to a plane problem by considering a thin slice of concrete having a thickness of the order of magnitude of the maximum aggregate size.

The failure of concrete cylinders in triaxial stress states might be described as follows:

At the early stage of loading, bond cracks lying mainly in the direction of the axial load will occur in the interfacial zones between aggregates and cement paste. According to plastic theory, under a certain combination of stresses, sliding displacements take place in the cement paste, and a yield line with the inclination γ, see Fig.4.2.1, will be formed in the cement paste. In normal strength concrete, the strength of most aggregates is higher than that of the cement paste. Thus, the yield line, if running into an aggregate particle, will not be able pass through, and is forced to go around the particle. Since bond cracks already exist around the aggregates, the yield line prefers to follow these cracks because this will consume less energy. Once the yield line passes around the aggregate, it will resume the original sliding pattern in the cement paste. The failure mechanism is schematically depicted in Fig.4.2.1. The aggregates have been drawn as spheres.

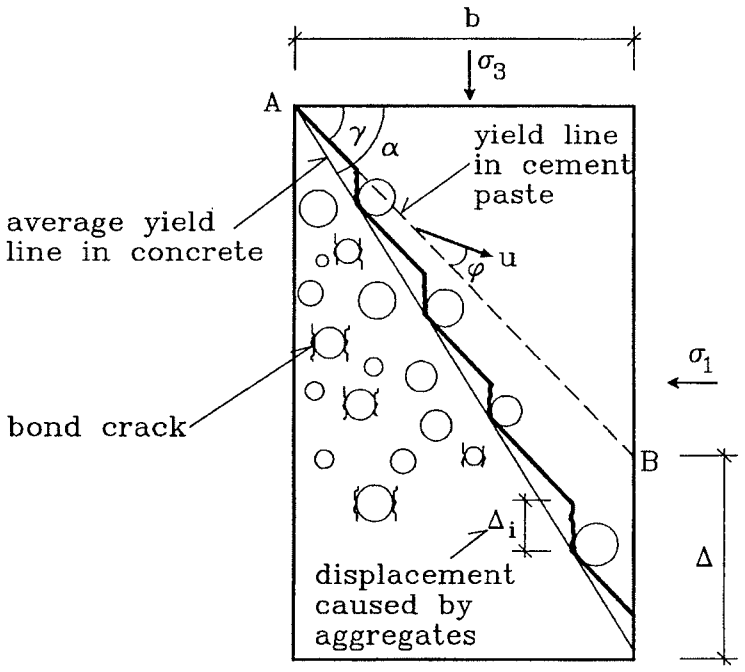

Fig.4.2.1 Shear failure mechanism in concrete in triaxial compressive stress states

The bond between aggregates and cement paste is reduced considerably by the cracks formed in the interfacial zone, but the magnitude of the reduction is not clear yet. It might be reasonable to assume that the bond is reduced to such an extent that its contribution to the resistance of sliding may be neglected. Thus, the function of the aggregates in shear failure of concrete is mainly to displace the yield line, which would have been formed in the cement paste, to a steeper position.

With this assumption, the dissipation along the bond cracks becomes zero, thus the energy dissipated along the yield line in concrete will equal that of a yield line in cement paste. The external work is however different.

From the analysis in the previous chapter, it appears that the apparent friction angle of cement paste φ actually is the angle β of the sliding surface formed in front of the hard unhydrated cement grains, and the relative displacement is at an angle $\beta=\varphi$ to the direction of the yield line. The yield line has an inclination

of γ. Due to the existence of aggregates, the cement paste in the concrete is in a very complex stress state and the average position of the yield line in cement paste has to be determined by optimization corresponding to each $\beta=\varphi$.

The vertical deviation or displacement of the yield line in concrete, at the edge of the cylinder, from the would-be yield line in the cement paste is designated by Δ, which is closely related to the number of aggregate particles the yield line runs into and the displacement caused by the individual aggregate particles.

To the author's knowledge, the problem of calculating Δ has never been touched upon, and it will only be possible to present a very approximate solution. Fortunately, it turns out that the result is not very sensitive to the displacement formula. The maximum displacement caused by an aggregate particle is of the order of magnitude d, the diameter of the particle, which is the essential thing to take into account

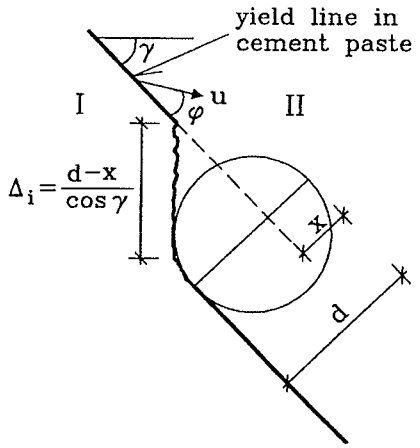

Fig.4.2.2 Displacement caused by an aggregate particle

Consider, see Fig.4.2.2, an aggregate particle with diameter d. For simplicity, the particle is assumed to be spherical. Microcracks are in the direction of the maximum compressive stress around the aggregate particle, i.e. vertical in the figure. Before the yield line in the cement paste "reaches" the particle, it will be displaced because the existence of the microcracks. The displacement of the yield line is designated by Δ_i.

The cement paste in the upper part II will move as a rigid body relative to the lower part I at an angle of φ to the yield line, i.e. it will move in the direction of the relative displacement u in Fig.4.2.2. Since the aggregates are much harder than the cement paste, the yield line will make a vertical jump when an aggregate stands in the way of the displacement. Along the vertical parts of the yield line a crack opening takes place.

If the yield line cuts the particle in the right hand side, it may be displaced in the way shown in Fig.4.2.3 to the left. Here the yield line AD, tangent to an adjacent aggregate particle, is in the direction of the yield line in the cement paste, while the yield line DE, tangent to the particle concerned, is in the direction of the relative displacement along the yield lines. When the adjacent particle is moved more to the right, a situation is reached where the yield line in the cement paste will not be affected at all by the particle considered.

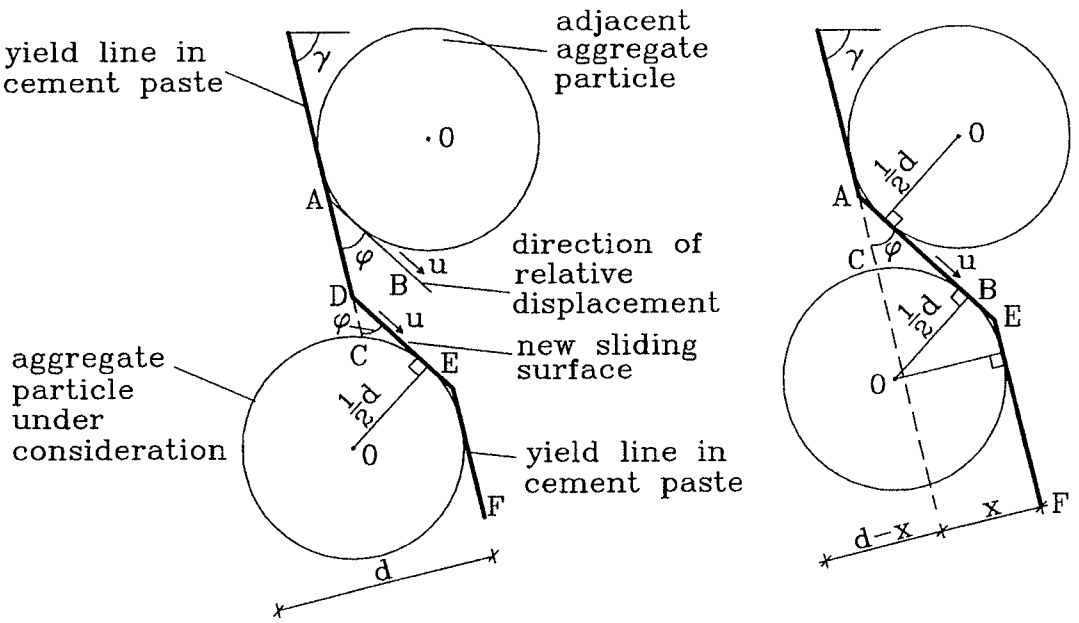

Fig.4.2.3

When the adjacent particle is moved more to the left, we have another limiting position where the part of the yield line having the direction of the displacement is tangent to both particles, see Fig.4.2.3 to the right. After the yield line in the

cement paste has passed the adjacent aggregate particle, we assume that the yield line is forced to displace as shown in Fig.4.2.2 if the line AB in Fig.4.2.3 to the left "hits" the particle concerned. If the line AB does not "hit" the particle, the yield line will be assumed to follow the direction of the displacement DE until it reaches the yield line EF which is tangent to the aggregate particle considered and having the direction of the yield lines in the cement paste. Thus, the maximum vertical displacement of the type shown in Fig.4.2.2 is found when AB is tangent to the particle considered as well as the adjacent particle.

To simplify the problem, the displacement of the yield line caused by the aggregates will be calculated by transforming the real particle system to an ideal particle system with identical spherical particles having the same volume ratio as the real particles. The particles are considered randomly distributed. In this way, the maximum displacement of the yield line caused by an aggregate particle is found to be

$$\Delta_{imax} = \frac{d-x}{\cos\gamma} \tag{4.2.1}$$

Here d is the diameter of the identical particles and

$$x = \frac{1}{2}d(1-\cos\varphi) + [\sqrt{a_m^2 - d^2} + \frac{1}{2}d\cdot\tan(\frac{1}{2}\varphi)]\cdot\sin\varphi \tag{4.2.2}$$

where a_m is the mean distance between the centers of the aggregate particles, and x refers to the situation shown in Fig.4.2.3 to the right.

The value of a_m is determined according to numerical stereology [70,2]. The mean free distance a_{free} between particles, i.e. a mean edge-to-edge distance, is

$$a_{free} = \bar{L}_3 \frac{1-\kappa_a}{\kappa_a} \tag{4.2.3}$$

κ_a being the volume ratio of aggregate particles, and $\bar{L}_3$ the mean intercept length of the particles considered as three-dimensional bodies. For spherical particles

$$\bar{L}_3=\frac{2}{3}d \tag{4.2.4}$$

Hence

$$a_m=d+a_{free}=\frac{1}{3}d\frac{2+\kappa_a}{\kappa_a} \tag{4.2.5}$$

By inserting eq.(4.2.5) into eq.(4.2.2), x can be calculated, and thus Δ_{imax} is determined. The average displacement caused by the particle will be

$$\bar{\Delta}_i=\frac{1}{2}\Delta_{imax}=\frac{1}{2}\frac{d-x}{\cos\gamma} \tag{4.2.6}$$

According to a theorem in stereology [70,2], already discussed in section 3.3.1, the volume ratio, area ratio and linear ratio are equal. Then the number of the aggregate particles cut by the yield line shown in Fig.4.2.1 will be

$$N=\frac{\kappa_a}{\bar{L}_3}L_{AC}=\frac{\kappa_a}{\frac{2}{3}d}L_{AC} \tag{4.2.7}$$

L_{AC} being the length of the yield line.

Therefore the total displacement Δ of the yield line will be

$$\Delta=N\cdot\bar{\Delta}_i=\frac{3}{4\cos\gamma}(1-\frac{x}{d})\kappa_a\cdot L_{AC} \tag{4.2.8}$$

The final formula for the displacement becomes

$$\Delta=\frac{3}{4\cos\gamma}(1-f(\kappa_a,\varphi))\kappa_a\cdot L_{AC} \tag{4.2.9}$$

Having denoted $x/d=f(\kappa_a,\varphi)$, i.e.x/d as a function of κ_a and φ.

From Fig.4.2.1, it is seen that

$$L_{AC}=\frac{b}{\cos\alpha}$$

Thus

$$\Delta=\frac{3}{4\cos\gamma}(1-f(\kappa_a,\varphi))\cdot\frac{b}{\cos\alpha}\cdot\kappa_a \tag{4.2.10}$$

The aggregates often have a laminated structure. The sliding resistance of the aggregates is therefore sensitive to the orientation of the lamination. When the direction of the sliding is close to the orientation of the layers, the sliding resistance will be reduced significantly. Besides, some of the aggregates may not be regarded strong compared with the cement paste, especially when dealing with high strength cement paste. Therefore, it is natural that not all of the aggregates take part in the displacing a yield line initiated in the cement paste. We term the ratio between the volume of aggregates that are capable of resisting the sliding and the total volume of aggregates as the effective ratio of aggregates, designated by $\lambda\leq 1$. Hence

$$\Delta=\frac{3}{4\cos\gamma}(1-f(\kappa_a,\varphi))\cdot\frac{b}{\cos\alpha}\cdot\lambda\kappa_a \tag{4.2.11}$$

Then, all of the aggregates are effective for $\lambda=1$, and $\lambda=0$ means that all of the aggregates are so weak that they can not resist the sliding. For concrete with normal aggregates, λ is close to 1, and λ decreases with increasing strength of cement paste.

In other related formulas κ_a should also be replaced by $\lambda\kappa_a$.

To get a glimpse of how the cracks and failure surfaces really are located in the triaxially tested specimens, some polished and thin sections were extracted from the specimens B035-2-13 in [92,1]. The size of the cylinder specimen was 100mm×200mm, and the uniaxial compressive strength was 43MPa. At the end of loading, the total deformation was about 60mm axially and about 30mm laterally. Two of the photos of the thin section are presented in Fig.4.2.4(a) and (b). About the details of the thin section technique, see [96,1]. In Fig.4.2.4(a), an "hourglass" failure pattern is clearly seen. In Fig.4.2.4(b), cracks in the boundaries between aggregate particles and cement paste in the direction of the axial load are created, and cracks are created even through the aggregates. Shear sliding surfaces can also be observed. The aggregates used in the mix was

(a).

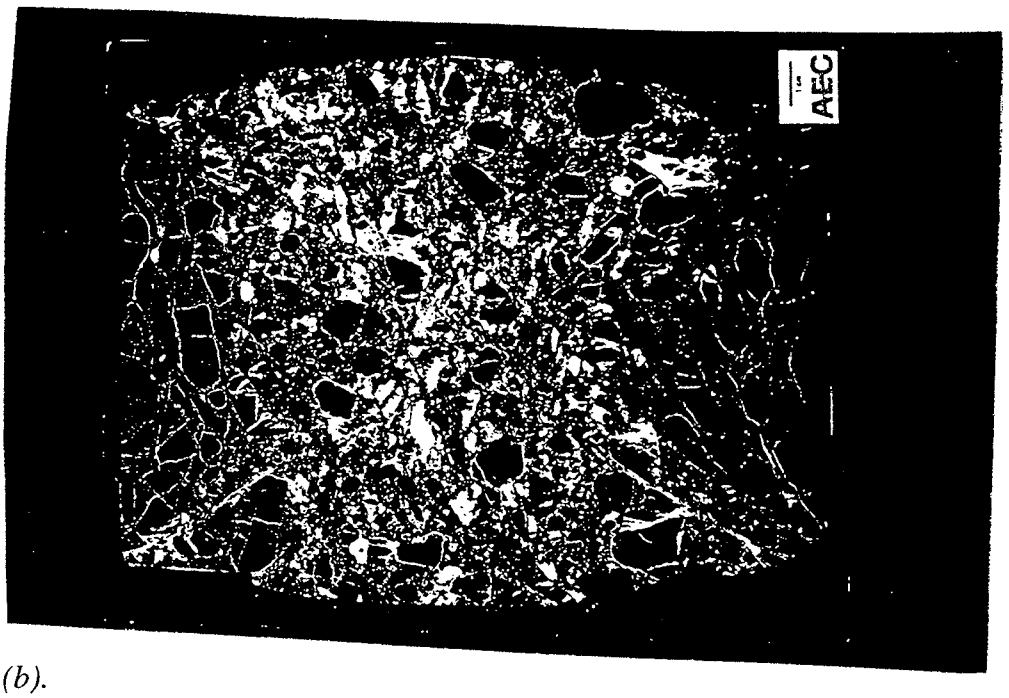

(b).

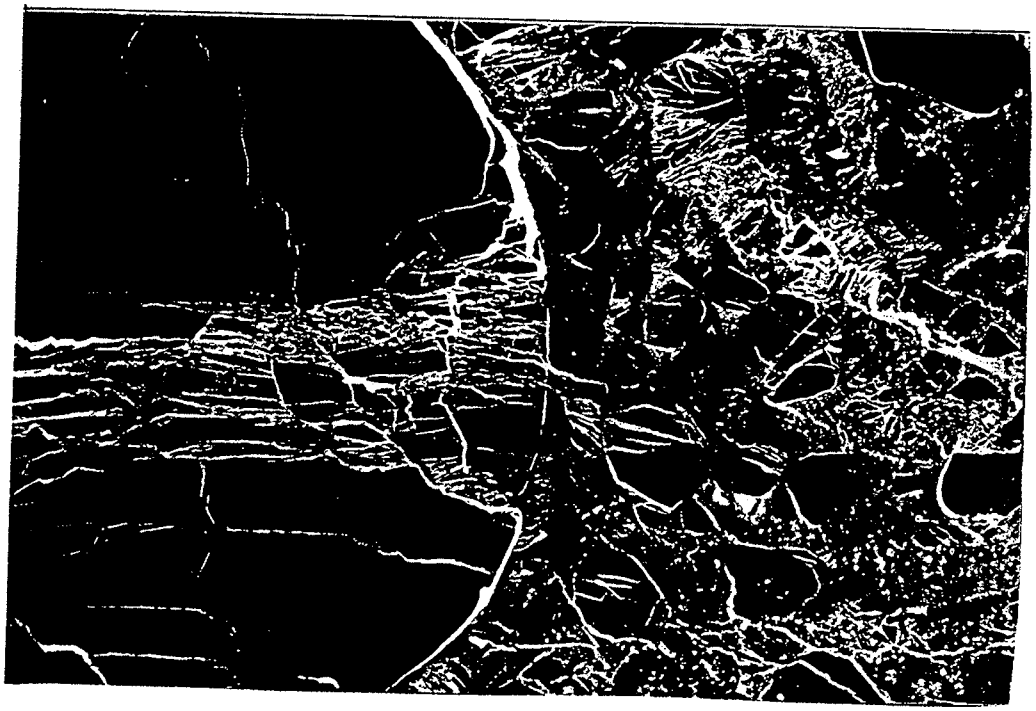

Fig.4.2.4 Photos of thin sections of triaxially tested specimens [96,1] (the light colour shows the cracks, the dark the aggregate particles and the cement paste, which may clearly be distinguished)

relatively weak, and this explains the cracks in the aggregates, and also justifies the introduction of the effective ratio of aggregates λ in the model.

The shear failure condition in τ-σ space for cement paste, obtained from the micromechanical model presented in the previous section, is re-illustrated in Fig.4.2.5.

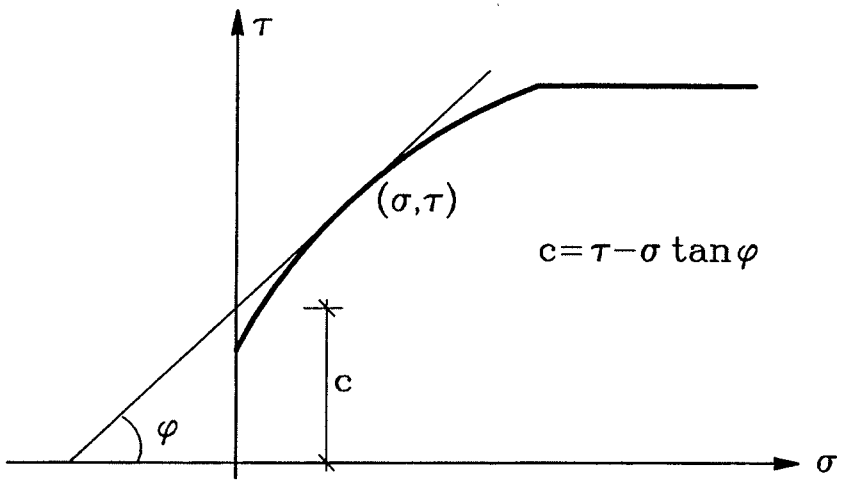

Fig.4.2.5 Shear failure condition of cement paste

Corresponding to every point on the curve, the values of τ, σ and the apparent friction angle φ are known. Since the plastic theory with its normality condition is valid for cement paste at a specific point of the curve, a straight line, tangent to the curve at this point, corresponding to the apparent friction angle φ and the apparent cohesion c will be found. This straight line may be identified with a Coulomb failure criterion with friction angle φ and cohesion c as shown in Fig.4.2.5. Then $c=\tau-\sigma\tan\varphi$, and it is possible to apply the formulas deduced for a Coulomb material in the present calculation.

If the yield line in cement paste is displaced as shown in Fig.4.2.2, the internal work dissipated in concrete will be equal to that along the yield line in the cement paste assuming no contribution from the vertical cracks. If the yield line is displaced by creating a new sliding surface as in Fig.4.2.3, another dissipation will be found. Calculations have shown that the difference between the two dissipations is small and can be ignored. Further, since the cohesion of cement

paste along the sliding surface close to an aggregate particle is difficult to estimate due to the microcracking in this area, the small difference between the dissipations will be neglected in the following calculations.

The internal dissipation thus becomes:

$$W_I = c \cdot u \cdot \cos\varphi \cdot L_{AB} \tag{4.2.12}$$

where

$$L_{AB} = \frac{b}{\cos\gamma} \tag{4.2.13}$$

The external work is

$$W_E = \sigma_3 \cdot b \cdot u \sin(\gamma - \varphi) - \sigma_1 \cdot b \tan\alpha \cdot u \cos(\gamma - \varphi) \tag{4.2.14}$$

The work equation $W_I = W_E$ results in

$$\sigma_3 = c \frac{\cos\varphi}{\cos\gamma \sin(\gamma - \varphi)} + \sigma_1 \frac{\tan\alpha}{\tan(\gamma - \varphi)} \tag{4.2.15}$$

The angle α may be determined geometrically. In Fig.4.2.1, it is seen that

$$b \cdot \tan\alpha = b \cdot \tan\gamma + \Delta \tag{4.2.16}$$

Substituting Δ with the expression from eq.(4.2.11) we get

$$\tan\alpha = \tan\gamma + \frac{3}{4\cos\gamma}(1 - f(\kappa_a, \varphi)) \cdot \frac{1}{\cos\alpha} \cdot \lambda\kappa_a \tag{4.2.17}$$

This formula gives the connection between the effective volume ratio of the aggregates $\lambda\kappa_a$ and the angle α determining the displacement of the yield line.

For $\varphi = 0$, we get $x/d = f(\kappa_a, \varphi) = 0$. By assuming $\gamma = 45^\circ$ as in a Coulomb material with a friction angle $\varphi = 0$, we get

$$\sin\alpha = \cos\alpha + \frac{3\sqrt{2}}{4} \cdot \lambda\kappa_a \tag{4.2.18}$$

In Fig.4.2.6 tanα is drawn as a function of $\lambda\kappa_a$ for $\varphi=0$ and $\gamma=45°$, using eq.(4.2.18). The result has been compared with the results of the procedure described using the optimized value of γ.

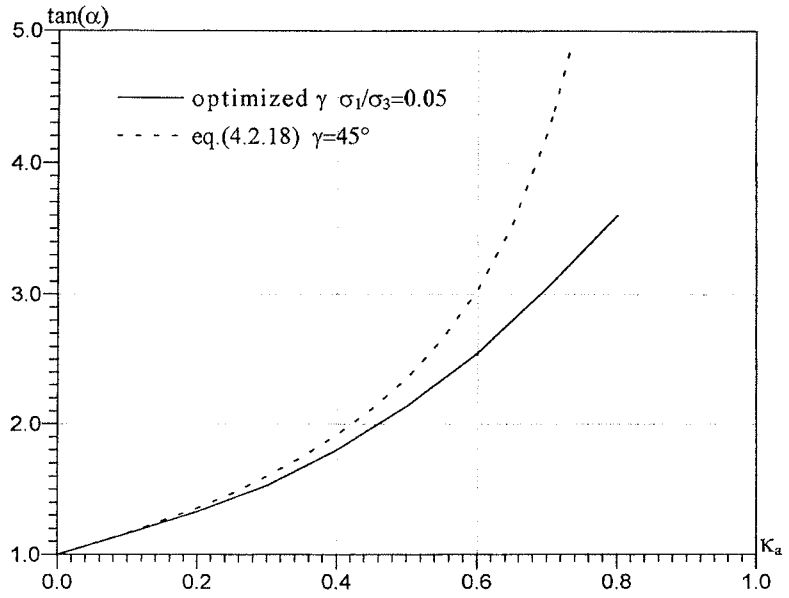

Fig.4.2.6 tanα as a function of $\lambda\kappa_a$ for $\varphi=0$

As will be demonstrated in the following, the value of γ obtained by optimization is related to the volume ratio of aggregates and the confining pressure, so is the value of tanα. The curve of tanα with optimized γ for $\varphi=0$ from the following calculations is shown as a solid line in the figure above. The optimization reduces the value of tanα substantially for the higher value of κ_a.

The load carrying capacity is now found by minimizing (4.2.15) with respect to γ and determining α by eq.(4.2.17).

Corresponding to an arbitrary point on the curve in Fig.4.2.5 with a specific apparent friction angle φ and a corresponding apparent cohesion c, a curve which is close to a straight line may be determined by eq.(4.2.15) as shown in Fig.4.2.7. In this way, a set of curves corresponding to different apparent friction angles are found.

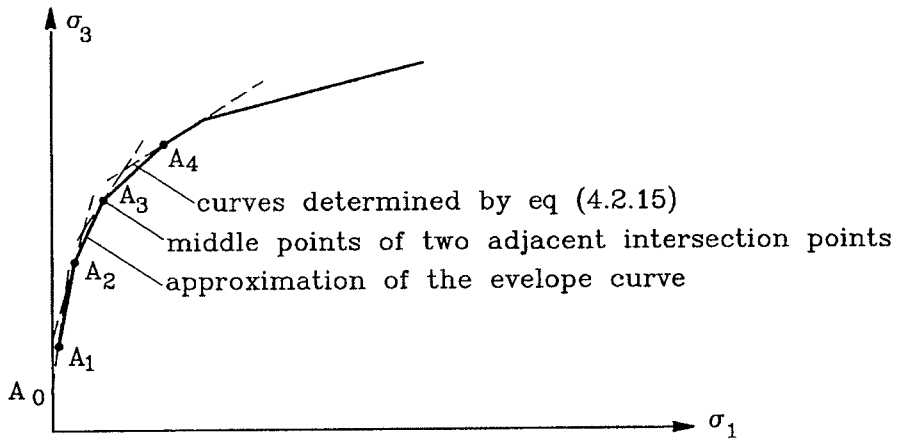

Fig.4.2.7

The envelope curve determined by the set of the curves is the failure condition for concrete in principal stress space.

The envelope curve can be approximated by connecting the middle points of two adjacent intersection points if the intervals between two adjacent points are sufficiently small. In this way, the failure condition for concrete is found, It is shown schematically in Fig.4.2.8.

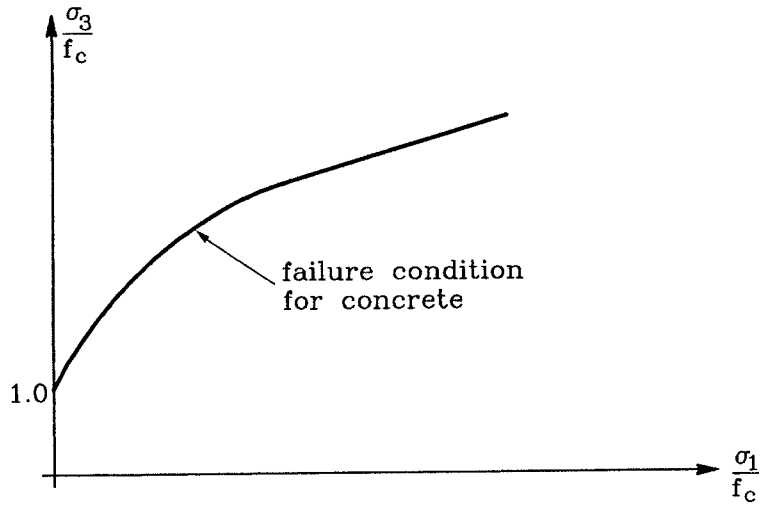

Fig.4.2.8 Failure condition for concrete in principal stress space

As mentioned before, the uniaxial compressive strength of cement paste and that of concrete is equal in this model.

It must be emphasized that while cement paste may be and has been in the model of this paper considered as an isotropic plastic material, this is not the case for concrete. This is due to the fact that concrete is assumed to be cracked in the interfacial zone of aggregate particles and cement paste in the direction of the largest principal stress σ_3. Thus the loading introduces anisotropy in the material. Therefore, for concrete, strictly speaking, it has no meaning to ask for the failure condition in τ-σ space. It is not defined in this model. Of course, an apparent τ-σ failure criterion might be determined from the σ_1-σ_3 failure condition in a similar way as it was done for cement paste, see section 3.3.2.

4.3 Parameter studies

Obviously, the prominent difference between the composition of concrete and cement paste is the addition of aggregates. We shall assume that the state of microcracking in the cement paste is not influenced by the addition of aggregates, and that the parameters of the model for concrete may be taken the same as for cement paste except that the yield line will be displaced by the resistance of the aggregates. Then the main factor which will influence the position of the yield line and the load carrying capacity is the effective volume of the aggregates determined by the parameter λ.

Fig.4.3.1 shows the failure conditions for different λ values. It is seen that the failure condition is greatly influenced by the value of λ. The higher the effective part of the aggregates, the steeper the yield line in concrete, and the higher the load capacity with the same lateral confining pressure.

4.4. Experimental verification

Regarding a review of triaxial tests of concrete, using either cylinders or cubes, see [92,2]. Test results from [92,1][95,1] are studied in detail in the following. Results of some tests by other researchers will be briefly compared with the calculations.

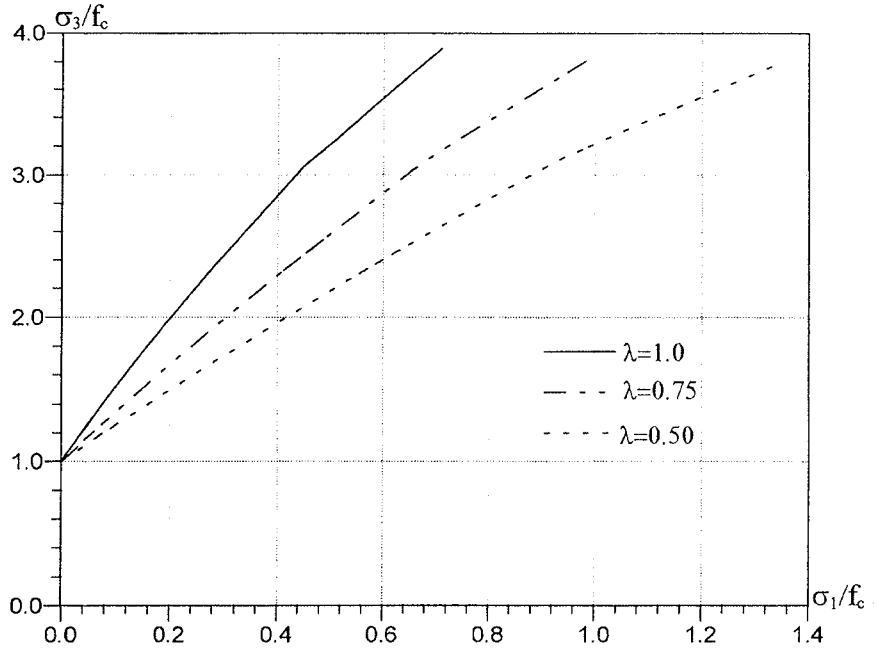

Fig.4.3.1 Shear failure conditions for different λ values

From the available test results for concrete and cement paste with the same or with close uniaxial compressive strengths, it appears that the ratios of f_{cc}/f_c for both materials are very close. Hence, the ratios of f_{cc}/f_c for concrete and for cement paste are assumed equal in the calculation. The way of determining the triaxial compressive strength f_{cc} is described in section 3.3.1.

About details on mix design, curing conditions and test procedures, the reader is referred to [92,1] and [95,1].

The uniaxial compressive strength measured from cylinders and the parameters applied in the calculations are listed in table 4.4.1.

Table 4.4.1 Uniaxial compressive strength and the parameters used in the calculations

test group	f_c (MPa)	κ_a	m' (%)	f_{cc}/f_c	η
B010	13.8	0.75	6.62	1.23	0.28
B035	40.7	0.69	9.20	1.50	0.43
B050	52.1	0.71	8.53	1.62	0.46
B070	70.8	0.72	8.81	1.66	0.48
B085	89.4	0.73	11.40	1.68	0.51
B100	104.4	0.72	11.97	1.74	0.54
B110	108.8	0.66	12.47	1.76	0.55

Note: 1) f_c is the mean uniaxial compressive strength for each test group.

2) The cement used was rapid hardening cement except for B100, where white cement was used.

3) m' is found by using the table A1.1, Appendix 1.

4) η is determined as for cement paste.

The ratio of f_{cc}/f_c as a function of f_c is depicted in Fig.4.4.1 where the best fit curve is also shown.

The comparisons between the calculation and the test results for various concrete strengths are shown in Fig.4.4.2 ~ Fig.4.4.9. The effective volume ratio of the aggregates $\lambda\kappa_a$ for different strengths is found by fitting the test results in the range of large confining stresses.

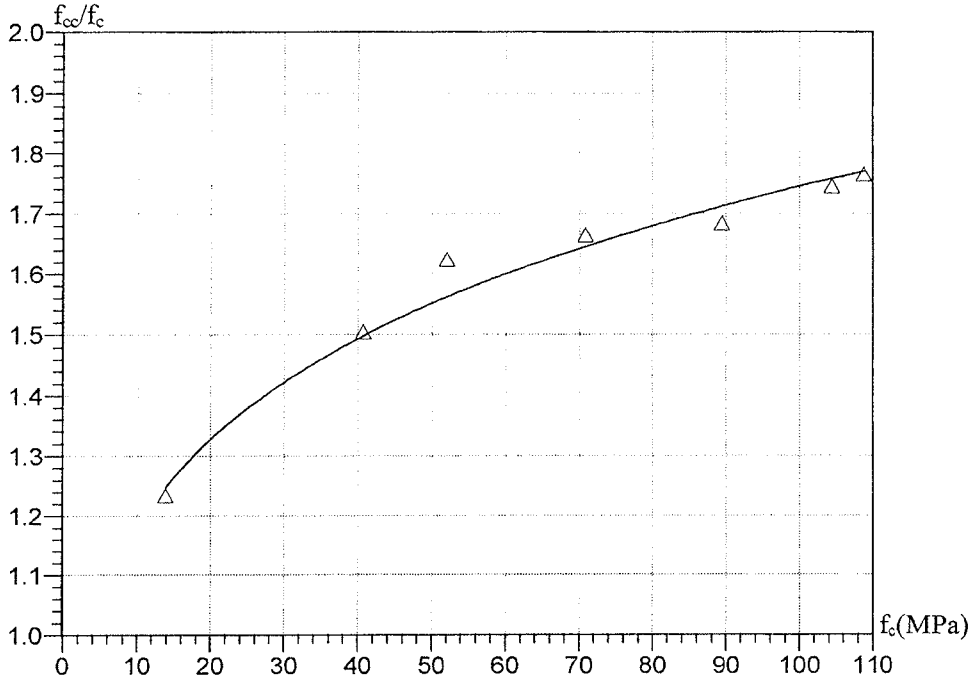

Fig.4.4.1 Ratio of f_{cc}/f_c versus f_c

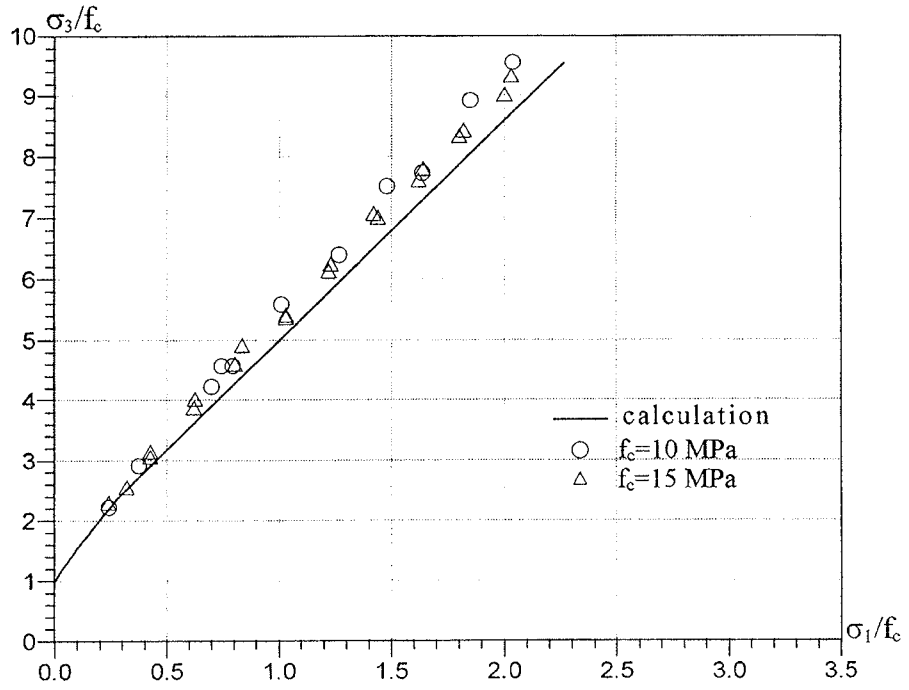

Fig.4.4.2 Comparison with test results for B010 with $\sigma_1/f_c<2.5$

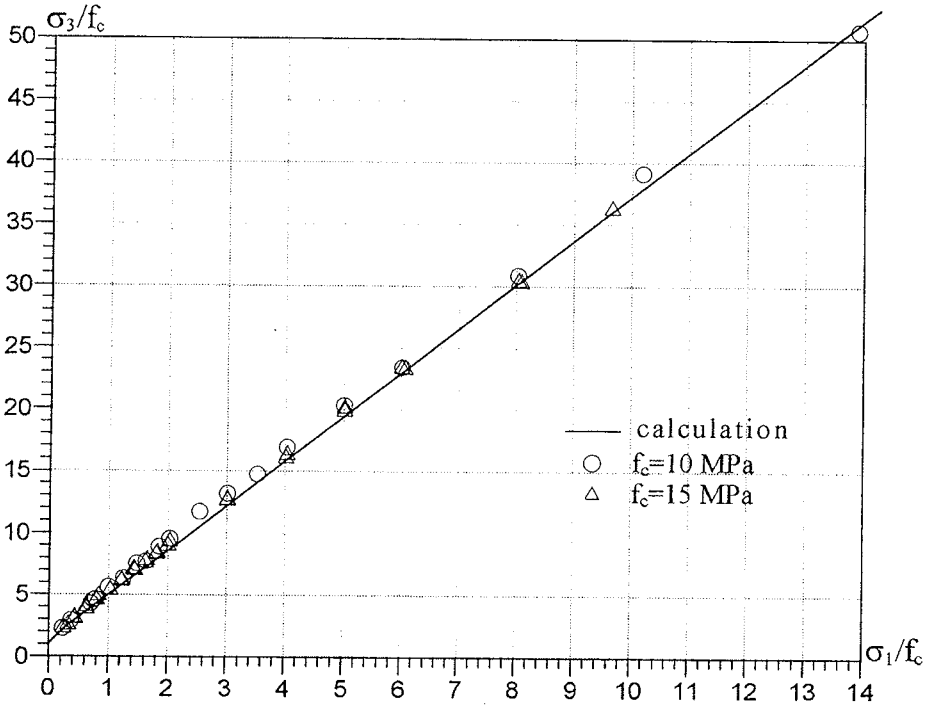

Fig.4.4.3 Comparison with test results for B010 with σ_1/f_c up to 14

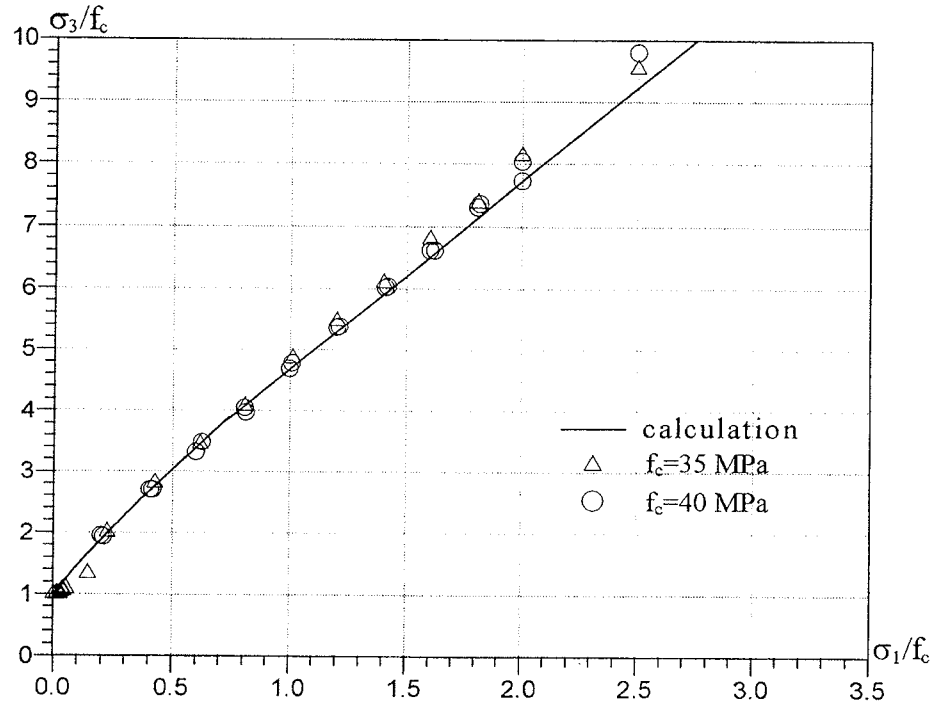

Fig.4.4.4 Comparison with test results for B040

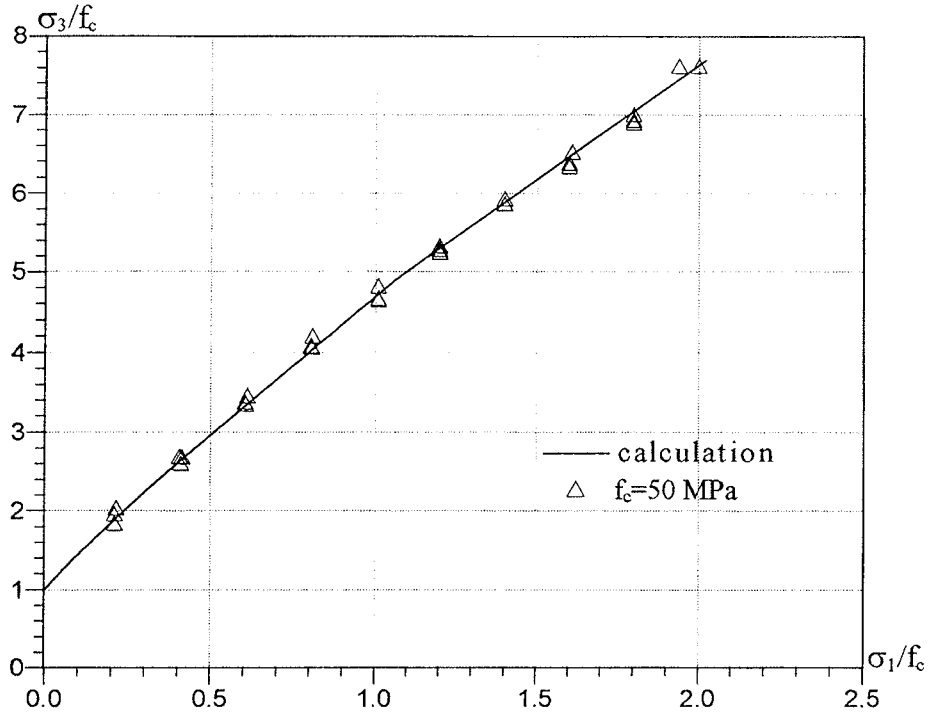

Fig.4.4.5 Comparison with test results for B050

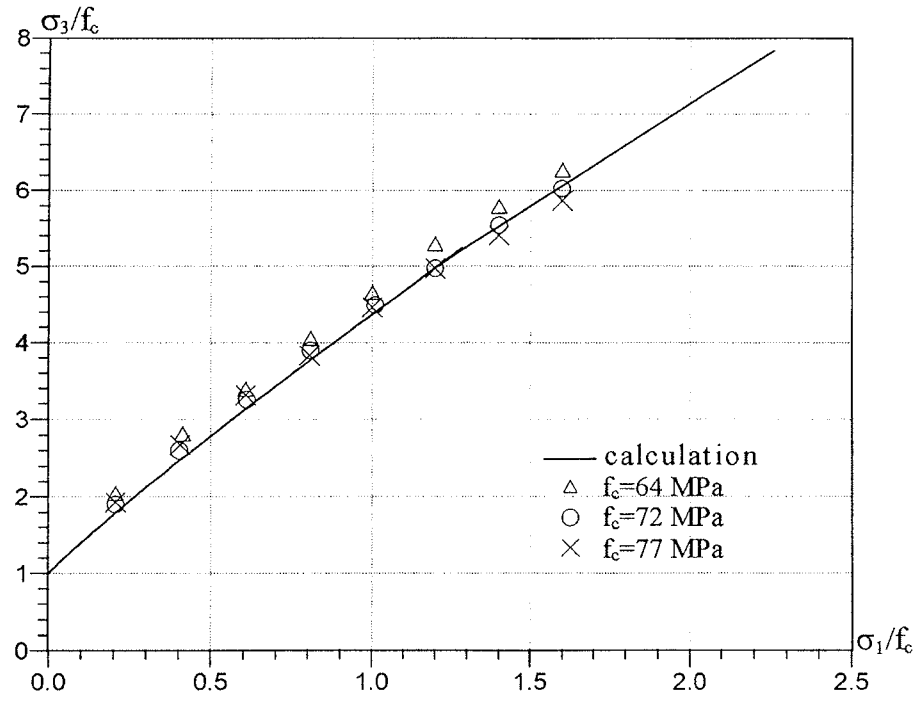

Fig.4.4.6 Comparison with test results for B070

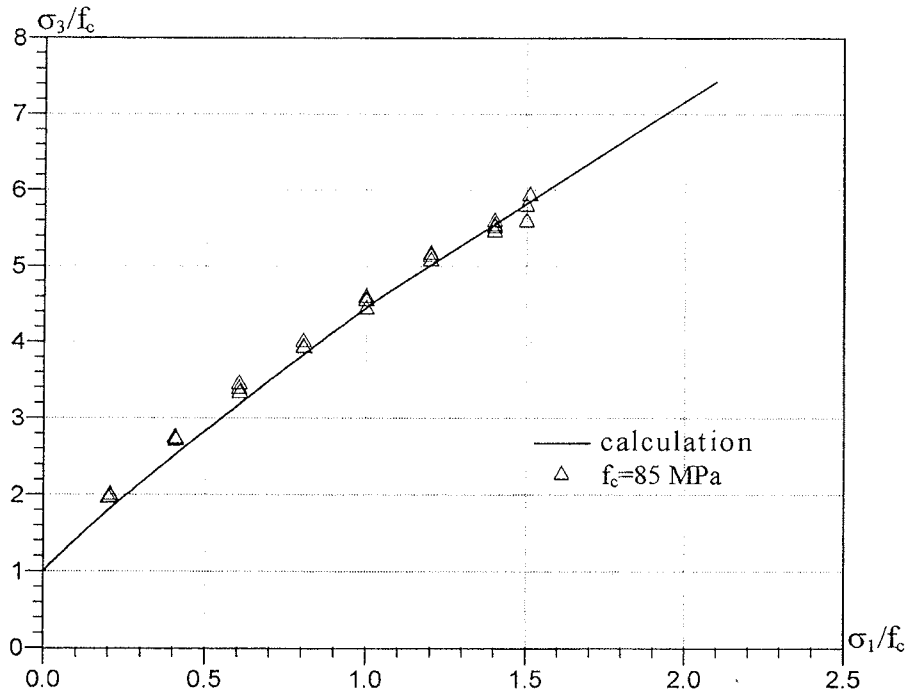

Fig.4.4.7 Comparison with test results for B085

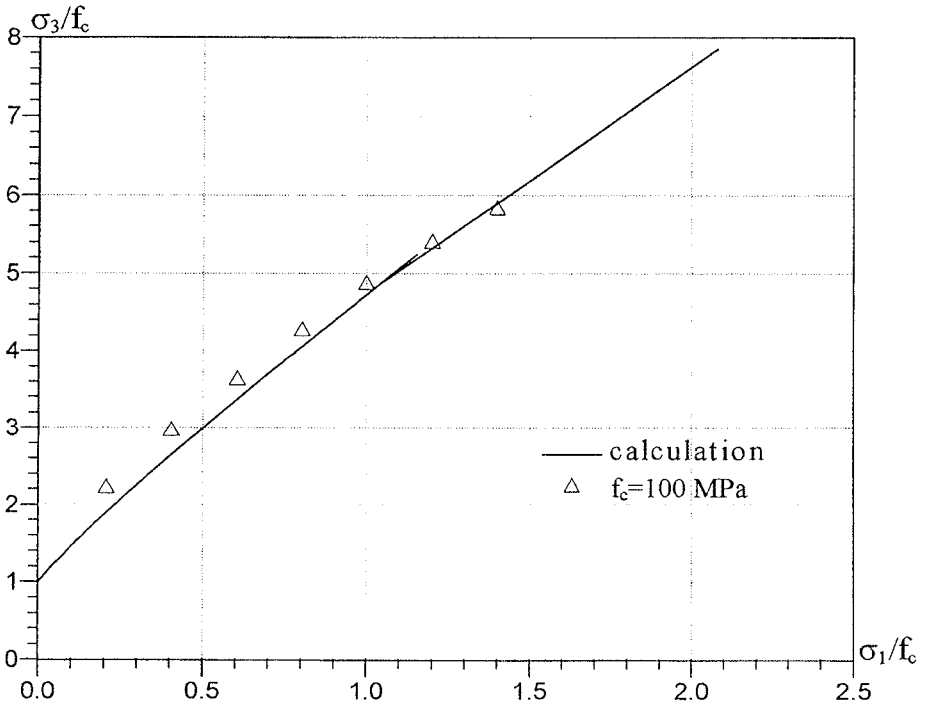

Fig.4.4.8 Comparison with test results for B100

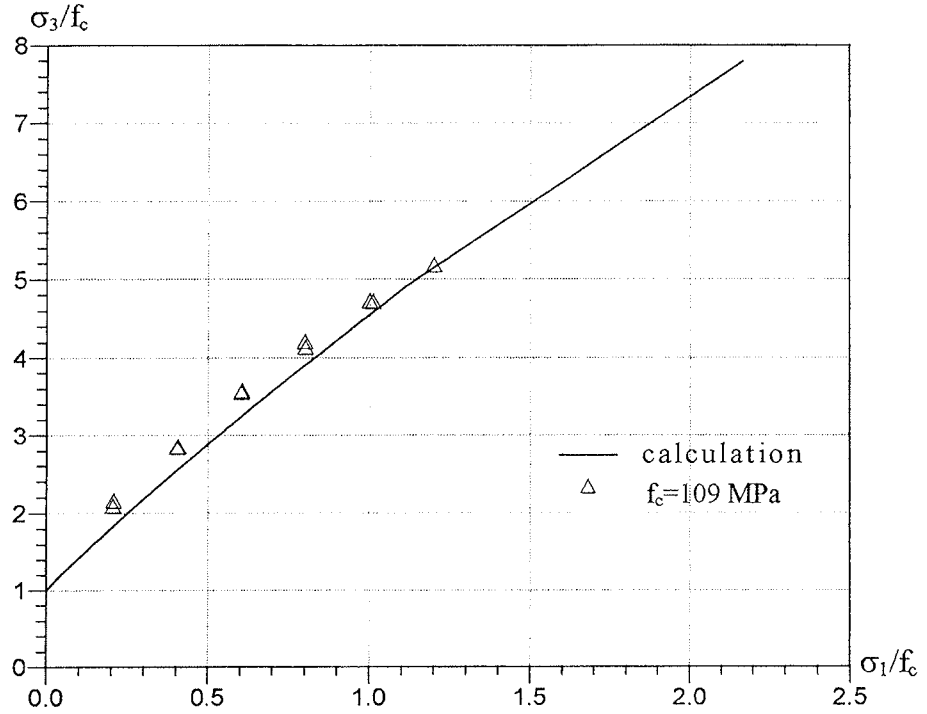

Fig.4.4.9 Comparison with test results for B100

For the test group B010, the lateral confining pressure reached a value as high as $14f_c$. It is observed in Fig.4.4.1 and Fig.4.4.2 that, for $\sigma_1/f_c>3$, σ_3 is still increasing approximately linearly with σ_1 but at a less increasing rate than that for $\sigma_1/f_c\leq 3$.

It appears that the agreement between the calculations and the test results is fairly good.

Test results using cylindrical specimens from other test series [28,1][52,1][70,-1][74,1][84,2] are compared with the calculation in Fig.4.4.10 ~ Fig.4.4.13. The parameters in the calculations are kept on the same values as above.

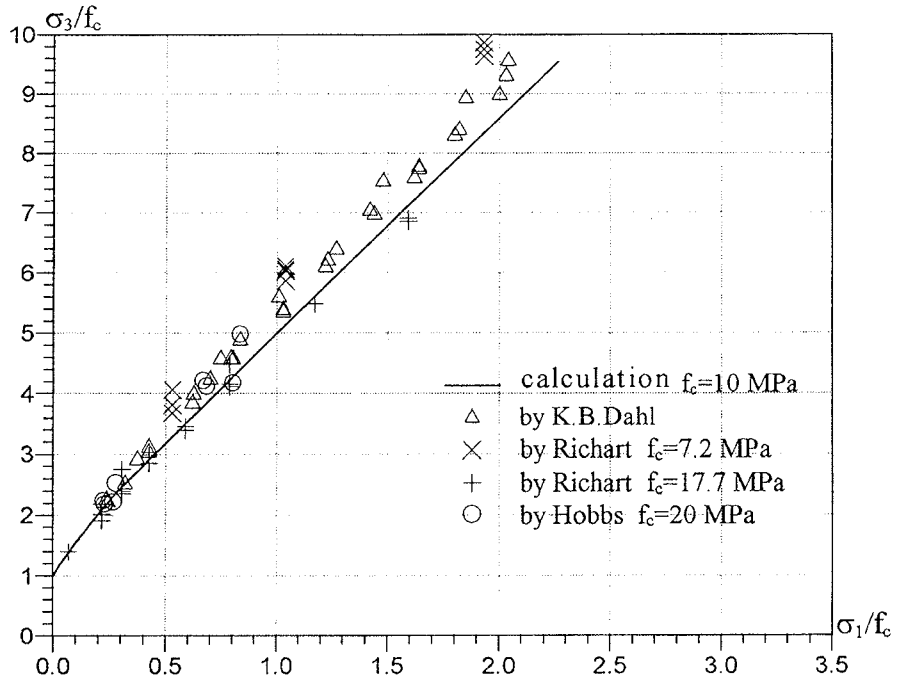

Fig.4.4.10 Comparison with test results from [28,1][74,1]

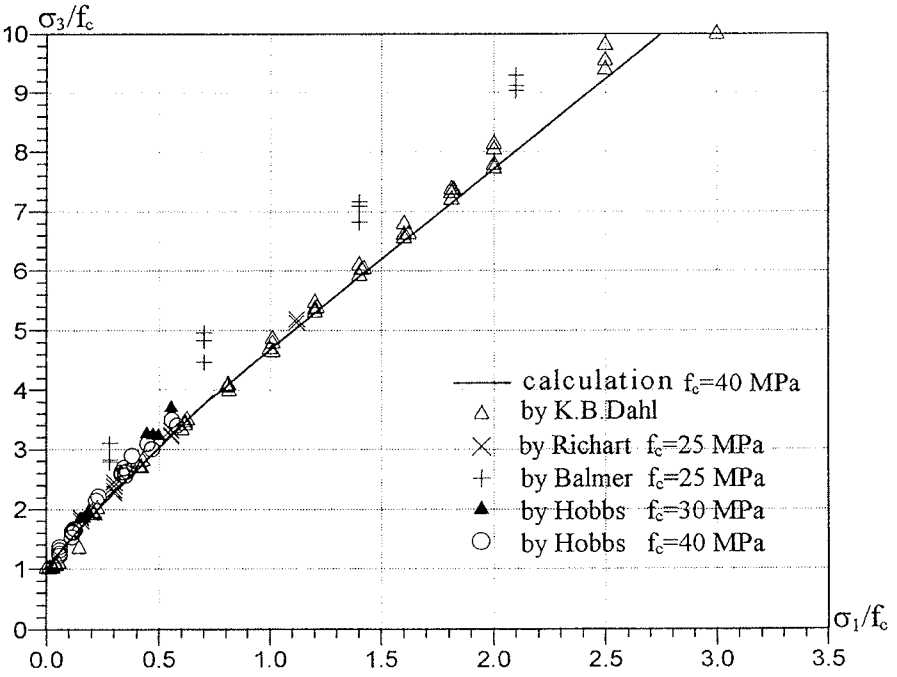

Fig.4.4.11 Comparison with test results from [28,1][52,1][70,1][74,1]

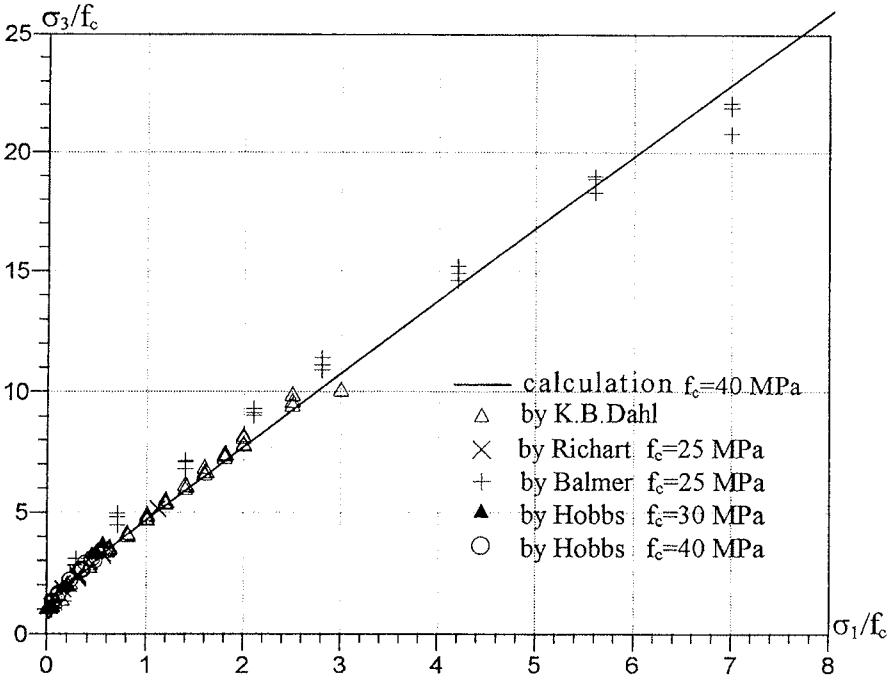

Fig.4.4.12 Fig.4.4.11 continued for large ratios of σ_1/f_c

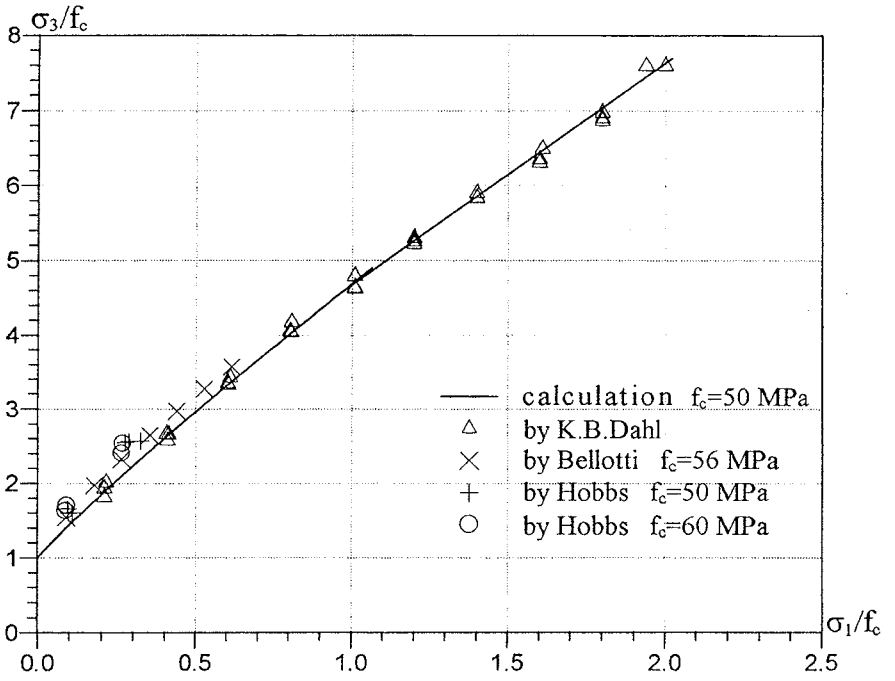

Fig.4.4.13 Comparison with test results from [84,1][74,1]

It is seen that the agreement between the tests and the calculation is fairly good. The increased rate of σ_3 versus σ_1 for small σ_1 values is similar to what was observed in [92,1].

As for pure cement paste, the hydration degree of concrete varies with the water/cement ratio. Hence, it is expected that, for higher concrete strength, the hydration degree will be lower, which results in a larger portion of hard unhydrated cement particles. Take the test group B070 as an example. If we calculate the volume ratio of hard particles based on the hydration degree as a function of the water/cement ratio as shown in Fig.3.5.4, m′=0.183 will be obtained. A corresponding σ_3-σ_1 curve for concrete is shown in Fig.4.4.14 where all the parameters have been adopted from the test group B070. In the figure, the curve obtained by applying m′ determined on the basis of the fixed hydration degree in table A.1.1 is also shown. It can be seen that the difference between
the two curves is not substantial even though the inclination of the curve in the transition part is raised up for larger m′. Therefore, in the following compari-

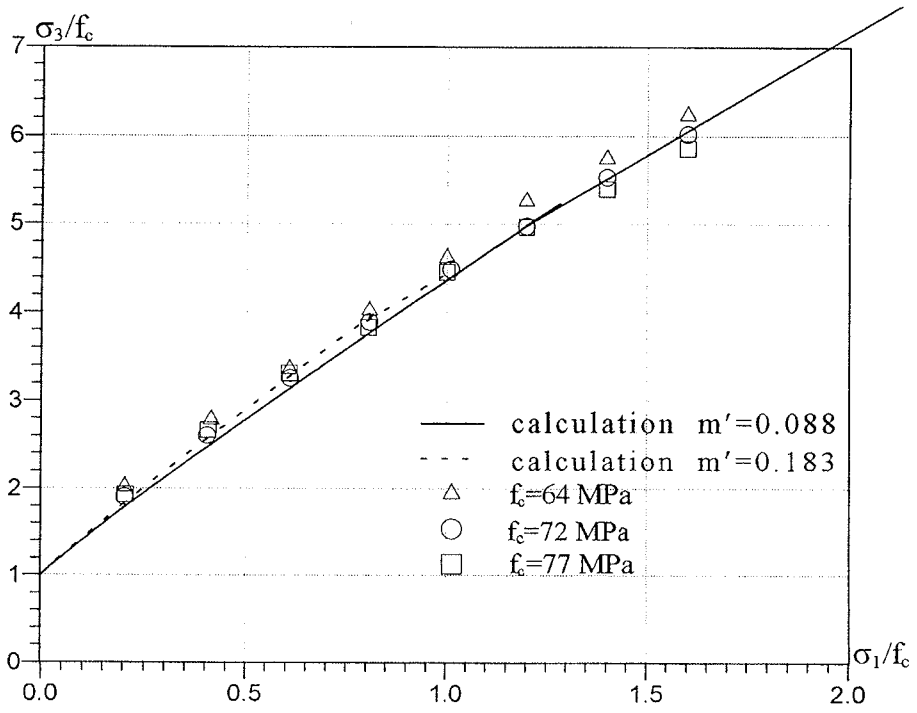

Fig.4.4.14 Calculations with different m′ for the test group B070

sons, the results based on the fixed hydration degrees in table A.1.1 will be used.

4.5 Friction angle of concrete

Since, according to the model, it is not possible to define a failure condition in τ-σ space for concrete due to the anisotropy introduced by the cracking, similarly it is not possible to define an angle of friction for concrete.

However, it might be interesting to compare the inclination of the σ_1-σ_3 curve for large side pressures with the inclination obtained for a Coulomb material with a corresponding value of the friction angle $\varphi_{con.}$.

Table 4.5.1 lists the parameter λ, the effective volume ratio of aggregate $\lambda\kappa_a$, the inclination of the σ_3-σ_1 curve $k=\tan\alpha/\tan\gamma$ under large confining pressure, and the friction angle $\varphi_{con.}$ for different test groups. Here $\sin\varphi_{con.}=(k-1)/(k+1)$ and k is taken from the calculation when the confining pressure is in the range of high confining pressures.

Table 4.5.1 Apparent friction angle for concrete

	B010	B035	B050	B070	B085	B100	B110
λ	1.0	0.97	0.92	0.84	0.83	0.89	0.93
$\lambda\kappa_a$	0.75	0.67	0.65	0.60	0.61	0.64	0.61
$k=\tan\alpha/\tan\gamma$	3.6	3.0	2.9	2.7	2.7	2.9	2.7
$\varphi_{con.}$	34.4°	30.0°	29.2°	27.4°	27.4°	28.3°	27.4°

In plastic theory, calculations based on the assumption of a Coulomb or a modified Coulomb material with the friction angle of φ=37°, in most cases, works well for normal strength concrete. However, the friction angle, deduced by the test results from [92,1][95,1], seems to vary with the strength of concrete. The value of $\varphi_{con.}$ versus f_c is depicted in Fig.4.5.1.

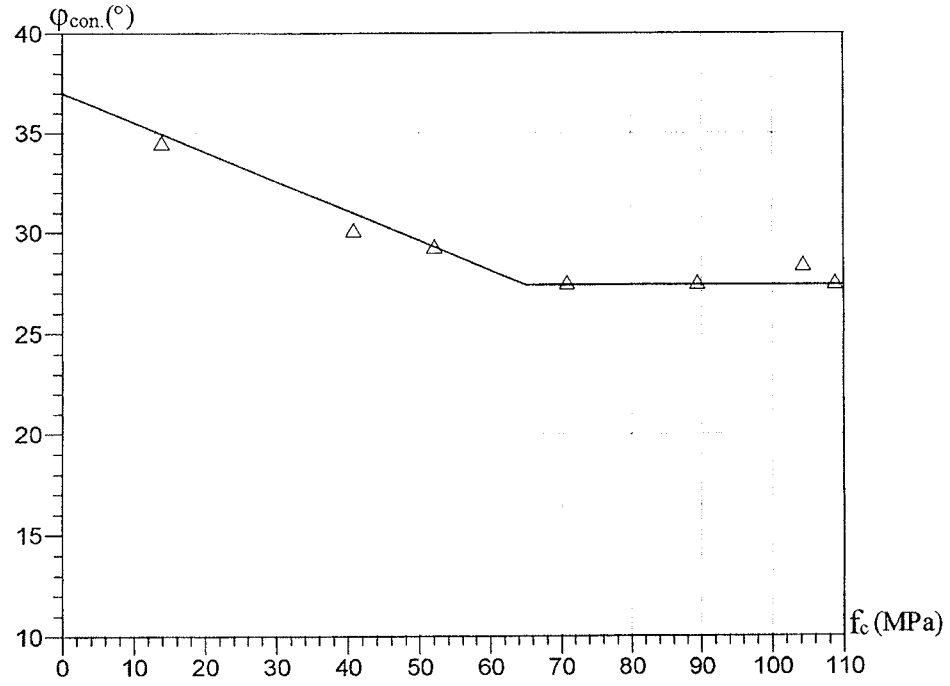

Fig.4.5.1 Friction angle for different strengths of concrete

It appears that $\varphi_{con.}$ decreases approximately linearly with increasing f_c up to about 70MPa. For f_c>70MPa, the friction angle seems to be a constant around 27°.

The reason for this is clearly that for the higher strengths, the effective volume ratio of the aggregates is lower than for the lower strengths, which will normally be the case.

In Fig.4.5.2 the effective volume ratio $\lambda\kappa_a$ has been plotted against the concrete strength f_c. The similarity of the two curves, Fig.4.5.1 and Fig.4.5.2, is evident.

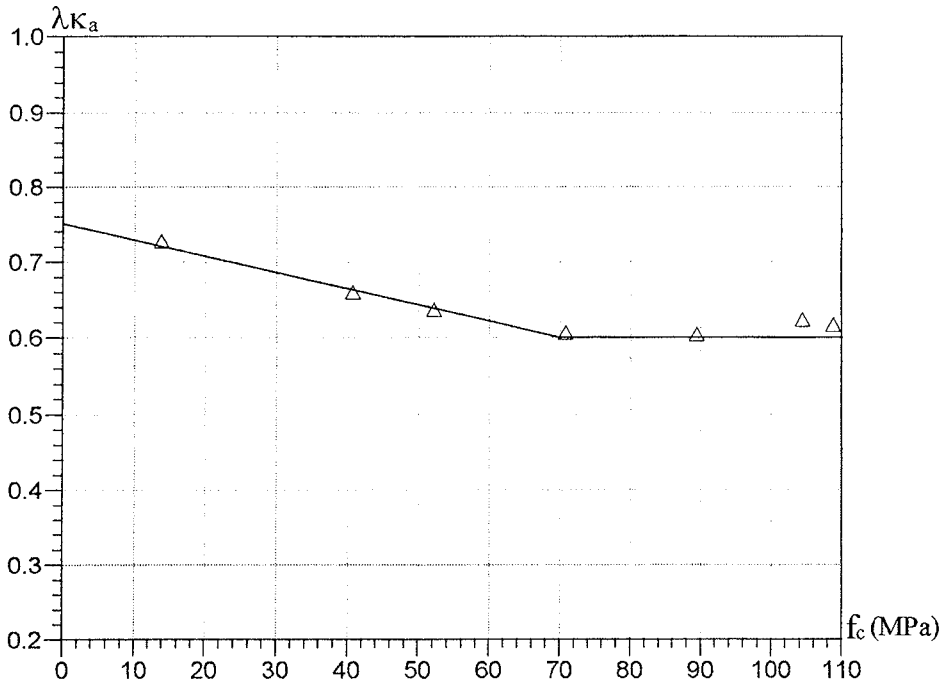

Fig.4.5.2 Effective volume ratio of aggregates for different strengths of concrete

4.6 Ratio of lateral strains to axial strains in uniaxial compression

The inclination k_0 of the σ_3-σ_1 curve at σ_1=0, the uniaxial compressive stress state, found for the different test groups is listed in table 4.6.1.

Table 4.6.1 Inclination of σ_3-σ_1 curve k_0 at σ_1=0 for the different test groups

test group	B010	B035	B050	B070	B085	B100	B110
k_0	6.3	5.1	4.8	4.3	4.3	4.8	4.5

These results are based on fixed hydration degrees of cement. Obviously, for high strength concrete, higher values of k_0 than those listed in the table above will be obtained if a hydration degree varying with the water/cement ratio is applied in the calculation. However, in what follows, we will use the values in the table.

We will now turn to the predictions of the model regarding strains. Consider

Fig.4.6.1 which is the same as Fig.4.2.1. The horizontal component of the displacement u is denoted u_1 and the vertical component u_3. We find

$$u_1 = u\cos(\gamma-\varphi) \qquad u_3 = u\sin(\gamma-\varphi) \tag{4.6.1}$$

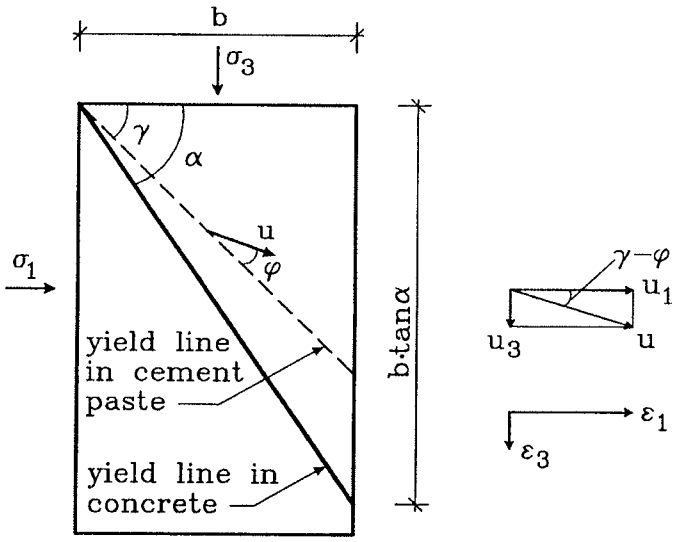

Fig.4.6.1

If the relative displacement u is shared uniformly by a large number of parallel yield lines, we get in the limit a homogeneous strain field characterized by a horizontal strain

$$\varepsilon_1 = \frac{u_1}{b} \tag{4.6.2}$$

and a vertical strain

$$\varepsilon_3 = \frac{u_3}{b\tan\alpha} \tag{4.6.3}$$

The ratio $\varepsilon_1/\varepsilon_3$ is therefore

$$\frac{\varepsilon_1}{\varepsilon_3} = \frac{\tan\alpha}{\tan(\gamma-\varphi)} \tag{4.6.4}$$

Normally there will also be an angular strain in these directions.

Having a single yield line, the average strains measured along the length b and btanα respectively of course will have the same ratio. However, when using other lengths the average strain will vary with the measuring length.

The strains could also be calculated by determining them in a coordinate system with one axis along the yield line and transferring to a coordinate system with horizontal and vertical axes respectively, see [84,1], section 3.4.2.

The strains calculated are to be considered as strain increments or time derivatives of strains at the onset of yielding.

Now comparing with formula (4.2.15), it appears that the normality condition is fulfilled, i.e. the strain increments ε_3 and ε_1 considered as a vector is a normal to the σ_3-σ_1 curve. This is valid even when the concrete material is not, according to the model, an isotropic plastic material, but a material with load induced anisotropy because of the cracking in the σ_3 direction.

It follows from the above that the ratio of the lateral strain increment to the axial strain increment at failure equals k_0 in uniaxial compression.

Fig.4.6.2 shows the curves of axial strain versus lateral strain in uniaxial compression, corresponding to different loading directions relative to the casting surface, obtained in [86,1]. The specimens were cubes. The water/cement ratio was 0.5 and the uniaxial compressive strength of the specimens was about 40MPa. In the tests, the specimens were loaded by means of brush bearing platens. Thus, the deformation constraints imposed by the loading system was minimized. It can be seen that the lateral strain when σ_3 is parallel to the casting surface is larger than when σ_3 is perpendicular to the casting surface. This is understandable because the concrete in sections parallel to the casting surface may have voids and more microcracks and thus larger deformations are expected.

(a).

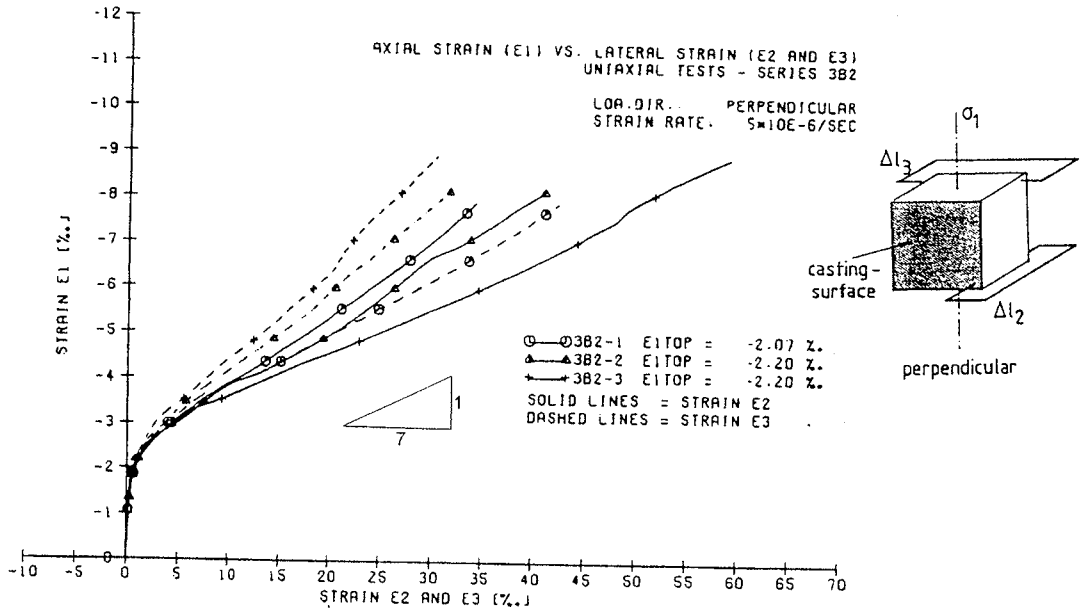

(b).

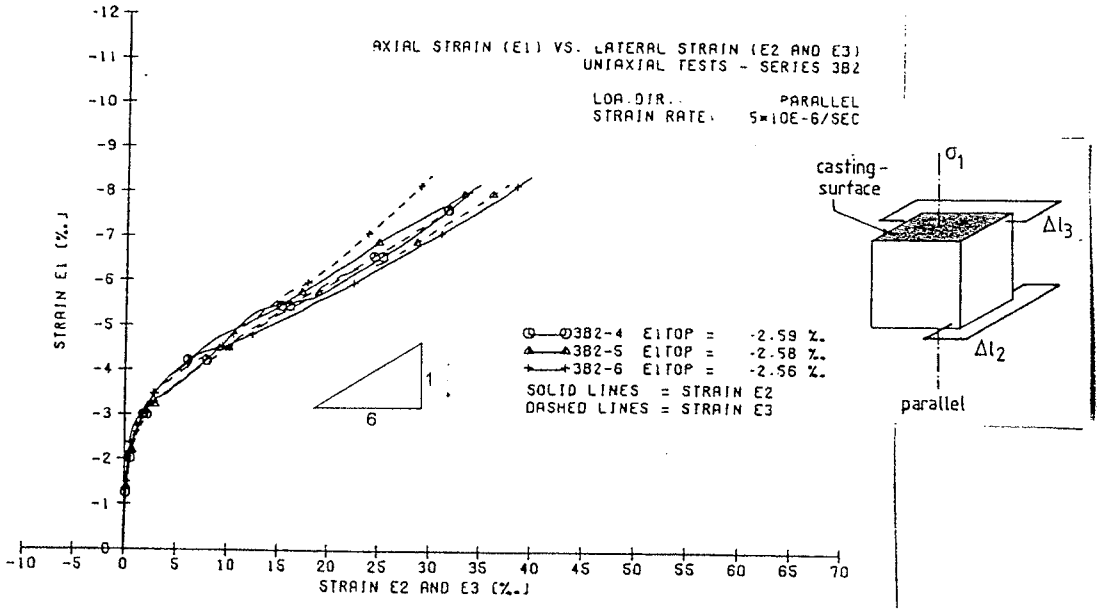

Fig.4.6.2 Axial strain versus lateral strain reported in [86,1]
Note: The notations used in the figure differ from that of the paper.

From the curves it is seen that the ratio of the lateral strain increments to the axial stain increments is about 7 when the axial load σ_3 is perpendicular to the

casting surface and about 6 when σ_3 is parallel to the casting surface. These values are close to the ones obtained in the calculations.

The result is quite remarkable since a considerable softening takes place after the peak value of the load is reached. It means that the model is able to predict the right order of the ratio of strain increments not only at the onset of yielding but also in the softening range. According to plastic theory for a Coulomb material with φ=37°, the ratio of the lateral strain increment to the strain increment in the σ_3-direction would be 4, which is too low.

4.7 Location of failure lines

In plastic theory for a Coulomb material, the yield line in a cylinder or prism is located as shown in Fig.4.7.1(a), i.e. the inclination of the yield line h/b becomes 2 if the friction angle of concrete is taken to be 37°.

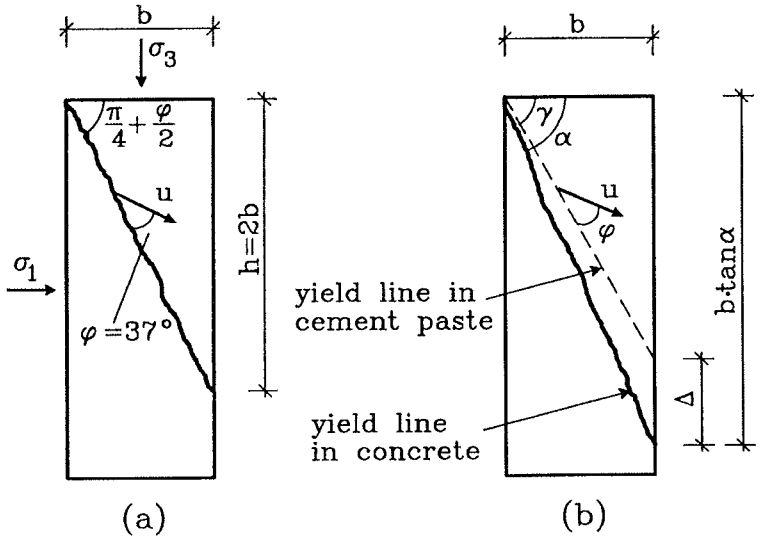

normal assumption *model of this paper*

Fig.4.7.1 Location of the yield line

According to the micromechanical model of this paper, the location of the yield line is as shown in Fig.4.7.1(b). The apparent friction angle of cement paste φ is related to the confining pressure, so is the inclination of the yield line tanα. The values of tanα for the different test groups under different lateral confining

pressures, expressed as a function of the ratio of σ_1/σ_3, are listed in table 4.7.1.

Table 4.7.1 Inclination of the yield line tanα at different ratios of σ_1/σ_3

test group	B010	B035	B050	B070	B085	B100	B110
σ_1/σ_3=0.00	5.1	3.4	3.2	2.8	2.8	3.0	2.8
σ_1/σ_3=0.05	3.3	2.9	2.8	2.6	2.6	2.7	2.6
σ_1/σ_3=0.10	2.8	2.6	2.6	2.4	2.4	2.5	2.4

Fig.4.7.2 shows pictures of specimens after failure taken from [86,1]. In the figure, (a) refers to constant stress ratio experiments and (b) to constant displacement ratio experiments. The uniaxial compressive strength of the specimens in the test series reported in [86,1] was close to that of the test groups B035 and B050. It may be verified that the values of the inclination found in the experiments are very close to what has been obtained in the calculations for the test groups B035 and B050 at σ_1/σ_3=0.05.

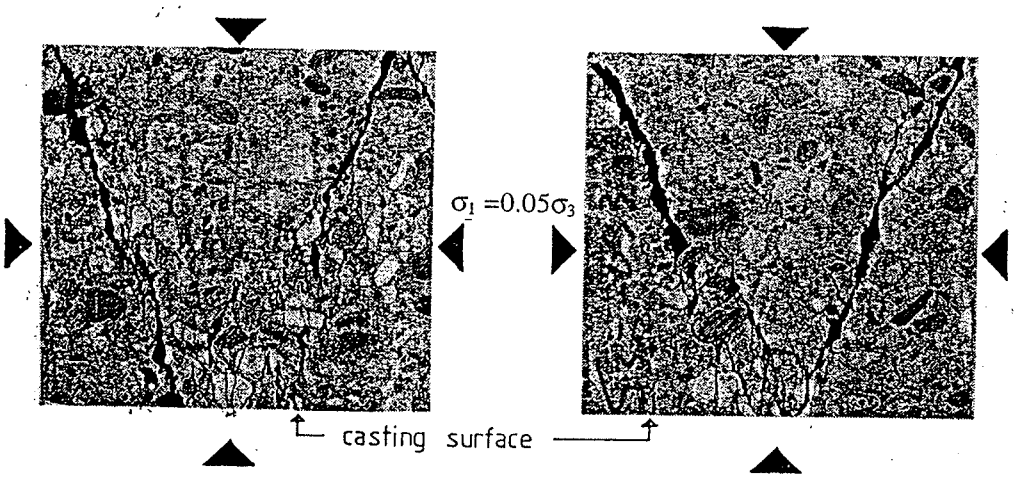

(a). constant stress ratio experiments

Fig.4.7.2 The location of yield lines with σ_1/σ_3=0.05 in specimens from [86,1]

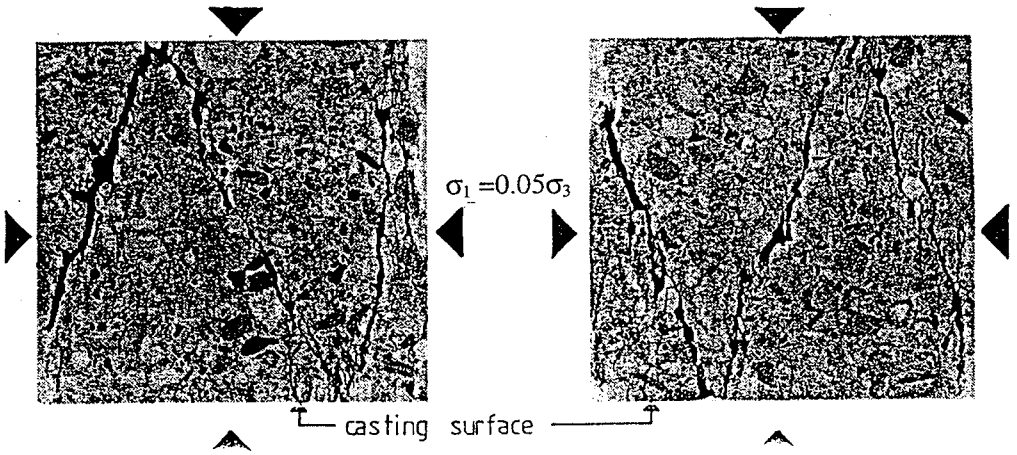

(b). constant displacement ratio experiments

Fig.4.7.2. (continued)

4.8 Effect of microcracking on the uniaxial compressive strength

It appears from the previous calculations that the strength is considerably affected by the extent of microcracking in the specimens. The damage factor η due to microcracking applied in the calculations is found by calibrating the parameters to give the result $\sigma_3=f_c$ when the lateral confining pressure $\sigma_1=0$. In other words, the value of η determined in this way may be regarded as an indication of the state of microcracking in the specimen when it has the measured uniaxial compressive strength. However, the extent of microcracking in the specimens may be increased due to change of curing conditions or due to chemical reactions and external loading. Thus, the strength is reduced correspondingly.

The uniaxial compressive strength found by the model with an increased damage factor η is designated by f_c^*. The ratio of f_c^*/f_c as a function of the damage factor η is depicted in Fig.4.8.1.

Fig.4.8.1 demonstrates that the uniaxial compressive strength decreases almost linearly with increasing damage factor. The decreasing rate for different

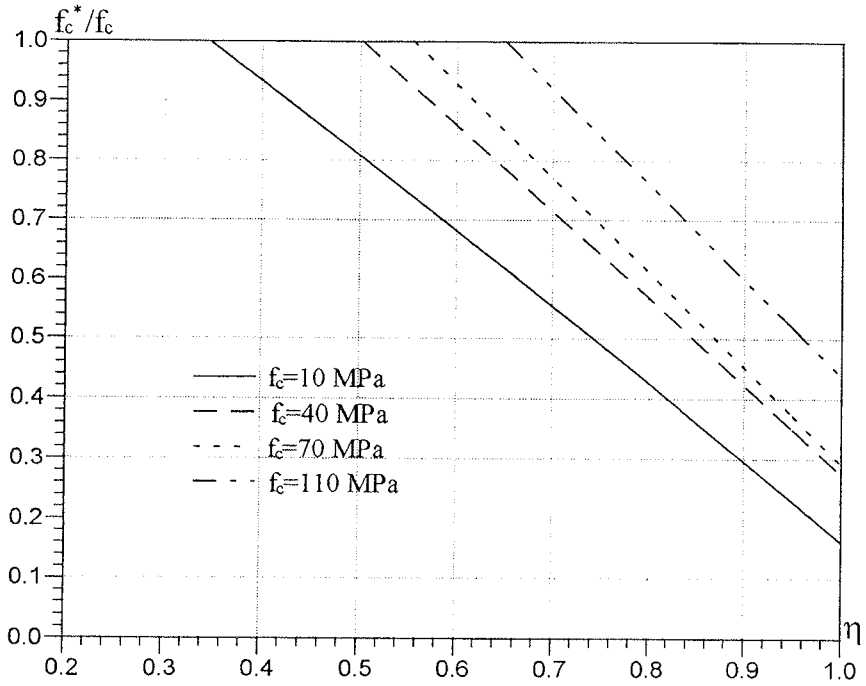

Fig.4.8.1 Influence of microcracking of concrete on the uniaxial compressive strength

strengths is approximately the same. The specimens with higher strength are more microcracked in the state of uniaxial compression.

The uniaxial compressive strength is reduced about 30% if the damage factor is increased by about 0.25.

In [93,2] the uniaxial compressive strength of concrete was measured as a function of the total number of cracks in the cement paste. The concrete had a rather high micro silica content (about 15%) and the internal cracks developed during a period of 12 years. Fig.4.8.2 shows a clear dependency of the compressive strength on the number of cracks.

As stated previously, the relationship between the damage factor η used in this paper and the number of cracks can not yet be established. The measurements in [93,2] seem to be the only one reported in the literature and they are probably not sufficient for a reliable calibration. Thus, the number of cracks can not yet be directly used in the model to predict the reduced strength. However, these

measurements confirm that the strength is strongly affected by the cracking of the material.

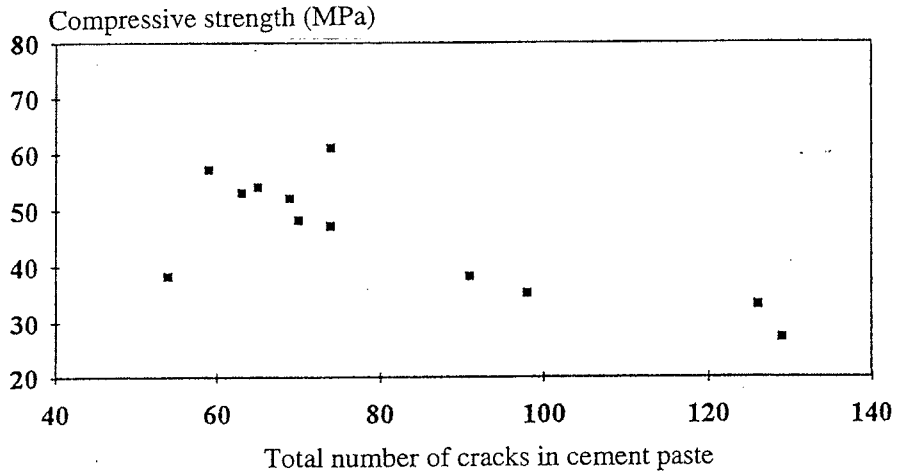

Fig.4.8.2 Compressive strength versus the total number of cracks in the cement paste [93,2]

4.9 Lower bound solutions

The model developed has been based on upper bound solutions since these are much simpler to deal with in this case compared with lower bound solutions. For a composite material like concrete lower bound solutions in general will be extremely complicated. However, to get an idea of how the stresses are carried, let us make a simple lower bound estimate in the case where the confining pressure is so high that the strength of the cement paste is not influenced by the unhydrated cement grains.

Further we assume that the aggregate particles are closely packed, so they may act as a granular friction material carrying the load by concentrated forces in the points of contact between the particles. These forces may of course have to pass through a thin layer of cement paste, since in concrete normally the cement paste volume is higher than the voids of the aggregates in dry condition. Otherwise the concrete will not be workable.

In Fig.4.9.1 the Coulomb yield conditions for cement paste and for the

aggregates are shown. The cement paste is a frictionless material with the cohesion c and the aggregate particles form a cohesionless material with the friction angle φ.

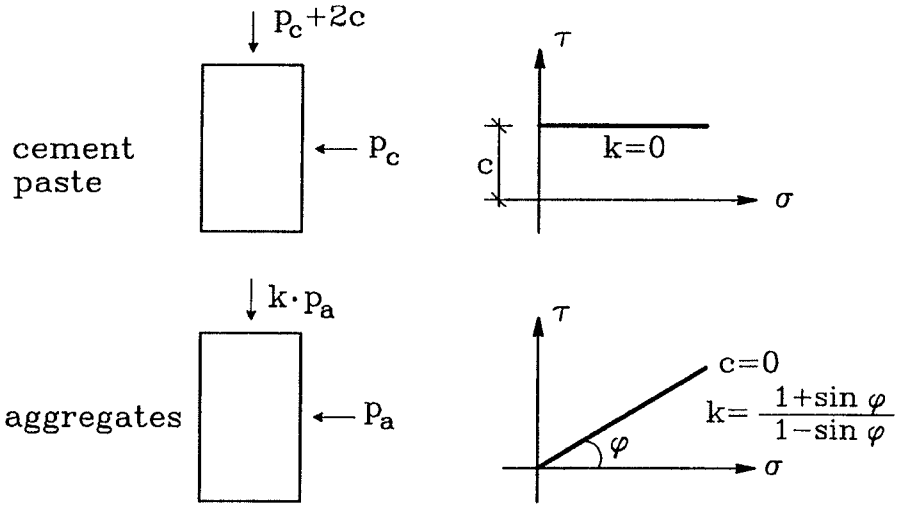

Fig.4.9.1

If the cement paste carries the confining pressure p_c, the axial stress carried by the cement paste will be p_c+2c. If the aggregates carry the confining pressure p_a, the axial stress carried by the aggregates will be kp_a, where $k>1$ is determined by formula (2.4.2.4). The stress field in the cement paste must be extended unchanged through the aggregate particles to fulfill equilibrium conditions.

If the total confining pressure is

$$\sigma_1=p=p_c+p_a \tag{4.9.1}$$

the total axial stress carried will be

$$\sigma_3=\sigma=p_c+2c+kp_a=p_c(1-k)+2c+kp \tag{4.9.2}$$

For a given confining pressure p the axial stress σ reaches the highest value when the confining pressure carried by the cement paste $p_c=0$, and we have

$$\sigma = 2c + kp \qquad (4.9.3)$$

This is precisely the type of load carrying capacity we have obtained for high confining pressure by means of the upper bound solutions.

If the friction angle of the aggregate particles is known, k may be calculated and the load carrying capacity for sufficiently high confining pressures may be obtained by means of formula (4.9.3).

For high confining pressure there is agreement between the upper bound and the lower bound solutions.

If this is the way the stresses are carried, the model may be said to provide a means of calculating the friction angle of the aggregate particles as a function of the effective volume ratio of aggregates.

For low values of aggregate volume ratios, it is not likely that the aggregate particles act simply by point contact, so the above stress field may be doubtful in this case. However, the upper bound solutions still seem to be able to predict the load carrying capacity accurately, also for low aggregate volume ratios.

Further, the upper bound method is probably the only simple way of dealing with the transition region from uniaxial stress to sufficiently high confining pressures, i.e. pressures for which the effect of the unhydrated cement grains is eliminated.

Finally, the upper bound method is the only method which may be used to give an estimate of the strain increments at failure and the locations of the yield lines. As appears from the above, the strain increments and the locations of the yield lines predicted by the model are quite different from what would be predicted by using the normality condition of the theory of plasticity and a Coulomb failure criterion.

These remarks justify the development of the model.

4.10 Conclusions and discussion

From the calculations and comparisons presented above, the following conclusions may be drawn:

1). The uniaxial compressive strength of cement paste and concrete are equal if the change of the microcracking state in the cement paste due to the addition of aggregates is small.

2). The function of aggregates, according to the model of this paper, is to displace the yield line which would be formed in pure cement paste to a steeper position. In triaxial compressive stress states, cracks around the aggregates lying mainly in the direction of the axial load are formed, and sliding occurs along yield lines in the cement paste which will bridge the cracks along the aggregate particles at failure. The inclination of the yield line in concrete depends on the effective part of aggregates, i.e. the part which can resist the sliding displacements. Normally, the higher the strength of the cement paste, the lower the effective part of the aggregates, and the flatter the yield line in concrete.

3). Compared with a Coulomb material, the apparent friction angle observed in tests decreases with increasing compressive strength of concrete when $f_c \leq 70$MPa and beyond this it is almost constant.

4). The Coulomb failure criterion, using a friction angle depending on the uniaxial compressive strength, is valid when the lateral confining pressure is relatively large. However, the apparent uniaxial compressive strength, which is found as the intersection point of the straight Coulomb line with the σ_3-axis, is higher than the measured uniaxial strength. In the transition region between the range where the straight Coulomb line is valid and uniaxial compression, a curved failure condition seems more rational.

It has to be emphasized that the model proposed here needs further refinements, regarding the location of the interfacial cracks and their directions, the description of microcracking in the cement paste, the influence of the water/ce-

ment ratio on the hydration degree of cement and several other minor points. However, from the results obtained, it seems that the load carrying capacity and the location of the yield lines may be predicted by the model fairly well.

On the basis of the analysis performed it is reasonable to conclude that compressive failures in concrete are not only governed by cracking in sections in the direction of the axial load but also to a large extent by shear failure in the cement paste. Therefore it seems impossible to predict compressive strengths only on the basis of Mode I crack growth using Fracture Mechanics.

V. Micromechanical modelling of failure of cement paste and concrete in tension

Since the tensile failure is much more brittle than the compressive failure, it is normally assumed that tensile failure must be described by a fracture mechanics approach. This is undoubtedly correct at least for larger specimens. However it would be interesting to investigate the results of a plastic calculation even for tension. The results may be valid for small specimens with a homogeneous stress field where crack growth plays only an inferior role.

5.1 Failure modelling of cement paste in pure tension

As stated in previous sections, when cement paste is subjected to compression, sliding surfaces are formed in front of the hard unhydrated cement particles. What will happen if the cement paste is subjected to pure tension?

Since the cement paste is microcracked because of shrinkage of the cement gel around the hard unhydrated cement grains and other reasons, it may be assumed that the most dangerous yield line will pass around the hard, unhydrated cement grains. Even if cracks are connecting all the cement grains, in a yield line a certain amount of energy is required to pull the embedded hard unhydrated cement particles out of the cement gel because a considerable sliding resistance around the hard unhydrated cement particles still remains. Hence, the bond between the hard particles and the cement gel will provide a certain sliding resistance. The relative displacement along the yield line may in pure tension be assumed to be perpendicular to the yield line. Therefore, bond cracks are assumed to be formed due to the loading in sections parallel to the yield line and we may neglect the contribution to the dissipation from such sections. What remains is the sliding resistance offered by sliding surfaces around the unhydrated cement particles which means that a zig-zag shaped yield line is formed as shown in Fig.5.1.1. The friction angle of hardened cement paste is assumed zero as in compression.

Since the unhydrated cement grains are pulled out from the side with the least resistance, the average depth for pull out is d/4, where d is the average diameter of the unhydrated cement grains. The state of microcracking in the cement paste is assumed the same as in compression. For convenience, the unhydrated cement grains are depicted as cubes in the following figures.

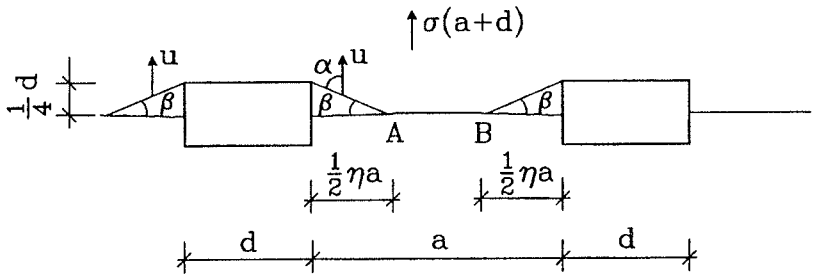

Fig.5.1.1 Failure mode of cement paste in pure tension

According to plastic theory, the internal work for this failure mechanism becomes, details see [77,1][84,1],

$$W_I=2\cdot u\cdot[\frac{1}{2}f_{cc}(1-\sin\alpha)+f_{tt}\sin\alpha]\cdot\frac{\frac{1}{4}d}{\sin\beta}+f_{tt}\cdot L_{AB}\cdot u$$

$$=\frac{1}{2}(\frac{1}{2}f_{cc}\frac{1-\cos\beta}{\sin\beta}+f_{tt}\cot\beta)\cdot d\cdot u+f_{tt}\cdot L_{AB}\cdot u \qquad (5.1.1)$$

where

$L_{AB}=(1-\eta)a$ if $d/\tan\beta<2\eta a$

$=a-d/2\tan\beta$ if $d/\tan\beta\geq 2\eta a$

The external work is

$$W_E=\sigma\cdot u\cdot(a+d)$$

The work equation $W_I=W_E$ yields:

$$\sigma=\frac{1}{2}(\frac{1}{2}f_{cc}\frac{1-\cos\beta}{\sin\beta}+f_{tt}\cot\beta)\frac{d}{a+d}+f_{tt}\frac{L_{AB}}{a+d}$$

As stated in section 3.3.1, the ratio of d/(a+d) is related to the volume ratio of the unhydrated cement particles by

$$\frac{d}{a+d}=\frac{3}{2}m'$$

Hence

$$\sigma=\frac{3}{4}\left(\frac{1}{2}f_{cc}\frac{1-\cos\beta}{\sin\beta}+f_{tt}\cot\beta\right)m'+f_{tt}\left(1-\frac{3}{2}m'\right)\frac{L_{AB}}{a} \qquad (5.1.2)$$

The minimum is obtained when $\beta=\beta_{min}$ where $\tan\beta_{min}=d/2a=1.5m'/(2-3m')$. Thus, the tensile strength for cement paste in pure tension, denoted by f_{tp}, obtained in this way is:

$$f_{tp}=\frac{3}{4}\left(\frac{1}{2}f_{cc}\frac{1-\cos\beta_{min}}{\sin\beta_{min}}+f_{tt}\cot\beta_{min}\right)m' \qquad (5.1.3)$$

In this failure mode, the tensile strength f_{tp} is closely related to the volume ratio of hard particles m′, but independent of the state of microcracking in the cement paste.

Parameters used for the calculations in the previous sections are adopted here. Some values of f_{cc} and m′ for cement paste are extrapolated from those valid for concrete with a similar uniaxial compressive strength f_c. The results of f_{tp} for different f_c are listed in table 5.1.1, where the value of m′ is estimated by assuming a fixed hydration degree of cement taken from table A1.1.

Since the hydration degree of cement varies with the water/cement ratio in the mix, calculations with m′ based on the curves of hydration degree versus water/cement ratio in Fig.3.5.4 have also been performed. The hydration degrees of cement corresponding to different water/cement ratios for each test group in [92,1] are listed in table A.1.1 in Appendix. The results are shown in table 5.1.2.

It can be seen that the ratio of f_{tp}/f_c is increased especially for higher value of m′ but not proportional, because the angle of the sliding surface changes considerably, too.

Table 5.1.1 Tensile strength f_{tp} with m′ based on fixed hydration degrees of cement

f_c (MPa)	f_{cc}/f_c	m′ (%)	f_{tt} (MPa)	β_{min} (°)	f_{tp} (Mpa)	f_{tp}/f_c (%)
10	1.23	6.62	1.11	3.2	1.0	10.1
40	1.50	9.20	2.45	4.6	2.2	5.5
50	1.62	8.53	2.85	4.2	2.6	5.2
70	1.66	8.81	3.41	4.4	3.1	4.4
85	1.68	11.4	3.78	5.9	3.4	4.1
110	1.76	12.47	4.40	6.6	4.1	3.7

Table 5.1.2 Tensile strength f_{tp} with m′ based on varying hydration degrees of cement

f_c (Mpa)	f_{cc}/f_c	m′ (%)	f_{tt} (Mpa)	β_{min} (°)	f_{tp} (Mpa)	f_{tp}/f_c (%)
10	1.23	6.62	1.11	3.2	1.0	10.1
40	1.50	11.34	2.45	5.9	2.2	5.4
50	1.62	13.35	2.85	7.1	2.5	5.1
70	1.66	18.45	3.41	10.8	3.2	4.6
85	1.68	25.34	3.78	17.0	4.4	5.1
110	1.76	36.10	4.40	30.6	9.2	8.3

Here, the tensile strength of unmicrocracked cement paste f_{tt} has been put equal to $\sqrt{0.1f_{cc}}$ as before. Obviously, by changing f_{tt}, f_{tp} will be changed correspondingly. However, more accurate values of f_{tt} are not available at the moment.

In the following, f_{tt} will be kept at the value stated.

5.2 Failure modelling of cement paste subject to shear tension

It would be interesting to compare the tensile strength obtained in the previous section with the tensile strength obtained as the limiting case $\tau=0$ of the shear model of section 3.3, where the sign of σ is changed, i.e. $\sigma<0$. In this way the whole shear failure condition in σ-τ space with the normal stress both tensile and compressive may be obtained as illustrated in Fig.5.2.1. The parameters for the test group B010 from [92,1] have been applied here.

The tensile strength for cement paste subjected to shear tension, which is found at the point where $\tau=0$, is designated by f_{ts}. The values of f_{ts} for test specimens of different uniaxial compressive strengths from [92,1] are listed in table 5.2.1. Here, the parameters applied in the calculation are the same as for the compressive calculation and m′ has been estimated using fixed hydration degrees of cement.

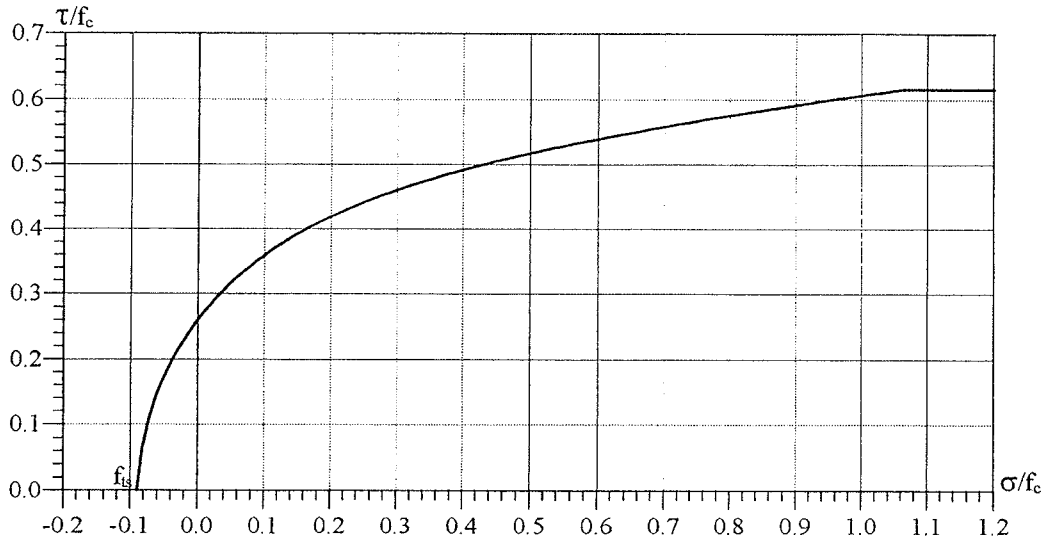

Fig.5.2.1 Shear failure condition with tensile as well as compressive normal stresses

Table 5.2.1 Tensile strength f_{ts} with m′ based on fixed hydration degrees of cement

f_c(Mpa)	10	40	50	70	85	110
f_{ts}(Mpa)	0.9	3.3	3.9	5.4	7.7	10.7
f_{ts}/f_c(%)	9.2	8.2	7.8	7.7	9.0	9.7

The influence of m′ on f_{ts} is the same as on f_{tp}.

Compared with the values of f_{tp}/f_c in table 5.1.1, it is seen that, using the same parameters in the calculations, the tensile strength of cement paste failing in pure tension is smaller than that when failing in shear tension. This implies that cement paste is more likely to fail in tension before any sliding can take place. This explains why cement paste is such a brittle material in pure tension.

Therefore, for $f_{tp}<f_{ts}$ a tension cut off must be introduced in the failure condition.

5.3 Failure of concrete in tension

The tensile behavior of concrete, compared with that of cement paste, is much more ductile, which has been observed in many tensile tests on concrete specimens. In [87,1] the influence of aggregate size under static and cyclic loading is studied. Two of the stress-deformation curves obtained in [87,1] are presented in Fig.5.3.1, where the maximum aggregate size D_{max} is 16mm and 32mm respectively. From the stress-deformation curves, it can be seen that, after the peak value of tensile stress is achieved, a rather sudden drop of the stress will occur followed by a softening branch. Sliding displacements probably take place after the dropping down in stress.

The failure occurring at the peak of loading is termed the primary failure in tension with the corresponding strength f_{tpc}, whereas the failure occurring when sliding takes place in the softening branch is termed the secondary failure in tension with the corresponding stress designated by f_{tsc}. The two different

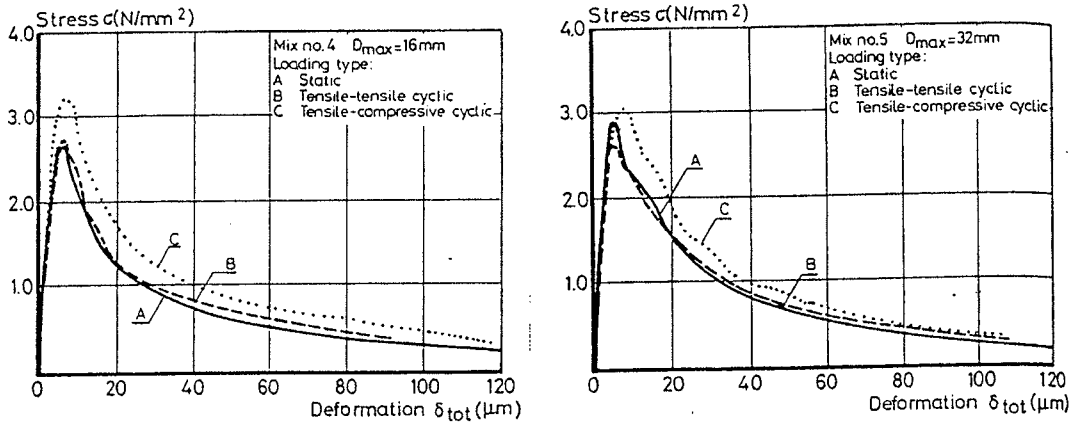

Fig.5.3.1 Average stress-deformation curves for concrete with different aggregate size [87,1]

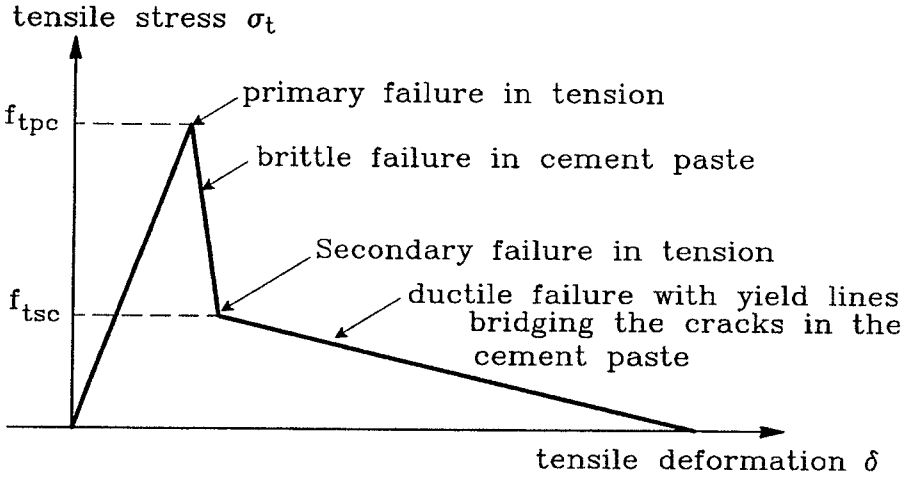

Fig.5.3.2 Simplified stress-deformation curve for concrete in tension

failures are illustrated in the simplified stress-deformation curve for concrete in tension as shown in Fig.5.3.2.

5.3.1 Primary failure in tension

The mechanism of the primary failure may be explained in the following way:

Prior to the peak of loading, cracks will mainly be found around the aggregates, namely the bond cracks, which are more or less perpendicular to the direction of the applied tensile force. At and after the peak of loading, cracks in the cement paste start to bridge those bond cracks, and longer cracks are formed. However, the aggregate particles will stop these cracks. Immediately after the peak it may therefore be assumed that we have a number of more or less parallel cracks stopped by aggregate particles.

Final failure can only take place by sliding failures bridging these cracks. Since the tensile failure in the cement paste is extremely brittle, the failure load corresponding to tensile failure in the cement paste and the load carrying capacity by bridging the tensile cracks can not be added, but the sliding resistance may of course replace the missing tensile stresses along the bond cracks. Therefore, it is natural to expect that the tensile strength corresponding to primary failure in tension equals the tensile strength of the cement paste, i.e. $f_{tpc}=f_{tp}$.

5.3.2 Secondary failure in tension

After the peak of loading is reached, yield lines bridging the tensile cracks in the cement paste are formed. Sliding displacements take place. As in compression, the yield line in the cement paste is displaced because of the aggregate particles being strong enough to resist the sliding through it. The yield line will pass around the aggregates by following the existing bond cracks. Thus, we have a failure pattern similar to that of concrete in compression but with the lateral stress being tensile.

As the tensile lateral stress increases, the displacement of the yield line caused by the aggregates will become larger and consequently the yield line in the cement paste gets steeper. We can not expect the formulas derived in section 4.2 to be valid for such steep yield lines, and it is also rather unlikely that the failure takes place in this way. A different failure pattern must exist. Instead of trying to obtain a failure curve by looking for a different displacement

expression, we will make the following simplifications. Since in the failure curve the distance between pure tension and uniaxial compression is rather short, we may draw a straight line to approximate the failure criterion between the state of uniaxial compression and the tension cut off. The slope of the straight line may be taken the same as the slope for uniaxial compression. The deviation caused by this approximation will be insignificant. In this way the problem is reduced to find the secondary tensile strength in concrete.

When concrete is subjected to pure tension, it is observed that along the fracture plane, most of the aggregate particles are pulled out with sliding surfaces formed around them. Analogous to the analysis of punching failure of concrete slabs subjected to concentrated loads, a similar analysis of shear failure in cement paste may be performed to obtain the secondary tensile strength.

Solutions for concrete slabs subjected to concentrated loads based on plastic theory may be found in [84,1]. The plastic solutions may be used in the following approximate way: consider a cylindrical control surface around the punch at a certain distance, then the average shear stress on the control surface at failure equals the tensile strength of concrete. The control surface is in [84,1] placed at a distance of half the depth of the slab. In the following, this method is applied to obtain the secondary tensile strength of concrete.

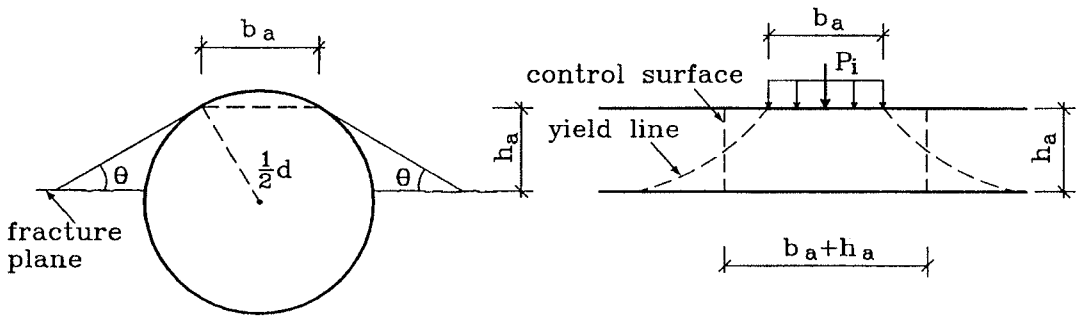

Fig.5.3.2.1

We assume that the aggregates are spheres. In pure tension, the fracture plane is perpendicular to the direction of the tensile force. Analogous to concrete

slabs, we imagine the fracture plane in cement paste as the bottom of the "slab", and the effective depth of the "slab" is the minor of the heights of the aggregates cut by the fracture plane. To transform the geometry of the problem to a punching failure in a slab, we simplify the curved yield lines to straight yield lines being tangents to the aggregate particles and forming an angle θ with the fracture plane. Thus a kind of "platform" is formed at the top of the sphere. A concentrated force is acting on this "platform", as shown in Fig.5.3.2.1. In this way, the length of the "concentrated loading area" b_a and the effective depth of the "slab" h_a is found. Taking into account of the random distribution of the aggregates, the average effective depth and the length of the loading area are found to be

$$h_a=\frac{1}{2}\cdot\frac{1}{2}d_i\cos\theta \tag{5.3.2.1}$$

$$b_a=d_i\sin\theta \tag{5.3.2.2}$$

where d_i is the diameter of the aggregate particles.

Since the cylindrical control surface is at a distance of half the depth from the loaded area, the diameter of the cylinder becomes b_a+h_a. Designating the tensile strength of cement paste by $f_{t.cement}$, we find the load carrying capacity of a single particle

$$\begin{aligned}P_i&=\pi\cdot(b_a+h_a)\cdot h_a\cdot f_{t.cement}\\&=\frac{1}{8}\pi d_i^2(\sin2\theta+\frac{1}{2}\cos^2\theta)\cdot f_{t.cement}\end{aligned} \tag{5.3.2.3}$$

The total force is

$$P=\sum P_i$$

Hence the average tensile stress becomes

$$f_{tsc}=\frac{P}{A}=\frac{\sum \frac{1}{8}\pi d_i^2(\sin 2\theta+\frac{1}{2}\cos^2\theta)\cdot f_{t.cement}}{A} \qquad (5.3.2.4)$$

where A is the total area under load.

The mean intercept area of a sphere, according to [70,2], is

$$\overline{A_i}=\frac{1}{6}\pi d_i^2 \qquad (5.3.2.5)$$

Thus eq.(5.3.2.4) can be rewritten as

$$f_{tsc}=\frac{3}{4}(\sin 2\theta+\frac{1}{2}\cos^2\theta)\cdot f_{t.cement}\cdot\frac{\sum \overline{A_i}}{A} \qquad (5.3.2.6)$$

Since according to the theorems of stereology, we have $\frac{\sum \overline{A_i}}{A}=\kappa_a$, κ_a being the volume ratio of the aggregates, we get:

$$f_{tsc}=\frac{3}{4}(\sin 2\theta+\frac{1}{2}\cos^2\theta)\cdot\kappa_a\cdot f_{t.cement} \qquad (5.3.2.7)$$

In punching shear of slabs the bottom of the yield line is normally found at a distance of $1.5h_a$ from the loaded area. This gives $\theta\approx 34°$. For punching in cement paste, no experimental data is available. To get a rough estimation, it might be reasonable to assume that the sliding surfaces become steeper than in concrete. For simplicity, we may take $\theta=45°$. By eq.(5.3.2.7) we get:

$$f_{tsc}\approx 0.94\kappa_a\cdot f_{t.cement} \qquad (5.3.2.8)$$

As discussed previously, the peak values of tensile stress for cement paste f_{tp} and the corresponding concrete f_{tpc} are equal. By putting $f_{t.cement}=f_{tp}=f_{tpc}$ the secondary tensile strength of concrete may be expressed by

$$f_{tsc}\approx 0.94\kappa_a f_{tpc} \qquad (5.3.2.9)$$

In this failure pattern, only relatively large particles can be effective. This means that the volume ratio of aggregates should exclude most of the sand. For normal concrete mixes, the volume ratio of this part is around 0.5~0.6. Thus eq.(5.3.2.9)

gives

$$f_{tsc} \approx \frac{1}{2} f_{tpc}$$

which is close to the plastic tensile strength of concrete usually applied in plastic calculations for concrete where the tensile strength is taken into account.

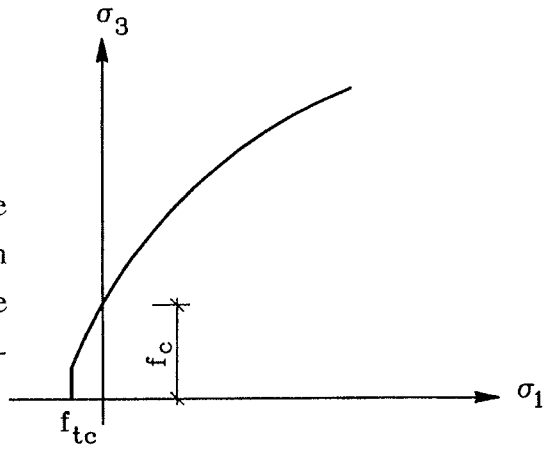

Fig.5.3.2.2

Hence, the failure criterion for concrete in the tensile zone is as illustrated in Fig.5.3.2.2.

5.3.3 Comparison with empirical formulas

Fig.5.3.3.1 shows the proposed uniaxial tensile strength of concrete in the CEB model code 1990 [90,1] and in DS411 [84,3] with some test data from [92,1] included.

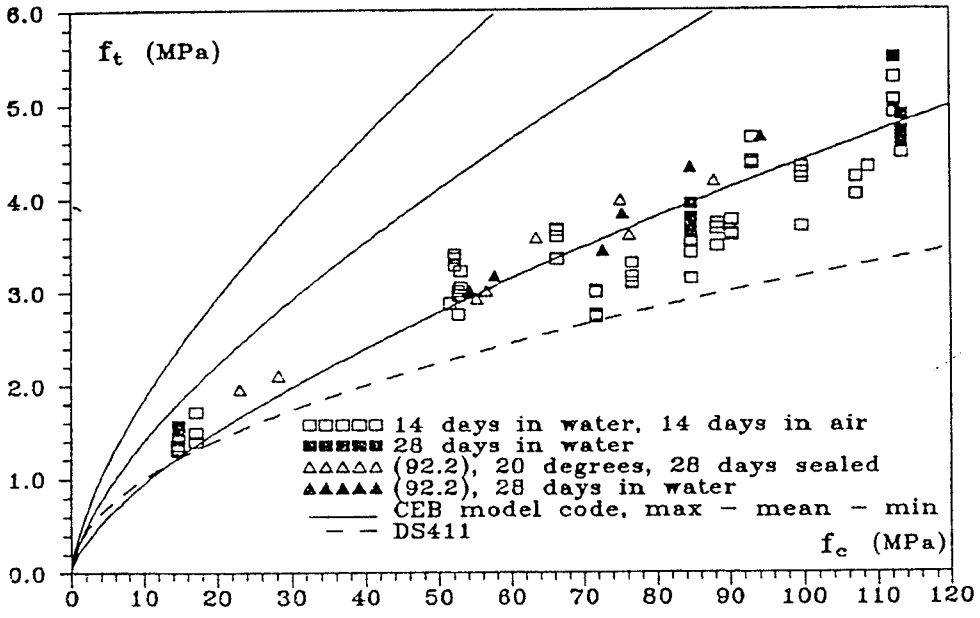

Fig.5.3.3.1 Uniaxial tensile strength of concrete proposed in the CEB model code 1990 [90,1] and in DS411 [84,3]

The uniaxial tensile strength formulas stated in [84,3] and [90,1] are:

$$f_t = 1.0\sqrt{\frac{f_c}{10}} \qquad \text{DS411 [84,3]}$$

$$f_t = 0.95\left(\frac{f_c}{10}\right)^{2/3} \qquad \text{CEB minimum [92,3]}$$

$$f_t = 1.4\left(\frac{f_c}{10}\right)^{2/3} \qquad \text{CEB mean [92,3]}$$

$$f_t = 1.85\left(\frac{f_c}{10}\right)^{2/3} \qquad \text{CEB maximum [92,3]}$$

Here, f_c and f_t are in MPa.

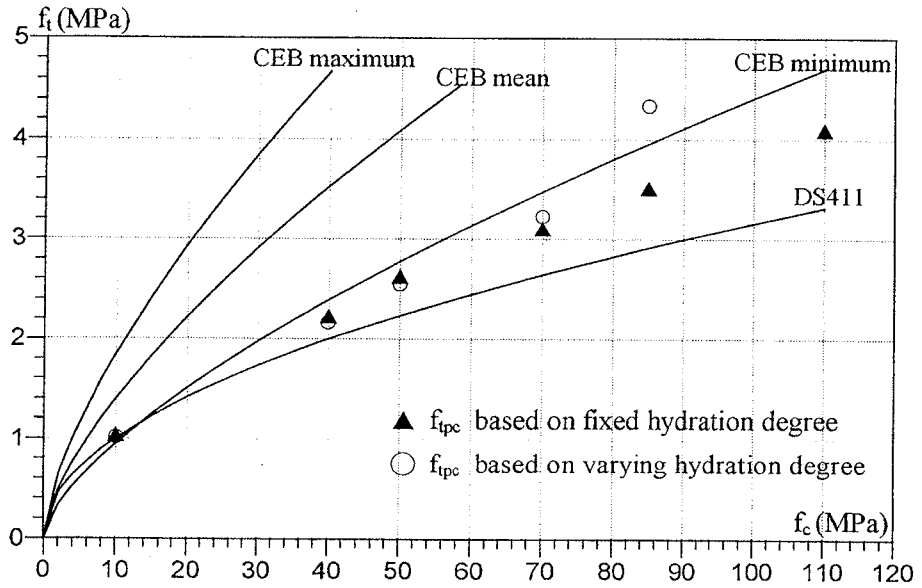

Fig.5.3.3.2 Comparison of f_{tpc} with proposed uniaxial tensile strengths in the CEB model code 1990 and in DS411

Normally, the uniaxial tensile strength measured in tests is the peak value which corresponds to the tensile strength in the primary failure f_{tpc} here. In Fig.5.3.3.2, the tensile strengths f_{tpc} obtained using m′ based on both fixed and on varying

hydration degrees of cement are compared with the proposed uniaxial tensile strengths in the CEB model code 1990 and in DS411.

It seems that the results of f_{tpc} from the calculation are around the CEB model code minimum tensile strengths.

The tensile strength f_{tpc} with m′ based on varying hydration degrees of cement are much higher than the normal values, especially for high strength concrete. Since a hydration degree varying with the water/cement ratio might be expected to be the most correct one, this discrepancy requires an explanation. The reason might be the state of microcracking. In the calculation, the extent of microcracking in the cement paste is determined by the condition that $\sigma_3=f_c$ when $\sigma_1=0$. The same state of microcracking has been used in compression and in tension. In this way, the influences imposed by the change of stress state from compression to tension and the addition of aggregates are not taken into consideration. Logically, the load induced extent of microcracking will be increased when the specimens are subjected to tensile stresses and when aggregates are added, especially for high strength concrete in which the cement paste is already in a severe microcracked condition. Tensile strengths are more sensitive to the change of the microcracking state than compressive strengths. Thus, for that reason the values of f_{tpc} obtained in the calculations may be higher than those measured, especially for high strength concrete.

5.4 Conclusions and discussion

Since little information on the tensile behavior of cement paste is available from the literature, the calculations carried out in this chapter are basically qualitative. From the above calculations and comparisons, the following conclusions may be drawn:

1). For cement paste, the failure mode of pure tension is normally decisive. The main factors that affect the tensile strength, besides the strength of unmicrocracked cement paste, is the volume ratio of hard unhydrated cement grains.

2). Two different failure modes are distinguished for concrete in tension: the primary failure mode and the secondary failure mode. The primary tensile strength corresponds to the peak value of the tensile stress-deformation curve, while the secondary tensile strength corresponds to the tensile stress where sliding displacements take place. The main factors which are influential on the values of tensile strengths of concrete are the effective ratio of aggregates as well as the volume ratio of hard unhydrated cement grains.

The sliding failure mechanism in the secondary failure in tension is probably the explanation why a number of solutions in plastic theory utilizing the tensile strength has been rather successful. The effective tensile strength to be used in the plastic solutions is around half of the value of f_{tpc}.

The results of the calculations are in reasonable agreement with the tensile strengths proposed in CEB model code and in DS411.

As discussed in the previous sections, the ways to determine the parameters in the model need more thorough investigations. In estimating the tensile strength of cement paste and concrete, the parameters are adopted without change from compression. This might be one of the reasons for deviations from the proposed tensile strengths used in codes.

Despite all the defects, it seems that the failure mechanism presented may lead to a reasonable understanding of the tensile behaviour of cement paste and concrete.

VI. PUSH-OFF TYPE TESTS

Shear transfer across a cracked plane of concrete is encountered frequently in practice. To investigate the shear behavior along cracked concrete surfaces, a push-off type set up has been applied worldwide.

In this section, a model to determine the shear carrying capacity of a cracked concrete surface is proposed based on the work presented in the previous sections. The validity of the model will be verified by test results.

6.1 Solutions according to plastic theory

Fig.6.1.1 shows schematically the type of specimens used in push-off tests. Two conditions of the specimens are normally tested. One condition is the so called monolithic case where no crack is made in the shear plane prior to loading, while in the other one a crack is deliberately produced in the shear plane before the specimen is loaded.

For uncracked concrete specimens, the stress states are rather complicated, and the failure is in most cases accompanied by local failure in the concrete close to the area of loads. The analysis of this type failure is beyond the scope of this thesis. Hence, in this section, we will primarily analyze the shear failure mechanism of cracked concrete specimens.

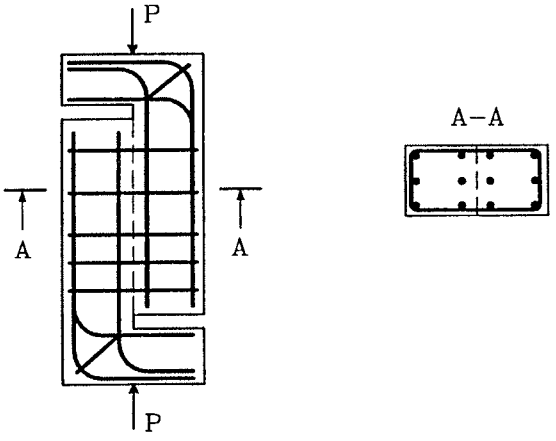

Fig.6.1.1 Schematic illustration of push-off test specimens

In [77,1] the shear problem in a joint was studied by B.C.Jensen. The analysis was based on the theory of plasticity. A shear failure mechanism was suggested by assuming a yield line in the shear plane. The relative displacement u is at an angle to the yield line, as shown in Fig.6.1.2. The upper bound solutions for such a shear failure mechanism are shown in Fig.6.1.3. and Fig.6.1.4. for the cases of plane strain and plane stress, respectively.

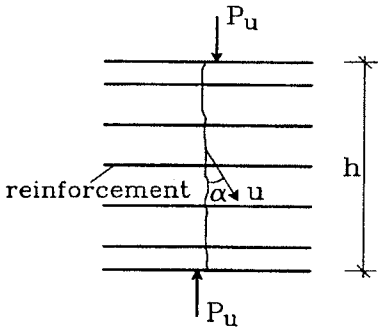

Fig.6.1.2 failure pattern

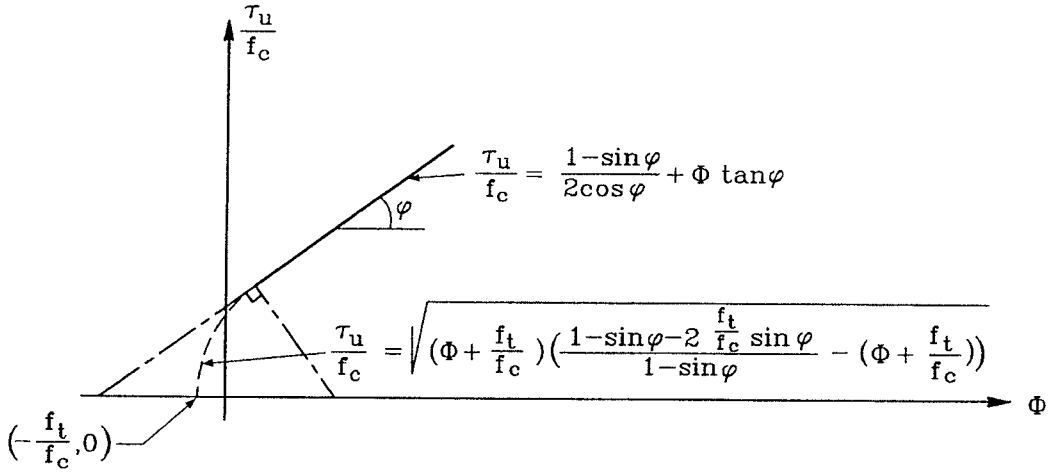

Fig.6.1.3 Shear carrying capacity in plane strain

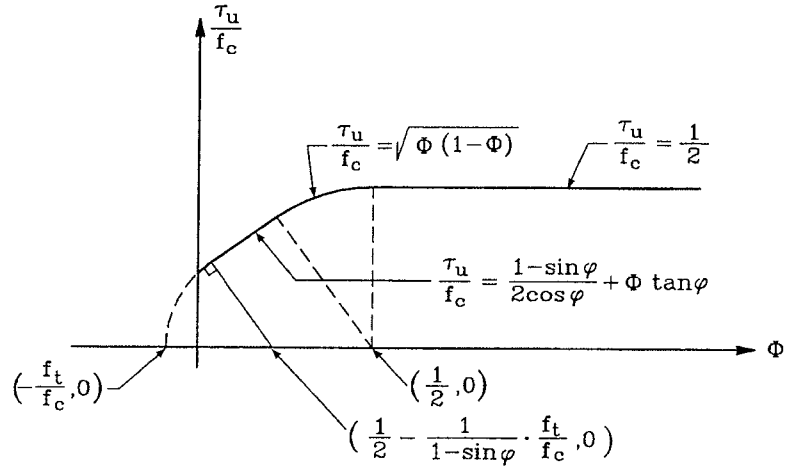

Fig.6.1.4 Shear carrying capacity in plane stress

In the figure $\Phi=A_s f_y/bhf_c$ is the mechanical reinforcement degree, f_y and f_c the yield stress of reinforcement and compressive strength of concrete respectively, and b and h the width and the height of the shear plane respectively.

By comparing with experimental results, the effectiveness factor was determined. It turned out that the ratio between the effectiveness factor for monolithic concrete specimens and that for cracked concrete specimens was about 1/0.7.

Obviously, cracking in concrete introduces a high degree of anisotropy and this is the reason for the reduction in shear carrying capacity of the specimens. How the cracking decreases the shear strength might be explained by the model presented in this paper.

6.2. Strength reduction due to cracking

Consider a concrete cylinder in the principal stress states shown in Fig.6.2.1(a). According to the failure mechanism presented in section IV, the yield line pattern is as illustrated by the dashed lines in the figure. For such a failure pattern, an average yield line, which is normally assumed if the material is imagined as homogeneous, may be defined as shown by the solid line in the figure. If, for simplicity, we assume the aggregate particles to be of equal size and uniformly distributed, it is easily seen that corresponding to a specific failure pattern, an average yield line is determined uniquely.

This may also be interpreted in the opposite way. Suppose an average yield line is defined for an imagined homogeneous concrete material, then the failure pattern in the real composite material will locate around the average yield line in a zig-zag shape consisting of the yield lines in the cement paste and the displacement of the yield line caused by the existence of aggregates.

If the average yield line is forced to follow an existing crack, as in the case of push-off tests with pre-made crack in the shear plane, the yield lines in the cement paste will be interrupted by the crack. The failure pattern will be as

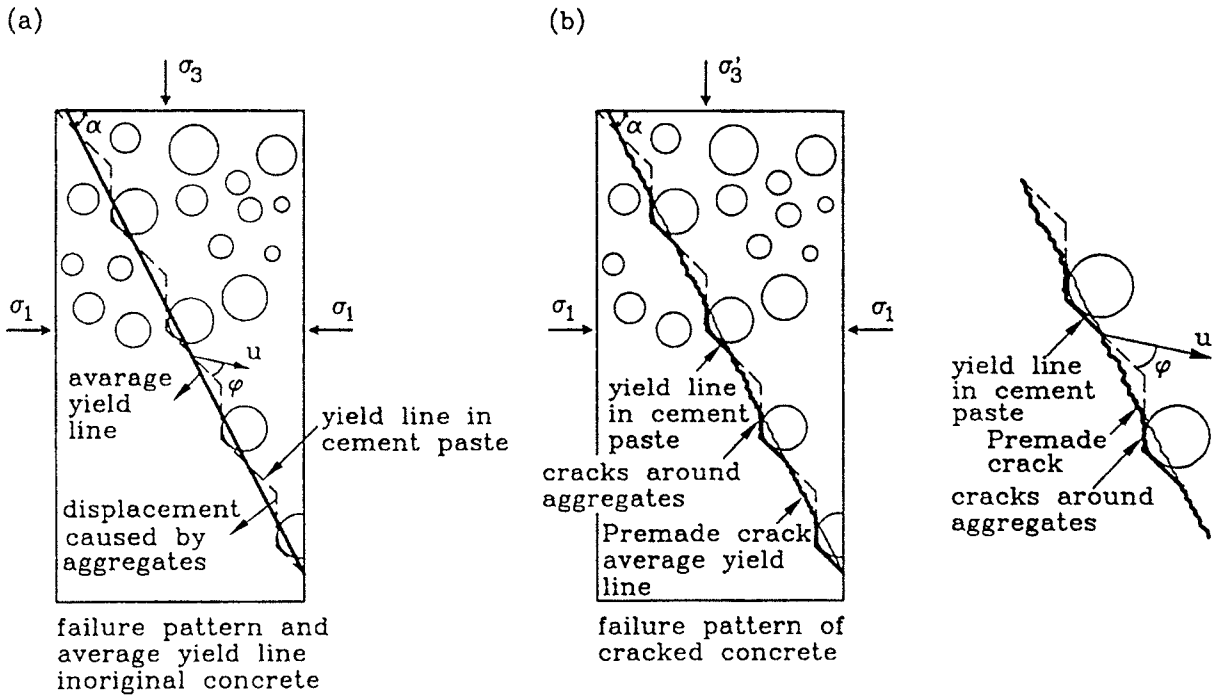

Fig.6.2.1 (a) Shear failure pattern and average yield line in original concrete
(b) Average yield line along an existing crack

shown in Fig.6.2.1(b). After passing an aggregate particle, the yield line in the cement paste will proceed until it meets the existing crack. Since the sliding resistance of cement paste is considerably weakened by the cracking, the failure will obviously choose the path of the crack. Thus, the failure pattern is composed of three parts: one part is the yield lines in the cement paste, second part is the pre-made crack and the third part is the load induced cracks in the loading direction. If the shear resistance along a cracked cement paste surface is assumed, as in the previous sections, to be reduced to such an extent that its contribution to the total resistance is negligible, this failure pattern shows that the reduction in strength of a cracked concrete specimen is due to the decrease of the total length of the yield lines in the cement paste.

In this section, the material without a pre-made crack is referred to as the original concrete.

6.3 Shear carrying capacity of cracked concrete

In Fig.6.2.1(b), if we assume that the aggregates are homogeneously distributed, then the average yield line will pass through the middle points of the yield lines in the cement paste.

The yield line pattern and the average yield line is determined as for the original concrete subjected to a lateral stress σ_1 and a longitudinal stress σ_3. The average yield line has the inclination α, as shown in Fig.6.2.1(a).

Disregarding the shear resistance of the yield line along the existing crack, the internal dissipation becomes

$$W_I' = \frac{1}{2} W_I = \frac{1}{2} cu \cdot \cos\varphi \cdot L_{AB} \tag{6.3.1}$$

where W_I is the internal dissipation for the original concrete and W_I' is the reduced internal dissipation in the cracked concrete. As before, c and φ are the apparent cohesion and friction angle, respectively, of the cement paste

corresponding to a specific stress state, and L_{AB} is the total length of the yield line in the cement paste.

The external work W_E is the same as in eq.(4.2.14), replacing the longitudinal stress σ_3 with σ_3'.

The work equation $W_E=W_I$ leads to

$$\sigma_3'=\frac{1}{2}c\frac{\cos\varphi}{\cos\gamma\sin(\gamma-\varphi)}+\sigma_1\frac{\tan\alpha}{\tan(\gamma-\varphi)} \tag{6.3.2}$$

To determine the normal stress σ and the shear stress τ in the average yield lines, we draw a Mohr's circle as shown in Fig.6.3.1. Then σ and τ may be determined by:

$$\sigma=\frac{1}{2}(\sigma_3'-\sigma_1)+\frac{1}{2}(\sigma_3'-\sigma_1)\cos2\alpha \tag{6.3.3}$$

$$\tau=\frac{1}{2}(\sigma_3'-\sigma_1)\sin2\alpha \tag{6.3.4}$$

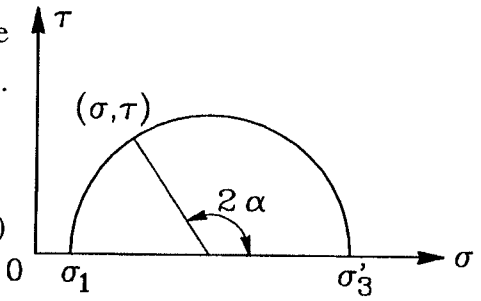

Fig.6.3.1

It should be emphasized that this failure pattern can only be realized when the normal compressive stress in the shear plane is relatively large. For small normal stresses in the shear plane, the shear failure is caused by overriding large aggregates, and the failure pattern will be different as described below.

When a concrete specimen is cracked prior to shear loading, the configuration of the pre-made crack is schematically shown in Fig.6.3.2. When forming the crack, a sort of punching out of the aggregates takes place, and sliding surfaces are formed around the particles in the matrix of the cement paste. When the cracked plane is subjected to shear force, the sliding surfaces which are on one side of the aggregate particles will be compressed, while the ones on the other side will become more open. A sliding surface will be formed in front of the aggregate particle. Since the strength is reduced along the cracked

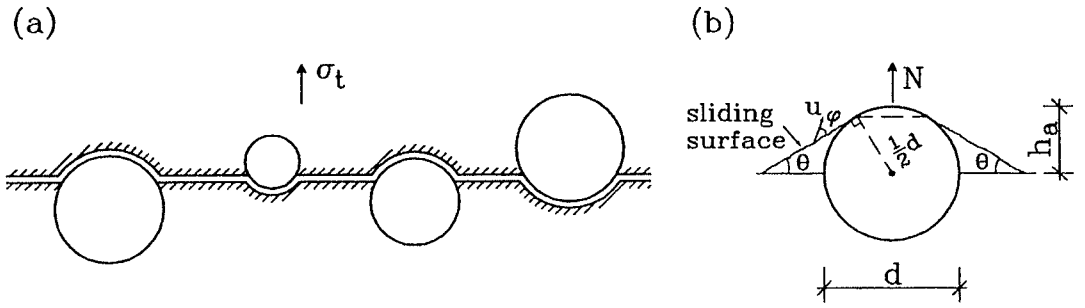

Fig.6.3.2 Configuration of a crack in concrete and punching out of an aggregate

surfaces, it would be natural for the yield line to choose the existing cracked surface, i.e. the failure takes place along the existing punching shear surfaces.

The failure of concrete subjected to tension is not yet known in details, and the punching out of aggregates is only one possible failure mode to describe the pulling out of the aggregates from the matrix of the cement paste. Details of the shape of the punching shear surfaces in cement paste are not available. To simplify the problem as in section 5.3.2, we assume that the aggregate particles are spheres and that the punching sliding surface has the shape of a truncated cone. The angle of the generatrix of the punching surface with the crack is denoted by θ.

Assuming the sliding surface tangential to the aggregate sphere, we can find the height of the sliding surfaces, and the mean value will be

$$h_a = \frac{1}{2}\cdot\frac{1}{2} d_i \cos\theta$$

The length of the sliding surface belonging to one aggregate particle in average becomes

$$\ell_{AB} = \frac{h_a}{\sin\theta}$$

The problem is treated as a plane strain problem. Along the cracked sliding surfaces, we assume the cohesion of concrete to be reduced to c', while the friction angle φ the same as in the original concrete. The relative displacement

u is at an angle of φ to the sliding surface.

Ignoring the contribution of resistance from the cracks in the shear plane and from the punching sliding surfaces behind the aggregates due to the reason that the width of these cracks will become larger during the process of loading, the internal dissipation is

$$W_I = \sum c' u \cos\varphi \cdot \ell_{AB}$$

The thickness of the specimen is a unit of length.

Inserting the expressions for h_a and ℓ_{AB}, we get

$$W_I = \frac{1}{4} cu \frac{\cos\varphi}{\tan\theta} \sum d_i \qquad (6.3.5)$$

The external work is

$$W_E = V \cdot u\cos(\theta+\varphi) - N \cdot u\sin(\theta+\varphi)$$

Denoting

$$\sigma = \frac{N}{L} \qquad \tau = \frac{V}{L}$$

we have

$$W_E = (\tau\cos(\theta+\varphi) - \sigma\sin(\theta+\varphi)) \cdot u \cdot L \qquad (6.3.6)$$

where L is the total length of the average yield line.

The work equation $W_I = W_E$ yields

$$\tau = \frac{1}{4} c' \frac{\cos\varphi}{\tan\theta\cos(\theta+\varphi)} \frac{\sum d_i}{L} + \sigma\tan(\theta+\varphi) \qquad (6.3.7)$$

According to the theorems in stereology, briefly presented in section 3.3, we have $\sum d_i/L=\frac{3}{2}\kappa_a$ where κ_a is the volume ratio of the aggregates. Thus

$$\tau=\frac{3}{8}c'\frac{\cos\varphi}{\tan\theta\cos(\theta+\varphi)}\kappa_a+\sigma\tan(\theta+\varphi) \tag{6.3.8}$$

For specific values of c' and φ, a straight line is defined by eq.(6.3.8). When c' and φ change successively, a set of straight lines are obtained. The envelope curve of these straight lines is the τ-σ relationship for a cracked surface.

The curve will be valid until it crosses the one found by eq.(6.3.3) and (6.3.4) at a certain value of σ.

The punching failure surfaces assumed in the matrix of cement paste need to be determined. In the punching shear failure analysis of concrete slabs, normal practice is to assume the bottom of the shear sliding surface being at a distance of approximately 1.5h from the concentrated load, where h is the effective depth of the slab. This gives $\theta\approx34°$. In the analysis the frictional angle of concrete is normally set to $\varphi=37°$. For cement paste, it might be expected that the sliding surfaces become steeper. Since the main purpose in this section is to get a qualitative estimation of the shear strength, we will not put much effort on studying the details in this respect. For simplicity, we set $\theta=45°$ in the calculation as in section 5.3.2. The cohesion c' is found by fitting the curve to the experimental data.

As the aggregates often are laminated, a portion of the aggregates will split during the process of producing the crack in the shear plane, especially for high strength concrete. This portion will be less or not at all effective in the shear resistance. In addition, some small aggregate particles are overridden when the initial crack width is relatively large. Thus, the effective volume ratio of aggregates for shear resistance will be less than that found from the mix design. The problem is to determine how much the effective volume ratio of aggregates is. No quantitative test data in this respect is available. For low and normal strength concrete, it may be reasonable to assume that most part of the

aggregates are effective.

Using the total volume ratio of aggregates in the calculation, it is found that approximately $c' \approx c/3$ where c is the cohesion of the cement paste in the original concrete.

In [77,1], it was demonstrated that the shear capacity of a cracked joint can not exceed the shear capacity of a monolithic concrete joint. This results in $\tau \leq \nu f_c/2$, where the effectiveness factor ν in [77,1] was found to be $\nu \approx 2/3$ for normal strength concrete. This value will be used in the following without further discussion.

6.4. Experimental verification

In the tests performed, the normal stress σ in the crack is normally produced by supplying the specimens with transverse reinforcement. When this reinforcement is assumed to yield, the σ-value may easily be calculated. In some tests σ is produced by an external normal force.

In this paper we will assume the behavior to be independent of whether σ is produced in one or the other way without further discussion.

Test results from [69,3][80,1][81,2][82,1][94,1] are quoted to compare with the theoretical calculations.

The parameters used in the theoretical calculations are adopted from the preceding sections for concrete with different compressive strengths. Due to the lack of detailed information about the materials used in the experiments from the above mentioned references, we have no possibility to accurately adjust the parameters in the calculations. Therefore, for the different compressive strengths the same data, as found in the preceding sections, are used.

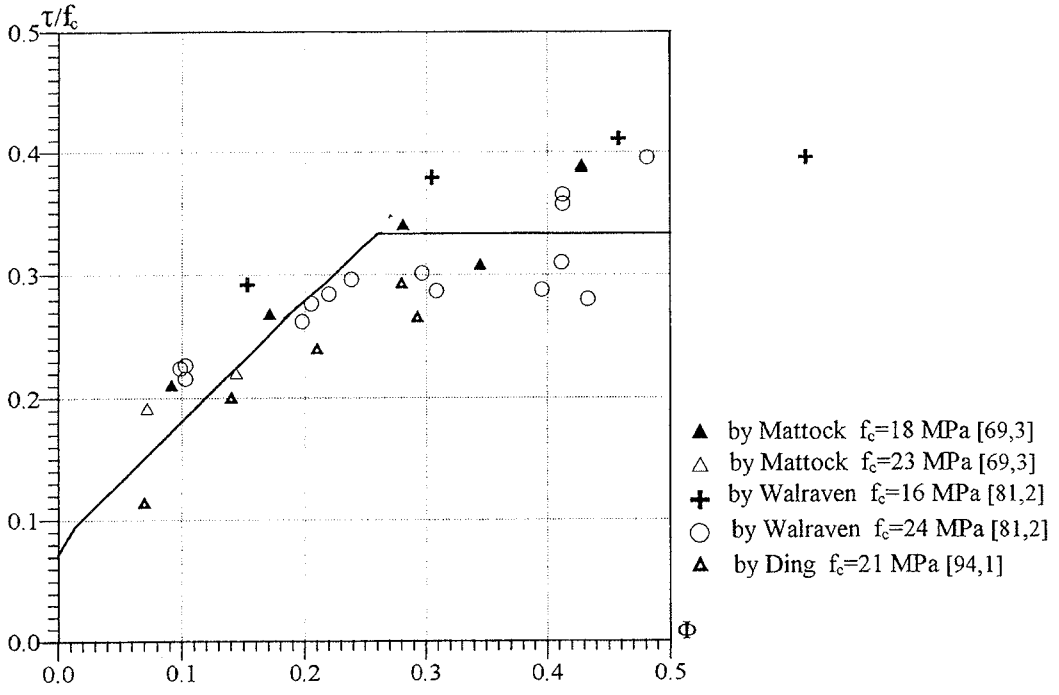

Fig.6.4.1 Comparison with test results for low strength concrete

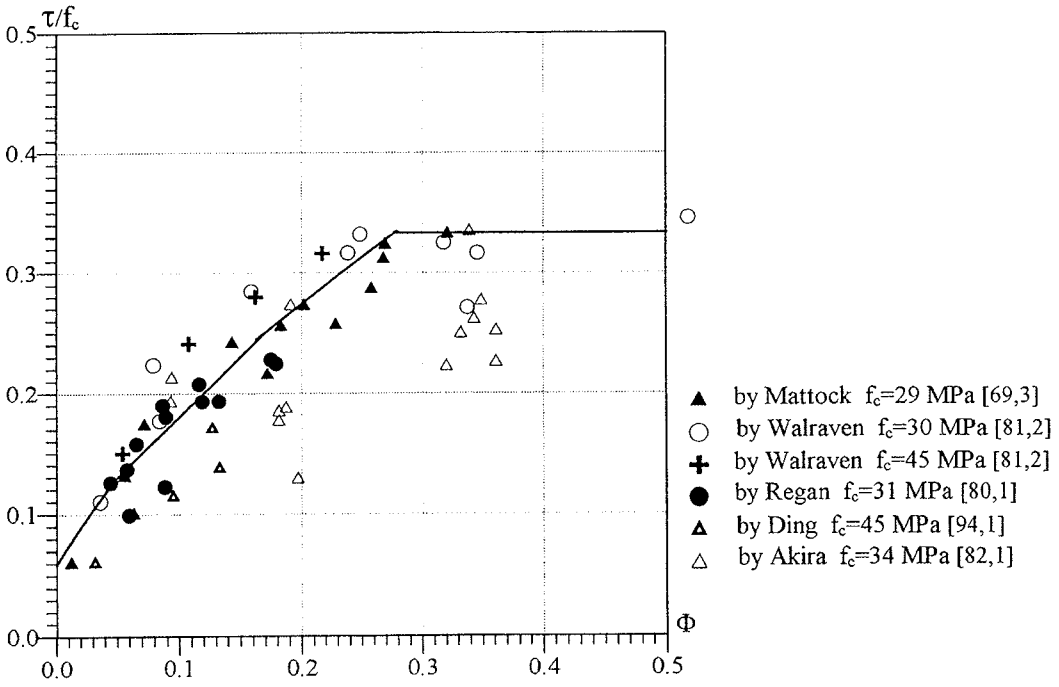

Fig.6.4.2 Comparison with test results for intermediate strength concrete

Fig.6.4.1 and Fig.6.4.2 show the comparison with test results. The calculations are performed for concrete with compressive strength f_c=10MPa and f_c=40Mpa.

The scatter of the push-off test results is recognized to be rather large due to the difficulties in controlling the crack width in the shear plane and in preventing local failures in the concrete. The influence of the initial crack width is shown in Fig.6.4.3. In this figure the ratio between the experimental results and the theoretical calculations as function of the initial crack widths w_0 [80,1][82,1] is plotted. It appears that when the initial crack width w_0 is less than about 0.5mm, the shear carrying capacity does not change substantially, while for w_0>0.5mm the shear capacity is reduced considerably with the increase of w_0. In the figure, two straight lines approximating this tendency are drawn. For w_0<0.5mm no reduction in the shear strength takes place, whereas for w_0>0.5mm the shear strength is reduced according to a straight line yielding the strength to half the value for w_0=1.0mm. This phenomenon can not yet be taken into account in the model.

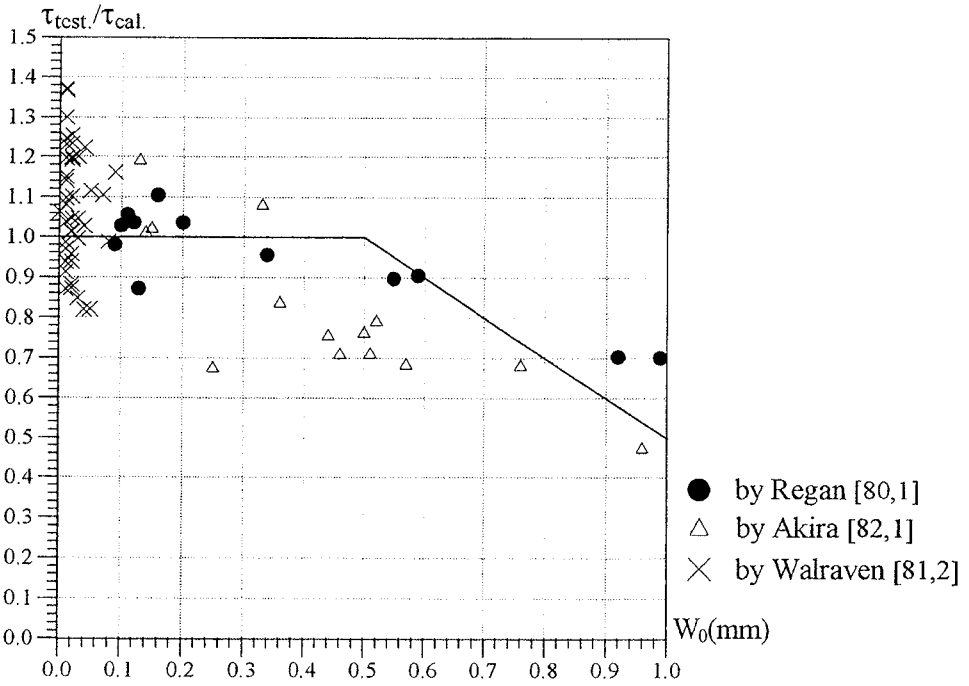

Fig.6.4.3 Influence of w_0 on the shear carrying capacity [80,1][81,2][82,1]

In some test series, the loading was stopped before it reached its ultimate value, as in [94,1] and [82,1]. Thus the measured maximum loads were less than the ultimate loads.

These might explain, to some extent, the large scatter in the test results. By checking the initial crack widths w_0 in the test series if they are available, and taking out those with w_0>0.7mm and also those where the ultimate loads were stated being not reached, we can obtain a better agreement as shown in Fig.6.4.4.

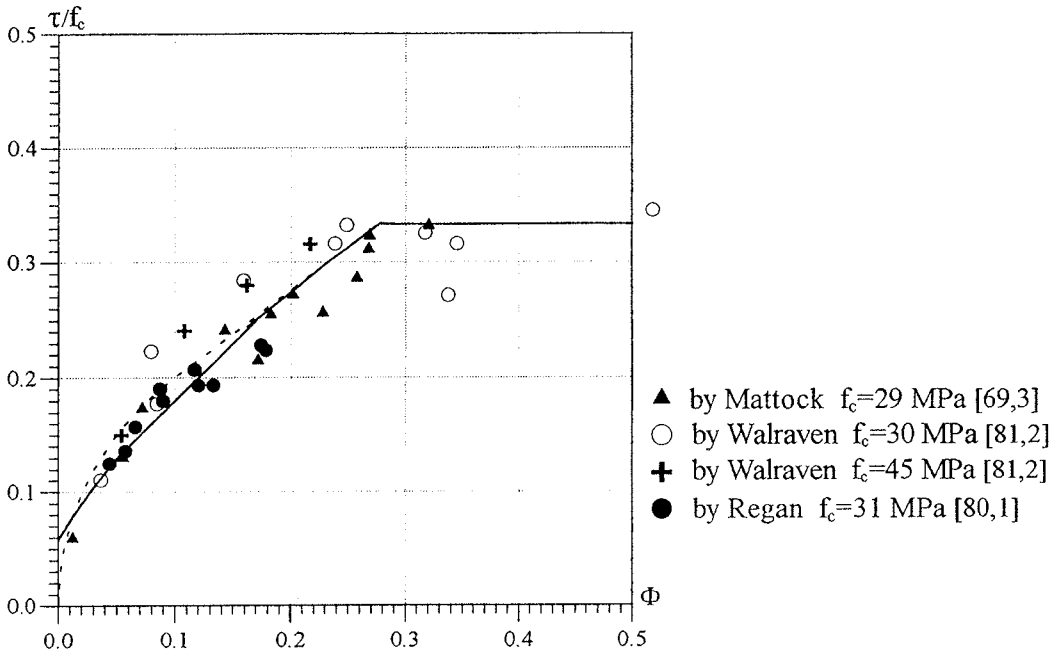

Fig.6.4.4 Comparison with test results with w_0<0.7mm

In Fig.6.4.4 the dashed line represents the result obtained by putting $c'=0.5c$, where c and c' are the cohesion of uncracked concrete and cracked concrete, respectively, into the usual plastic theory with $\varphi=37^\circ$ and the tensile strength in the crack $f_t=0$, see [77,1]. It appears that the shear capacities predicted by the two curves are rather close. This justifies the application of the usual plastic solution by choosing $c'=\nu_s c$ with $\nu_s=0.5$ when the concrete is cracked. The parameter ν_s is termed the sliding reduction factor of a crack and was used in

part 1 of this thesis [94,2] to determine the shear capacity of non shear reinforced beams.

6.5 Conclusions

The models presented in this part verify the fact that cracking in concrete reduces its strength. When the normal stress is at a low level, the reduction is mainly due to the reduced cohesion along the yield lines, whereas when the normal stress is at a higher level, the reduced length of the total yield lines in the cement paste is the main reason. By assuming the aggregate particles are evenly distributed in the matrix, the length of the yield line in the cement paste around the crack is reduced to half of that in the uncracked state.

Good agreement between the calculation and the test results is obtained. The comparison with test results shows that in case of cracked concrete, it is reasonable to assume the cohesion in the crack c' is reduced to half of that of uncracked concrete c. Thus, by setting the sliding reduction factor ν_s=0.5, the usual plastic solution can be applied in practice with reasonable accuracy.

VII. CONCLUSIONS

In this report a micromechanical shear failure mechanism in cement paste and concrete is proposed. The model is based on the fact that cement paste as well as concrete is in a microcracked state during loading or even prior to loading, and the observation from experiments that under triaxial compressive stress states cement paste may be considered as a perfectly plastic material.

In the model, hard particles from the unhydrated cement grains and the aggregates, which normally have higher strength than the cement gel, are assumed to exist in the matrix. The friction angle of cement paste is $\varphi=0$, and sliding surfaces are assumed to be created in front of the unhydrated cement grains. The microcracks in concrete are mainly in the direction of the axial load, and during failure the sliding surfaces in the cement paste will bridge the cracks along the aggregates. Hence, the function of the aggregate particles in concrete is to displace the yield lines in the cement paste to steeper positions.

The model leads to the following conclusions:

1). The compressive failure in concrete is not only governed by the cracking in the direction of the axial load but also to a large extent by shear failure in the cement paste.

2). The shear resistance of cement paste is mainly influenced by the microcracking state and the volume ratio of the unhydrated particles. When the lateral confining pressure is relatively large, the Coulomb failure criterion may be applied with the friction angle $\varphi=0$. The apparent friction angle of cement paste observed in experiments is probably due to the sliding surfaces formed in front of the unhydrated cement grains. These sliding surfaces may also explain why cement paste appears as a very brittle material in unconfined conditions.

3). Compared with a Coulomb material, the apparent friction angle of concrete observed in experiments decreases when increasing the compressive strength up

to a certain value, and beyond that it is almost a constant.

4). The shear failure criterion for concrete appears to consist of two parts: the usual Coulomb failure criterion when the lateral confining pressure is relatively large, and a transition curve between the uniaxial compression and the point where the Coulomb failure criterion becomes valid. The shape of the transition curve depends on the composition as well as the microcracking state of the material.

5). For concrete in tension, two failure modes are distinguished: the primary failure and the secondary failure. The tensile strength obtained in the secondary failure mode where sliding in cement paste occurs may explain the physical reasons for the effective tensile strengths used in the plastic theory of concrete.

6). For cracked concrete, the shear resistance along the crack can, with a reasonable accuracy, be counted to be half of that of uncracked concrete, resulting in a sliding reduction factor due to cracking ν_s=0.5. In this way, the usual plastic solutions for shear can be applied on cracked concrete by multiplying the usual effective strength of concrete with a factor ν_s=0.5.

Good agreement between the calculation and test results is found. Furthermore, a number of experimental facts about concrete and cement paste can be rationally explained by this model.

Naturally, the model is rather rough compared with the complexity of the problems we are dealing with. However, the essentials of the physical background of the compression failure, tensile failure and shear failure can be grasped by this model, and that is what the paper has endeavored to demonstrate.

REFERENCES

[28,1] F.E.Richart, A.Brandtzaeg and R.L.Brown:
A study of the failure of concrete under combined compressive stresses
University of Illinois Engineering Experiment Station, Bulletin No.185, 1928

[47,1] T.C.Powers and T.L.Brownyard:
Studies of the physical properties of hardened Portland cement paste (Nine parts)
Journal of the American Concrete Institute, Vol.43,(Oct.1946-April 1947)

[52,1] G.Balmer:
A general analytical solution for Mohr's envelope
ASTM Proceedings, 1952, pp.1260-1271

[54,1] J.W.Fabry, G.G.Balmer and V.Jones:
Triaxial strength tests of neat cement and mortar cylinders
United States Department of the Interior Bureau of Reclamation,
Concrete Laboratory Report No.C-779, Denver, Colorado, Nov.1954

[58,1] T.C.Powers:
Structure and physical properties of hardened Portland cement paste
Journal of the American Ceramic Society, Vol.41 No.1, 1958

[59,1] J.H.Taplin:
A method for following the hydration reaction in Portland cement paste
Australian Journal of Applied Science, Vol.10, No.3, 1959, pp.329-345

[61,1] T.N.W.Akroyd:
Concrete under triaxial stress
Magazine of Concrete Research, Vol.13, No.39, Nov.1961

[63,1] Thomas T.C.Hsu, F.O.Slate, G.M.Struman and G.Winter:
Microcracking of plain concrete and the shape of the stress-strain curve
Journal of the American Concrete Institute, Vol.60, Feb. 1963, pp.209
223

[66,1] R.H.Mills:
Factors influencing cessation of hydration in water cured cement paste
Highway Research Board, Washington, Special Report 90, pp.406-424, 1966

[66,2] J.R.Sims, N.W.Krathl and S.P.Victory Jr.:
Triaxial tests of mortar and neat cement cylinders
Anniversary Volume of the International Association for Bridge and
Structural Engineering, 1966, pp.481-495

[69,1] N.J.Gardner:
Triaxial behavior of concrete
Journal of the ACI, Feb. 1969, pp.136-146

[69,2] Shingo Seki, Kiyoshi Kasahara, Takeo Kuriyama and Makoto Kawasumi:
Relation between compressive strength of concrete and the effective cement-water ratio calculated from the hydration rate of cement
ACI Journal, March 1969, pp.198-201.

[69,3] J.A.Hofbeck, I.O.Ibrahim and A.H.Mattock:
Shear transfer in reinforced concrete
ACI Journal, Feb.1969, pp.119-128.

[70,1] D.W.Hobbs:
Strength and deformation properties of plain concrete subject to combined stress. Part 1: Strength results obtained on one concrete.
Cement and Concrete Association, report 42.451, Nov. 1970

[70,2] E.E.Underwood:
Quantitative stereology
Addison-Wesley Publishing Company, Inc. 1970

[71,1] G.E.Pellissier and S.M.Purdy:
Stereology and quantitative metallography
A symposium presented at the 74th annual meeting, American Society for Testing and Materials, Atlantic City, N.J., June-July 1971, ASTM Special Technical Publication 504.

[72,1] A.H.Mattock and N.M.Hawkins:
Shear transfer in reinforced concrete - recent research
PCI Journal, March-April 1972, pp.55-75.

[74,1] D.W.Hobbs:
Strength and deformation properties of plain concrete subject to combined stress. Part 2: Results obtained on a range of flint gravel aggregate concrete.
Cement and Concrete Association, report 42.497, July 1974

[74,2] R.Palaniswamy and S.P.Shah:
Fracture and stress-strain relationship of concrete under triaxial compression
Proceedings, ASCE V.100, No. ST5, May 1974

[77,1] B.C.Jensen:
Some applications of plastic analysis to plain and reinforced concrete

Institute of Building Design, Technical University of Denmark, Report No.123, Denmark, 1977

[79,1] M.Modèer:
A fracture mechanics approach to failure analyses of concrete
Materials Division of Building Materials, University of Lund, Report TVBM-1001, Lund Sweden, 1979

[80,1] Y.D.Hamadi and P.E.Regan:
Behavior of normal and light weight aggregates beams with shear cracks
The structural Engineer, Vol.58B, No.4, Dec.1980.

[81,1] A.M.Neville:
Properties of Concrete
Pitman Book Limited, 3rd edition,1981

[81,2] J.C.Walraven and H.W.Reinhardt:
Theory and experiments on the mechanical behavior of cracks in plain and reinforced concrete subjected to shear loading
Heron, Vol.26, 1981, No.1_A.

[82,1] A.Nishimura, M.Fujii, A.Miyamoto and S.Yamada:
Shear transfer at cracked section in reinforced concrete
Transaction of the Japan Concrete Institute, Vol.4, 1982, pp.257-268.

[83,1] S.Mindes:
Mechanical performance of cementitious systems
Structure and Performance of Cement, Chapter 7, edited by P.Barnes, Applied Science Publishers, 1983

[84,1] M.P.Nielsen:
Limit analysis and concrete plasticity.
Prentice-Hall, Inc. Englewood Cliffs, New Jersey, 1984.

[84,2] R.Bellotti and E.Ronzoni:
Results of tests carried out on cylindrical concrete specimens subjected to complex stress state: A critical analysis.
Int. Conf. on Concrete under Multiax. Cond., RILEM, Press de l'Universite Paul Sabatier, Toulouse, May 1984, pp.53-74

[84,3] DS411. Betonkonstruktioner.
Dansk Standard, DS411, 3rd edition, March 1984.

[85,1] P.J.Gustafsson:
Fracture mechanics studies of non-yielding materials like concrete
Modelling of tensile fracture and applied strength analyses.
Division of Building Materials, Lund Institute of Technology, Report TVBM-1007, Lund Sweden 1985

[86,1] J.G.M.van Mier:
Fracture of concrete under complex stress.
Heron, Vol.31 No.3, 1986

[86,2] T.C.Hansen:
Physical structure of hardened cement paste. A classical approach.
Materials and Structures, Vol.19, No.114, 1986, pp.423-436.

[87,1] S.Wolinski, D.A.Hordijk, H.W.Reinhardt and H.A.W.Cornelissen:
Influence of aggregate size on the fracture mechanics parameters of concrete.
The International Journal of Cement Composites and Lightweight Concrete, Vol.9, No.2, May 1987, pp.95-103.

[90,1] CEB Model Code 1990.
Comite Euro-International du Beton, Bulletin d'Information no.203, 1991.

[92,1] Kaare K.B.Dahl:
A failure criterion for normal and high strength concrete.
Technical University of Denmark, Department of Structural Engineering, Report R No.286, 1992

[92,2] Kaare K.B.Dahl:
A constitutive model for normal and high strength concrete.
Technical University of Denmark, Department of Structural Engineering, Report R No.287, 1992

[92,3] Kaare K.B.Dahl:
The calibration and use of a triaxial cell.
Technical University of Denmark, Department of Structural Engineering, Report R No.285, 1992

[93,1] R.A.Vonk:
A micromechanical investigation of softening of concrete loaded in compression.
Heron, Vol.38 No.3, 1993

[93,2] Ryå-broen: Forsøg med silicabeton - Egenskabsudvikling 1981-1993. Vejdirektoratet Broområdet, Betons holdbarhed, Rapport nr.6, 1993

[94,1] Liu Weiqing, H.E.Jensen, Ding Dajun and M.P.Nielsen: Experimental report on the mechanical behavior of cracks in reinforced concrete subjected to shear loading. High Performance Concretes in the 90'es, Report 7.7, Department of Structural Engineering, Technical University of Denmark, March 1994.

[94,2] J.P.Zhang: Strength of cracked concrete, Part 1 -Shear strength of conventional reinforced beams, deep beams, corbels, and prestressed reinforced concrete beams without shear reinforcement. Technical University of Denmark, Department of Structural Engineering, Report R No.311, 1994

[95,1] T.C.Hansen: Triaxial tests with concrete and cement paste. Technical University of Denmark, Department of Structural Engineering, Report R No.319, 1995

[96,1] T.S.Hansen and B.Andersen: General Description of cracks and other strain markers in concrete cylinders from triaxial compression tests - An investigation of fluorescein impregnated thin sections. AEC Consulting Engineers A/S, Report AEClab96-001, 1996.

Appendix 1. Estimation of Volume Ratio of Hard Unhydrated Cement particles in Hardened Cement Paste

According to investigations in the field of hydration of cement, it appears that, for normal cement cured under normal conditions, complete hydration of the cement even after long time of curing is difficult to achieve, if not impossible. A fraction will remain unhydrated. These unhydrated cement grains possesses a higher strength than cement gel.

In determining the volume ratio of hard unhydrated cement grains, the contribution from the addition of fly ash and micro silica must be taken into account as well.

A simple way to estimate the volume ratio of hard unhydrated cement grains is suggested in the following.

The volume ratio of unhydrated cement particles in hardened cement paste may be determined by:

$$m' = \frac{V_{unh.}}{V} \tag{A1.1}$$

$$V_{unh.} = (1-m)\cdot V_{cement} + (1-\alpha)\cdot V_{MS} + (1-\beta)\cdot V_F \tag{A1.2}$$

$$V = V_{cement} + V_{water} + V_{MS} + V_F \tag{A1.3}$$

$$V_{cement} = \frac{C}{\rho_C} \qquad V_{water} = \frac{W}{\rho_W} \qquad V_{MS} = \frac{MS}{\rho_{MS}} \qquad V_F = \frac{F}{\rho_F}$$

Here

- m' : volume ratio of unhydrated cement particles in hardened cement paste
- $V_{unh.}$: volume of unhydrated cement particles
- V : total volume of the hardened cement paste
- V_{cement}, V_{water}, V_{MS}, V_F

: volume of unhydrous cement, water, dry micro silica and fly ash, respectively

C, MS, F
: weight of unhydrous cement, dry micro silica, and fly ash, respectively

W : weight of total water, including that from micro silica slurry

m,α,β : hydration degree of cement, micro silica, and fly ash, respectively

ρ_C, ρ_{MS}, ρ_F, ρ_W
: density of dry cement, dry micro silica, fly ash and water, respectively

At a certain age after casting, the hydration state of cement depends on the type of cement, the fineness of the cement grains, the water/cement ratio, the curing temperature and the humidity, etc. For a rough estimation, the values of the hydration degree of cement at various ages are listed in table A1.1 for 3 different types of cement cured under normal conditions [**.*].

Table A1.1. Hydration degrees for 3 types of cement [86,2]

type / age(days)	PC	RHC	WRHC
1	0.3	0.4	0.4
3	0.5	0.6	0.5
7	0.6	0.7	0.6
14	0.65	0.8	0.7
28	0.7	0.8	0.75
91	0.8	0.9	0.9

Note: PC - Ordinary Portland Cement
RHC - Rapid Hardening Cement

The hydration of micro silica is a chemical reaction between calcium hydroxide, water and micro silica. This reaction therefore has to await the production of calcium hydroxide from the hydration of the cement. The hydration of micro silica leads to the formation of some calcium silicate hydrate crystals, which are much smaller than the hydration products of the cement grains. This is the reason why a very dense structure is obtained by adding micro silica to the mix.

The hydration mechanism of micro silica is not yet well understood. At early age, the hydration degree of micro silica is lower than that of cement due to the delay mentioned. For simplicity, we assume α=0.7 for rapid hardening cement at the age of 28 days after casting.

Normally, fly ash is used as replacement of some cement in the mix design. Only part of it is composed of material containing SiO_2. The other part of fly ash consists of particles which can be hardly regarded as hard grains compared with the unhydrated cement particles and can not be counted as effective resistance against sliding. This implies that this part of fly ash perhaps should better be regarded as "dust" in the shear resisting mechanism.

The hydration of fly ash is also delayed. At the age of 28 days, maybe about or less than 50% of the hydratable matter is hydrated. The actual hydration degree of fly ash is difficult to estimate. For simplicity, we assume that 50% of the fly ash is hydratable and that the hydration degree of the hydratable matter of fly ash at the age of 28 days is 0.5. Thus, in eq.(A1.2) to get the portion of the hard particles from fly ash we may put $1-\beta=0.25$.

In the test series reported in [92,1][94,1], the densities of the dry cement and fly ash are respectively ρ_C=3100 ~ 3200kg/m^3 and ρ_F=2200kg/m^3. Micro silica slurry, a solution of micro silica, with 51.6% dry-matter, was used in some of the mixes. The density of the micro silica slurry is 1391kg/m^3, and the density of dry micro silica is $\rho_{MS}\approx$2200kg/m^3.

In the calculation of the volume ratio of hard particles for the mixes in [92,1][94,1], the following values of parameters are used:

ρ_C=3150kg/m^3 ρ_W=1000kg/m^3 ρ_{MS}=2200kg/m^3 ρ_F=2200kg/m^3
MS=0.516$W_{MS\text{-}slurry}$
W=$W_{miximg\text{-}water}$+(1-0.516)$W_{MS\text{-}slurry}$
m=0.7 for PC, 0.8 for RHC and 0.75 for WRHC.
1-m=0.3 for PC, 0.2 for RHC and 0.25 for WRHC.
1-α=0.3 1-β=0.25

Here, $W_{MS\text{-}slurry}$ is the weight of the micro silica slurry.

As known, for a specific type of cement under the same curing conditions, the effective water/cement ratio is the primary influential factor on the hydration degree of cement. The results from [59,1]69,2] show clearly that low hydration degree may be expected when the water/cement ratio goes down. This will yield a larger portion of hard unhydrated cement grains, especially for high strength cement paste and concrete. Based on the curve of hydration degree in [59,1], shown in Fig.3.5.4, the hydration degrees of cement and concrete with the water/cement ratios from the mix design in the test series [92,1] may be estimated and the results are listed in table A1.2.

Table A1.2 Hydration degrees based on [59,1]

	B010(P)	B035(P)	B050	B070(P)	B085	B100	B110
W/C	1.32	0.69	0.64	0.50	0.39	0.28	0.26
m	0.80	0.72	0.71	0.64	0.54	0.46	0.44

Note: the symbol (P) represents cement paste specimens.

As mentioned above, the contribution of micro silica to the content of hard particles in cement paste is not clear. It might be possible that the hydration products from micro silica may be strong enough to be regarded as hard

particles regarding sliding resistance. To get an upper limit of m′ in this case, we put the α=0.

Table A1.3 lists the volume ratios of hard particles estimated on the basis of varying hydration degrees of cement m and α=0 as well as with fixed hydration degrees of cement m and α=0.7. The mix design is from [92,1].

Table A1.3 Volume ratios of hard particles m′ in cement paste and concrete [92,1]

test series		B010(P)	B035(P)	B050	B070(P)	B085	B100	B110
m′ (%)	α=0.7	6.62	9.20	8.53	8.81	11.40	11.97	12.47
	α=0	6.62	11.34	13.35	18.45	25.34	33.70	36.10

The method suggested here is an approximate way to estimate the content of hard particles in hardened cement paste and in concrete. Undoubtedly it will give the right order of magnitude. More accurate estimation needs further investigation.

AFDELINGEN FOR BÆRENDE KONSTRUKTIONER
DANMARKS TEKNISKE UNIVERSITET

Department of Structural Engineering and Materials
Technical University of Denmark, DK–2800 Lyngby

SERIE R
(Tidligere: Rapporter)

R 317. JAGD, LARS, CHRISTOFFERSEN, JENS, NIELSEN, M.P.: The HOTCH–POTCH Disk Element – Finite Element for Analysis of Reinforced Concrete Disks. 1994.
R 318. JAGD, LARS, CHRISTOFFERSEN, JENS, NIELSEN, M.P.: The HOTCH–POTCH Disk Element – Finite Element for Analysis of Reinforced Concrete Shells. 1994.
R 319. HANSEN, THOMAS CORNELIUS: Triaxial Tests with Concrete and Cement Paste. 1995.
R 320. PETERSEN, R.I., AGERSKOV, H., MARTINEZ, L. LOPEZ, ASKEGAARD, V.: Fatigue Life of High–Strength Steel Plate Elements under Stochastic Loading. 1995.
R 321. Resuméoversigt 1994 – Summaries of Papers 1994.
R 322. IBSØ, JAN BEHRENDT: Fatigue Life Prediction of Welded Joints Based on Fracture Mechanics and Crack Closure. 1995.
R 323. NIELSEN, CLAUS VESTERGAARD: Ultra High–Strength Steel Fibre Reinforced Concrete. Part I. Basic Strength Properties of Compresit Matrix. 1995.
R 324. NIELSEN, CLAUS VESTERGAARD: Ultra High–Strength Steel Fibre Reinforced Concrete. Part II. Structural Applications of Compresit. 1995.
R 1. R.I. PETERSEN, H. AGERSKOV & L. LOPEZ MARTINEZ: Fatigue Life of High–Strength Steel Offshore Tubular Joints, 1996.
R 2. Resuméoversigt, ABK 1995 – Summaries of Papers, ABK 1995.
R 3. SCHAUMANN, JETTE: Lignocellulosematerialers vandbinding. 1996.
R 4. RASMUSSEN, K.J.R.: State of the Art of Numerical Simulation and Computational Models in Coupled Instabilities. 1996.
R 5. JAGD, LARS KRISTIAN: Non–linear Seismic Analysis of RC Shear Wall. 1996.
R 6. NIELSEN, LAUGE FUGLSANG: Lifetime and residual strength of wood, subjected to static and variable load. 1996.
R 7. NIELSEN, LAUGE FUGLSAND: Træthed og reststyrke i beton og andre viskoelastiske materialer med ældning. 1996.
R 8. Ninth Nordic Seminar on Computational Mechanics. Redigeret af LARS DAMKILDE. 1996.
R 9. HANSEN, THOMAS CORNELIUS: Fatigue in High Strength Steel. A new approach to predict crack propagation behaviour. 1996.
R 10. HANSEN, THOMAS CORNELIUS: Fatigue in Welded Connections. A new approach to predict crack propagation behaviour. 1996.
R 11. HANSEN, THOMAS CORNELIUS, AND OLSEN, DAVID HOLKMANN: Fracture and crack growth in concrete. A new approach to predict crack propagation behaviour. 1996.
R 12. HOANG, LINH CAO AND NIELSEN, M.P.: Continuous Reinforced Concrete Beams – Stress and Stiffness Estimates in the Serviceability Limit State. 1996.
R 13. NIELSEN, LAUGE FUGLSANG: Composite Analysis of Concrete. Creep, Relaxation, and Eigenstrain/Stress. 1996.
R 14. PEDERSEN, CARSTEN: New Production Processes, Materials and Calculation Techniques for Fiber Reinforced Concrete Pipes. 1996.
R 15. NIELSEN, J.A., H. AGERSKOV AND T. VEJRUM: Fatigue in Steel Highway Bridges under Random Loading. 1997.
R 16. HOANG, LINH CAO: Shear Strength of Non–Shear Reinforced Concrete Elements. 1997

Abonnement 1.7.1997 – 30.6.1998 kr. 130,–
Subscription rate 1.7.1997 – 30.6.1998 D.Kr. 130.–.